

AN APPLICATION OF HOMOMORPHIC DECONVOLUTION  
TO LORAN-C SIGNAL PROCESSING

Robert John Wenzel

Library  
Naval Postgraduate School  
Monterey, California 93940

AN APPLICATION OF HOMOMORPHIC DECONVOLUTION TO LORAN-C SIGNAL PROCESSING

by

Robert John Wenzel

B.S., U.S. Coast Guard Academy

(1969)

SUBMITTED IN PARTIAL FULFILLMENT OF THE

REQUIREMENTS FOR THE DEGREES OF

ELECTRICAL ENGINEER

AND

MASTER OF SCIENCE

at the

MASSACHUSETTS INSTITUTE OF TECHNOLOGY

June 1974

Signature of Author . . . . .  
Department of Electrical Engineering, May 10, 1974

Certified by . . . . .  
Thesis Supervisor

Accepted by . . . . .  
Chairman, Departmental Committee on Graduate Students

T 16 1544



-2-

# AN APPLICATION OF HOMOMORPHIC DECONVOLUTION TO LORAN-C SIGNAL PROCESSING

by

Robert John Wenzel

Submitted to the Department of Electrical Engineering on 10 May 1974 in partial fulfillment of the requirements for the Degrees of Electrical Engineer and Master of Science.

## ABSTRACT

The performance of Loran-C receivers is severely limited by contamination introduced by multipath propagation effects. Echo removal by discrete generalized linear filtering is considered as a method of reducing the effects of the contamination. The signals can be described as consisting of repeated, known, composite signals with short echo arrival times, in noise. Since the signals are repeated, and stable, they can be averaged to increase the effective signal to noise ratio. The homomorphic deconvolution technique is applied to simulated signals and a determination of the averaging time needed for satisfactory performance is made.

Aside from the Loran-C application, the report presents a detailed study of the computational aspects involved in deriving the complex cepstrum. Since the signal is known, the effects of noise and aliasing can be precisely identified. In particular, conventional phase unwrapping methods are questioned for certain classes of signals.

THESIS SUPERVISOR: Russell M. Mersereau

TITLE: Research Associate, Department of Electrical Engineering



# ACKNOWLEDGEMENT

I would like to take the opportunity to thank the Digital Signal Processing Group of the Research Laboratory of Electronics for making available the computer time necessary for the completion of this thesis. I am also grateful for the information on the Loran-C system provided by Jim Doherty and Bill Schorr.

Most importantly, a good deal of thanks is extended to Doctor Russell Mersereau whose time and advice was always available to help me organize the direction of the research.





## TABLE OF CONTENTS

		<u>Page</u>
Chapter 1	INTRODUCTION	10
	1.1 Loran-C System Description	11
	1.2 Homomorphic Deconvolution	23
Chapter 2	PROBLEM FORMULATION	32
Chapter 3	DECONVOLUTION OF NOISELESS SIGNALS	41
	3.1 Sequence of Estimation	42
	3.2 Estimation of $g_a(n)$	46
	3.3 Estimation of $p_a(n)$	49
	3.4 Performance of Estimators	56
	3.5 Application to Simulated Signals	62
Chapter 4	DISTORTED SIGNALS	68
	4.1 Distorted Basic Waveform	68
	4.2 Distorted Echoes	74
Chapter 5	NOISY SIGNALS	78
Chapter 6	CONCLUSIONS	97
	BIBLIOGRAPHY	100
Appendix A	COMPLEX CEPSTRUM DERIVATIONS	101
	A.1 Basic Waveform, Arrival Time Coincident With Sampling Time	101
	A.2 Basic Waveform, Arrival Time Between Sampling Times	103
	A.3 Multipath Impulse Train	105
	A.4 Cepstrum for Exponentially Weighted Signals	108



TABLE OF CONTENTS  
(Continued)

	<u>Page</u>
Appendix B     PHASE UNWRAPPING CONSIDERATIONS	111
Appendix C     TRANSFORM PHASE CORRECTION METHOD	139
Appendix D     MORE GENERAL NOISE DFT DERIVATION	144



## LIST OF FIGURES

	<u>Page</u>
Figure 1-1 Loran-C Chain Pulse Transmission Scheme	13
Figure 1-2 Loran Propagation Paths	14
Figure 1-3 Skywave Arrival Times	15
Figure 1-4 Skywave Magnitudes	15
Figure 1-5 Composite Received Signal	16
Figure 1-6 Pulse Phase Code	17
Figure 1-7 Envelope Deriver and RF Samplers	18
Figure 2-1 Generation of Complex Envelope	33
Figure 2-2 Realization of Sampled Complex Envelope	34
Figure 2-3 Homomorphic Filter Input-Output	40
Figure 3-1 Cepstrum of Simulated Received Signal	43
Figure 3-2 Simulated $x(n)$ Sequence	45
Figure 3-3 Simulated $y(n)$ Sequence	47
Figure 3-4 Comparison of $g(n)$ and $p(n)$	48
Figure 3-5 Expected Form of $p_a(n)$	50
Figure 3-6 Homomorphic Filter-Estimator	55
Figure 3-7 Simplified Signal to be Estimated	56
Figure 3-8 Estimator Performance Curve	60
Figure 5-1 Frequency Plot of Signal and Noise	85
Figure 5-2 Vector Diagram of Signal and Noise	85
Figure 5-3 LOG-DFT Filtering Effect	87
Figure 5-4 Development of Noisy Cepstrum	89
Figure 5-5 + 40 db SNR LOG DFT	92



LIST OF FIGURES  
(Continued)

	<u>Page</u>
Figure 5-6 + 30 db SNR LOG DFT	93
Figure 5-7 + 20 db SNR LOG DFT	94
Figure 5-8 + 40 db SNR Cepstrum	95
Figure 5-9 + 30 db SNR Cepstrum	96
Figure B-1 Uncorrected Phase Curve	111
Figure B-2 Corrected Phase Curve	113
Figure B-3 Corrected Phase Curve - Final Version	113
Figure B-4 Vector Representation of $P(e^{j\omega})$	115
Figure B-5 $P(e^{j\omega})$ Phase and Magnitude	116
Figure B-6 $P(e^{j\omega})$ With Linear Phase	117
Figure B-7 Vector Representation of $P(e^{j\omega})$ With Linear Phase	118
Figure B-8 $P(e^{j\omega})$ Phase, $B_1 > 1$	119
Figure B-9 Real and Imaginary Part of $e^{-n}u_{-1}(n)$ DFT	123
Figure B-10 Magnitude and Phase of $e^{-n}u_{-1}(n)$ DFT	124
Figure B-11 Magnitude and Phase of Loran-C Signal Transform	125
Figure B-12 Vector Representation of $P(e^{j\omega})$	126
Figure B-13 Uncorrected Phase Curve: No Echo, No Linear Phase	131
Figure B-14 Uncorrected Phase Curve: No Echo, With Linear Phase	132
Figure B-15 Log Magnitude and Phase: One Echo, No Aliasing	133
Figure B-16 Log Magnitude and Phase: One Echo, With Aliasing	135
Figure B-17 Corrected Phase Curve: No Aliasing	137
Figure B-18 Corrected Phase Curve: With Aliasing	138
Figure C-1 Vector Representation of $P(e^{j\omega})$ With Extra Exponential Weighting	139





LIST OF FIGURES  
(Continued)

	<u>Page</u>
Figure C-2    Complex Cepstrum: Conventional Phase Unwrapping	142
Figure C-3    Complex Cepstrum: Modified Phase Unwrapping	143
Figure D-1    Model of Non-White Noise Sample Generator	144
Figure D-2    No Title	147
Figure D-3    No Title	149
Figure D-4    Non-White Noise DFT Variance	149



# LIST OF TABLES

	<u>Page</u>
Table 3-1 Results of Simulation, No Distortion, One Echo Zero Phase	63
Table 3-2 Results of Simulation, No Distortion, One Echo Non-zero Phase	64
Table 3-3 Results of Simulation, No Distortion, One Echo Groundwave and Skywave at Arbitrary Phases	65
Table 3-4 Results of Simulation, No Distortion, One Echo Skywave Larger than Groundwave	65
Table 3-5 Results of Simulation, No Distortion, Two Echoes	67
Table 4-1 Comparison of A Priori Estimate Error and $\hat{p}_a(n)$	71
Table 4-2 Comparison of Revised A Priori Estimate Error and $\hat{p}_a(n)$	73
Table 4-3 Results of Simulation, Distorted Echo	77



## Chapter 1

### INTRODUCTION

The digital signal processing technique referred to as Homomorphic Deconvolution has met with some success, in a number of diverse applications, in suppressing signal contamination introduced by a multipath propagation medium. Another possible application is to Loran-C, a low frequency electronic navigation system, in which the performance is severely limited by the effects of such contamination. It is the purpose of this thesis to study the applicability of the technique to various aspects of Loran-C signal processing.

In this Chapter, a brief description of the Loran-C system and Homomorphic Deconvolution is presented. In Chapter 2, the task of the homomorphic filter in the Loran-C case is formulated. In Chapter 3, the filtering technique is developed and the results of simulated filtering in the noiseless case are presented. Chapter 4 presents the theory and a simulated example of the effects of signal distortion. Chapter 5 includes a theory of the effect of white gaussian noise on the processing and includes examples to verify the theory. In Chapter 6, the effects of the various assumptions and simplifications made are discussed and the results of the preceding chapters are examined to determine the applicability of the method. The examples presented are simulations performed on an IBM 370 general purpose computer.



## 1.1 Loran-C System Description

Loran-C is an electronic navigation system which belongs to a broad class of systems referred to as hyperbolic, a characterization based on straightforward geometric considerations. If radio signals are simultaneously transmitted from two different locations, they will, in general, arrive at some arbitrary third location at two different times. To the extent that the speeds of propagation along the two paths are equal and known, a measurement of the difference in times of arrival provides a corresponding measure of the difference in distances involved. The locus of points with a constant difference in distance from two reference points is a hyperbola. A receiver which determines this time difference and identifies the proper reference points provides information sufficient to define a navigational line of position. Two or more such lines of position can be used to obtain a fix - the location of the receiver.

Various hyperbolic systems with origins in the late 1930's have evolved into today's alternatives. Of these, it may be said, the one which meets the most general operational requirements is the Loran-C system. The advantages of Loran-C can, in short, be attributed to the following.

1. Use of a frequency band (90 to 110 kHz) which provides for extended range and exhibits excellent propagation properties.
2. Use of a pulsed signal format. This increases average transmitted power and permits signal coding to facilitate





transmitting station identification and to reduce the effects of interference.

3. Improved measurement precision obtained by coarse measurement of the envelope followed by fine tune measurements based on the signal rf carrier.<sup>1</sup>

In Loran-C, the hyperbolic navigation concept is realized in a somewhat complex manner. There are a number of modifications to the simple scheme as previously described. While the modifications make the system appear involved, they are seen to be well founded and straightforward when systematically examined.

A first consideration is the operation of the transmitting stations. These are grouped into chains whose configurations, subject to practical constraints, provide geometrically optimal accuracy and coverage. An example of a simple chain to analyze is the so-called triad which consists of stations denoted master, slave X and slave Y. The transmissions consist of groups of pulses on a 100 kHz carrier frequency: the master transmits nine pulses in a group while the slaves each transmit eight pulses in a group. In practice, the stations do not transmit simultaneously. The slave stations incorporate known transmission delays relative to the master so that, within the service area of a triad, reception is typically as depicted in figure 1-1. Transmission timing is controlled so that the groups are received in the order and intervals shown. The transmission delays guarantee that there will be no overlap of the groups. In this example, the transmission sequence is repeated every 50,000 microseconds - the chain pulse group repetition interval. Different chains are distinguished by



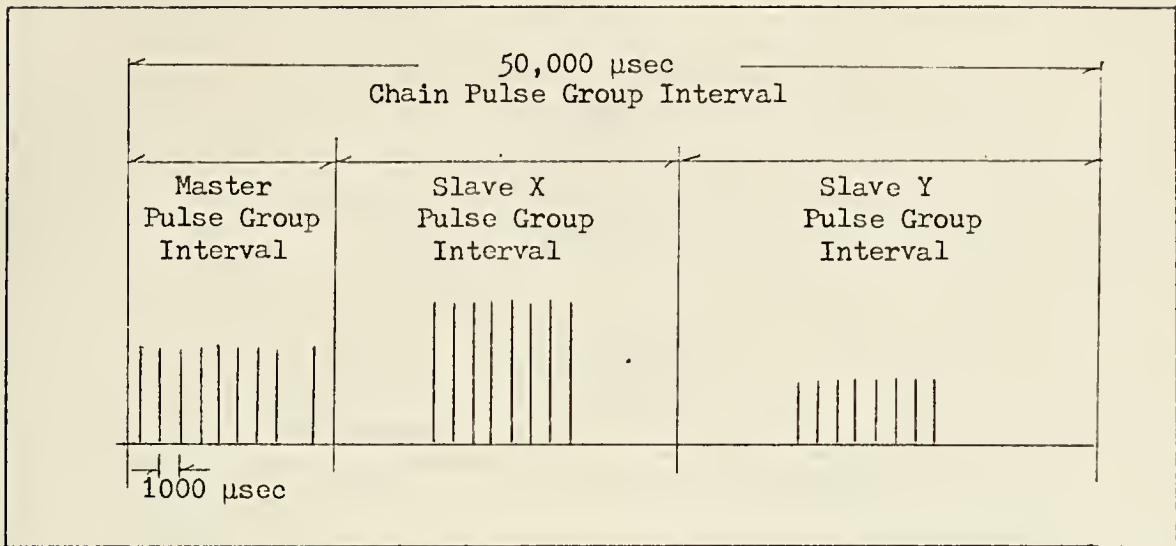


Figure 1-1 Loran-C Chain Pulse Transmission Scheme

different group repetition intervals. Consequently, by means of a correlation type operation applied over a number of repetition intervals, a receiver can discriminate between signals transmitted from adjacent chains.

The stations also employ a pulse phase code in the transmission. This allows enhanced discrimination between signals from competing chains and overcomes some of the problems introduced by skywave contamination.

The term skywave refers to the multipath propagation phenomenon depicted in figure 1-2. The high accuracy and coverage advantages of Loran-C depend on the use of measurements obtained from signals arriving via the stable groundwave propagation mode at extended ranges. The reception of skywaves, whose arrival times are highly dependent upon unpredictable ionospheric properties, causes severe signal processing problems. The nature of the important properties of the



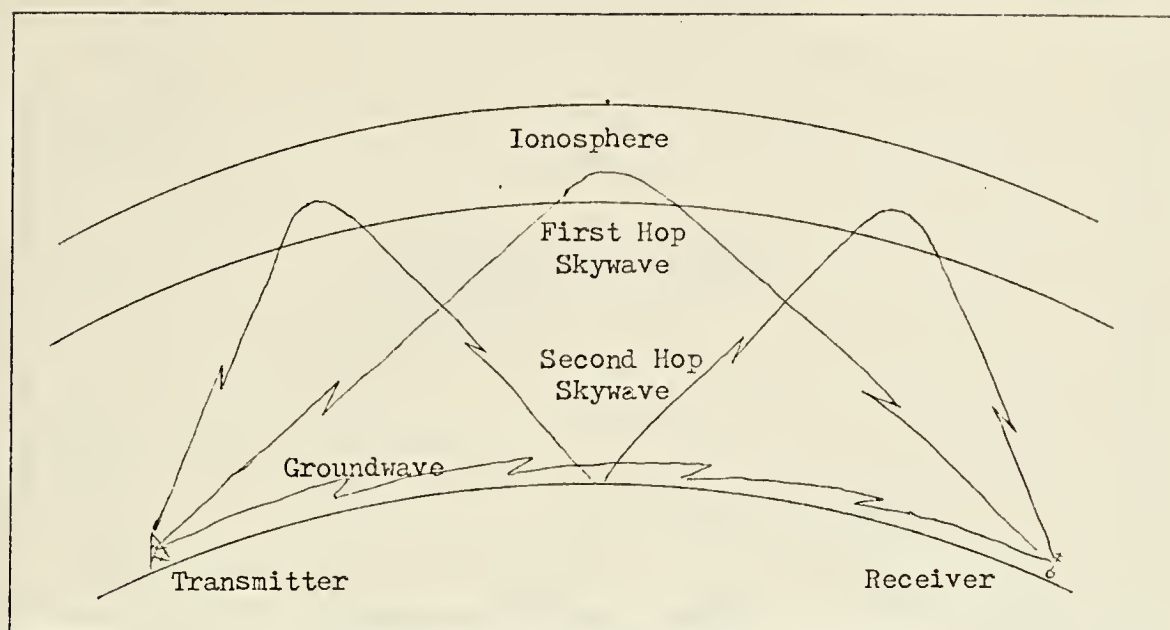


Figure 1-2 Loran Propagation Paths

multipath medium, at Loran-C frequencies, is illustrated in figures 1-3 and 1-4. It can be seen that the times of arrival can be as short as about 35 microseconds after the arrival of the groundwave for strong first hop skywaves at extended ranges. Additionally, arrival times can be delayed as long as about 1500 microseconds for higher order hops under some conditions. An explanation of how these effects are overcome requires a further description of the transmitted signal format and a brief description of receiver detection methods.

All transmitting stations attempt to generate pulses of the same form which can be described as  $t^2 e^{-\alpha t}$  with  $\alpha$  such that a peak occurs 65 microseconds after the beginning of the pulse. Such a pulse has an effective duration of 250 to 300 microseconds. An example which combines the two most deleterious effects of the multipath contamination is illustrated in figure 1-5. For clarity, the magnitudes



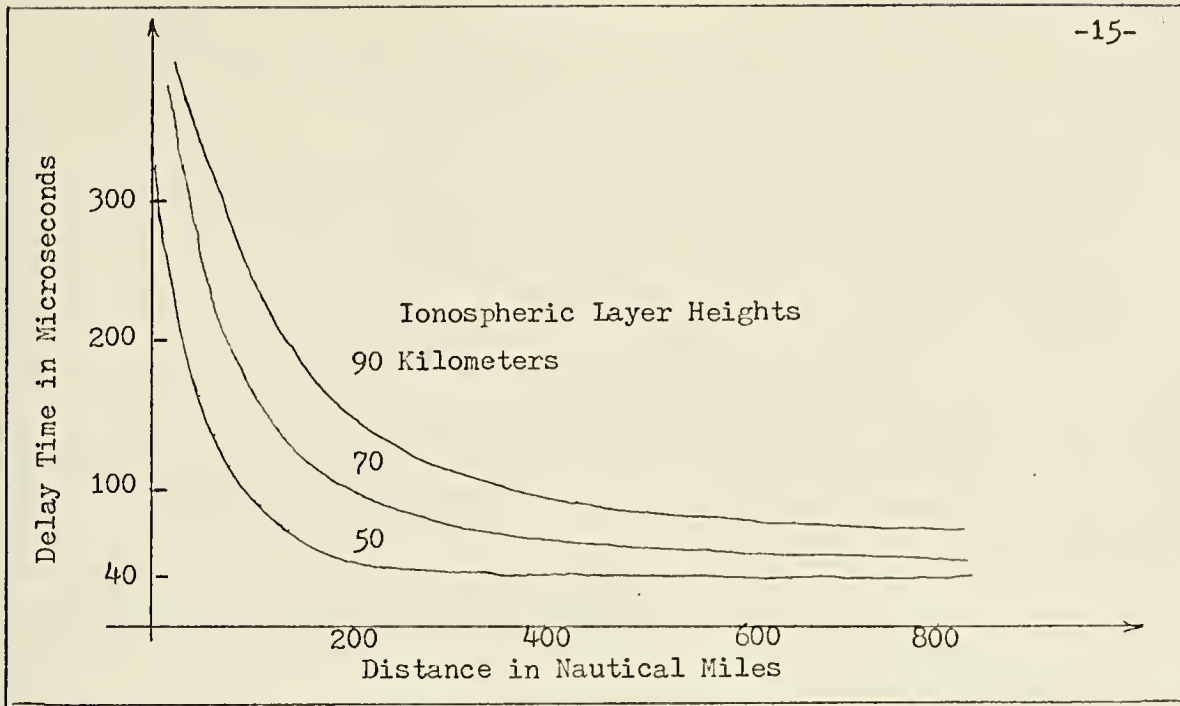


Figure 1-3 Skywave Arrival Times

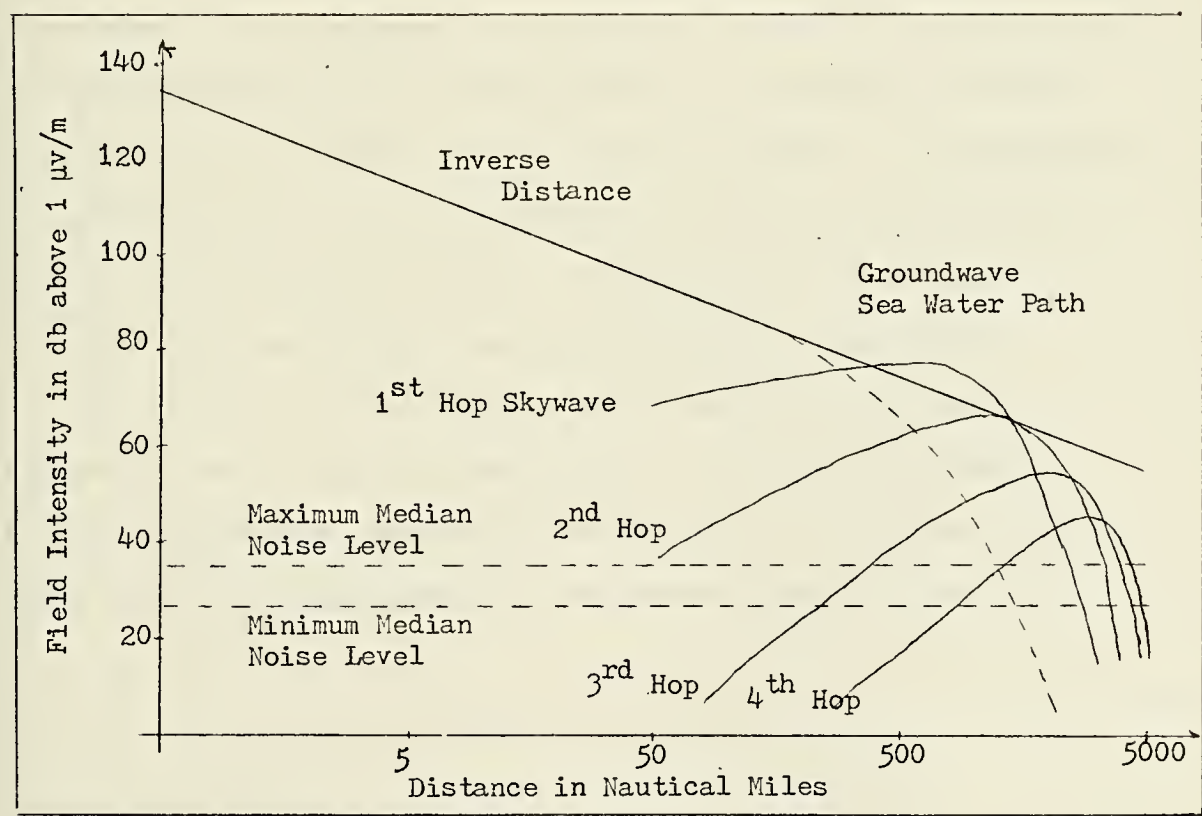


Figure 1-4 Skywave Magnitudes





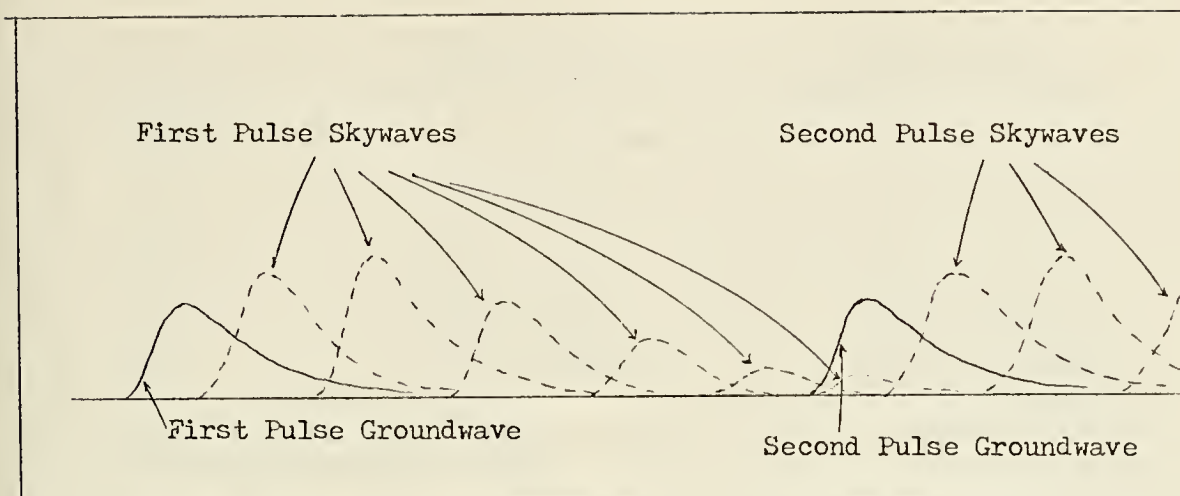


Figure 1-5 Composite Received Signal

of the separate components of the signal have been superimposed.

The effects of the contamination can be grouped into two categories. The groundwaves are overlapped by skywaves associated with the same transmitted pulse. These skywaves correspond to low order hops and may be many times larger than the groundwave. The groundwaves are also overlapped by much delayed, high order hops associated with the preceeding transmitted pulse. These skywaves will be fairly well attenuated and smaller than the groundwaves they overlap.

The problems of long delayed skywave interference is easily overcome by use of a pulse phase coding. The phase of the transmitted signal carrier is systematically varied in  $180^{\circ}$  steps from pulse to pulse in accordance with the scheme shown in figure 1-6.



Repetition Interval	Any Master Station	Any Slave Station
First	+ - - + + + +	+ - + - + + - -
Second	+ + - - + - + -	+ + + + + - - +
Third	same as first	same as first
Fourth	same as second	same as second
etc.	etc.	etc.

Figure 1-6 Pulse Phase Code

As an example of the use of the code, consider the effect of the sixth hop skywave in figure 1-5 which will cause problems by overlapping the next groundwave. It can be verified from figure 1-6 that the code can be represented as a signal,  $s(t)$ , with the property that  $s(t)$  and  $s(t-T)$  are orthogonal when averaged over two pulse group repetition intervals, where  $T$  is a multiple of 1000 microseconds. Since the effect of the sixth hop skywave is to create a signal  $s(t) + A s(t-T)$ , if the received signal is correlated with  $s(t)$ , this type of interference is removed.

The effects of the interference caused by low order skywaves are not so easily overcome. Use is made of the fact that the groundwave travels the most direct path and is therefore guaranteed to arrive before any of the skywaves associated with the same transmitted pulse. Consequently the first portion of the groundwave is free of contamination of this type and can be used to make the time measurements. This portion, however, can not be assumed, a priori, to be much more than the first 30 microseconds of the pulse.

The measurement technique proceeds in two steps. First it is



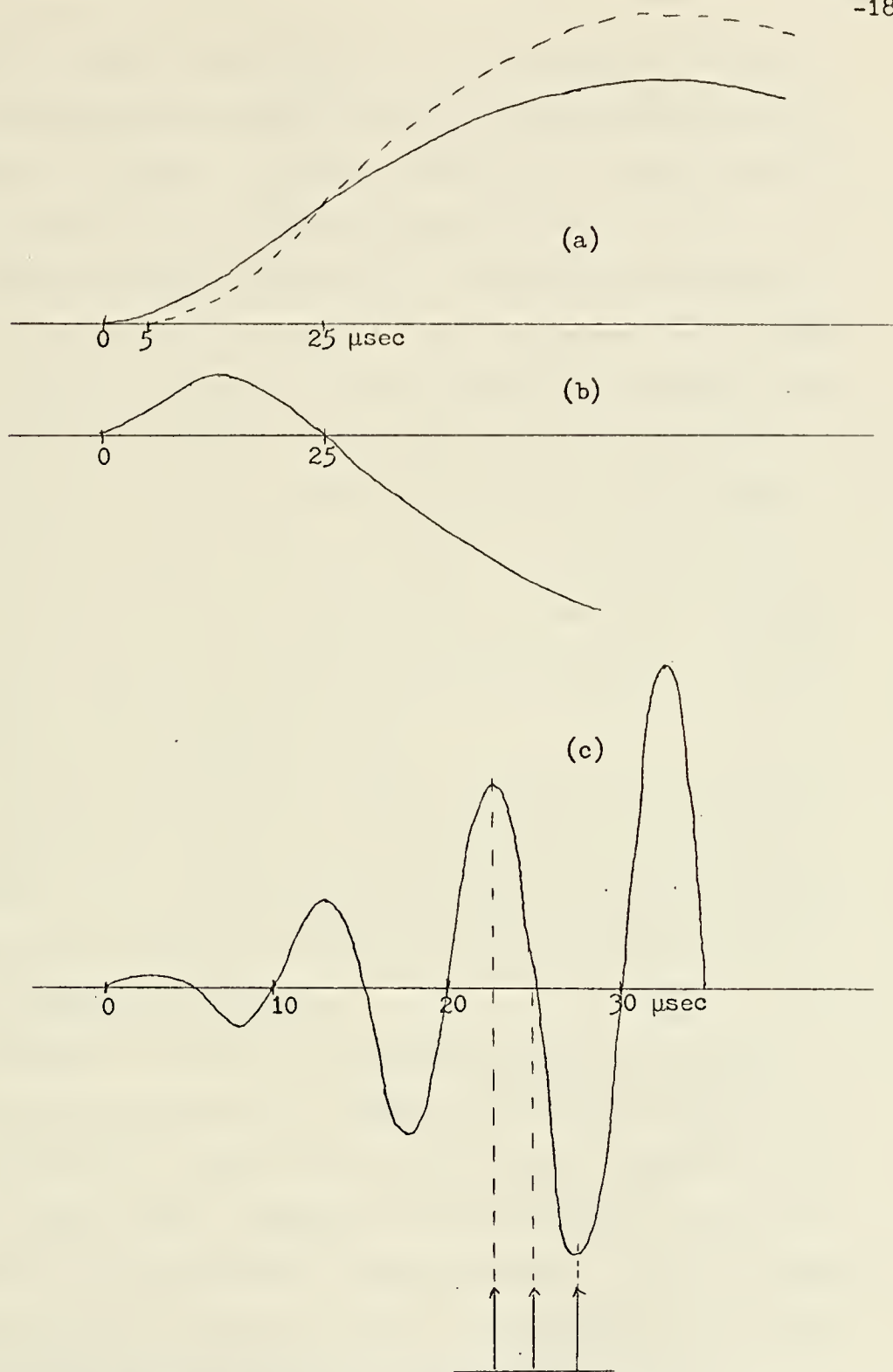


Figure 1-7 Envelope Deriver and RF Samplers



attempted to identify some point on the leading edge of the pulse. Since this point must be within the first 30 microseconds after the beginning of the pulse, it is clear that this is a severe constraint on a pulse which has an effective bandwidth of only 10 kHz.

A typical technique employed is to process the pulse envelope so as to produce a zero crossing at the 25 microsecond point. This is accomplished by delaying the received signal 5 microseconds and scaling it to produce what is represented by the dashed line in figure 1-7(a). This is then subtracted from the original signal - the solid line in figure 1-7(a) to produce the derived envelope of figure 1-7(b). The zero crossing is then detected and sampling strobes are centered at the estimated 25 microsecond point of the rf signal as shown in figure 1-7(c).

With the strobes located as shown, the middle one will obtain a zero sample value while the other two will obtain values with a known ratio. If the strobes were not centered properly, different values would be obtained, producing an error signal which can be used to reposition the strobes.

In practice, of course, the signals are noisy so that both steps in the procedure must be accomplished via measurements on a number of pulses - as many as 64 or 128 or more - depending on the signal to noise ratio. Typically, the most difficult step in the procedure is the envelope zero crossing deriving. The zero crossing measurement must be accurate to within 5 microseconds or the fine tune measurement that follows will be made on the wrong cycle of the carrier. In this regard, a final characteristic of the signals





should be presented.

The propagation paths involved do constitute dispersive media so that the signals received are not quite identical to those transmitted. The distortion in the shape of the envelope is slight - so much so that even though there are different propagation paths involved, the skywaves may be modelled as perfect echoes of the groundwave. The major effect of the propagation paths is the introduction of a phase shift of the pulse envelope relative to the carrier.

In effect, the envelope and carrier propagate at different velocities. Since the final time difference measurement is based on the carrier times, the carrier propagation times are calibrated for measuring distances. While the phase shift, for the groundwave, is typically not enough, by itself, to cause a cycle ambiguity in the detection, it does require that the envelope derivation have accuracy somewhat better than 5 microseconds.

With the preceding as background, some aspects of system performance can be presented. Inaccuracies can be introduced by any number of sources in the system. These can be loosely grouped into a few categories and statistically described. Receiver error will have a standard deviation of from 20 to 100 nanoseconds depending on the degree of sophistication. Chain synchronization includes the results of many effects and may be described as introducing an error with a standard deviation of about 50 nanoseconds. Noise induced errors can have a standard deviation of from about 20 nanoseconds for 0 db SNR to about 250 nanoseconds for -20 db SNR. The implications of these times can be seen from an example. If a total



error of about 100 nanoseconds is present, this corresponds, via a speed of propagation conversion, to a distance error of about 30 meters.

The numbers presented above for the error statistics were purposely given without mention of important descriptive parameters. For example, a figure for the error caused by atmospheric noise is completely meaningless without a detailed description of the particular receiver detection procedure - particularly the sample averaging or integration time involved (50 seconds in the case of the above figures). The geometry of the chain and the receiver position must also be specified: the fix obtained from lines of position intersecting at right angles can be expected to have an error almost an order of magnitude smaller than if the lines were nearly asymptotic and at extreme ranges. Without going into great detail, the performance can be simply summarized.

1. Position errors vary from a few tens of meters to not more than about 200 meters within the coverage region.
2. The only hyperbolic navigation systems that are competitive in performance have a coverage range limit of less than 200 miles. Loran-C has a nominal coverage range of about 1000 miles.
3. The receiver generally contributes the smallest percentage of the total error.

In spite of the third property, improved receiver performance is constantly strived for since it indirectly effects many of the other sources of error. Chain synchronization is a single example of



such a source. Transmission timing is controlled by passive Cesium Beam frequency standards located at each station. As precise as these may be, there will be, over a period of time, relative phase drifts between the stations of a chain. These phase drifts are observed by monitoring stations which use the most sophisticated receivers and periodic corrections are ordered to maintain synchronization to within 100 nanoseconds. Clearly, if more sensitive receivers were available, this monitoring process could be made more responsive to oscillator phase discrepancies.

Speculation on means of achieving improved processing schemes is tempting and many faceted. One aspect to be considered is that an optimum receiver need not totally restrict the measurements to be made in the portion of the groundwave that is perfectly free from skywave contamination. If, for example, the sampling strobes are centered at the 30 microsecond point rather than at the 25 microsecond point, the signal to atmospheric noise ratio would be improved. In such a case, it might result that the third strobe would be sampling a signal contaminated by a skywave. In many cases however, the skywave would be of such a low power level at the sampling point that the increase in total noise power - atmospheric noise plus skywave interference - is more than offset by the increase in signal power. The implementation of the resulting adaptive time filter would require the knowledge of skywave relative magnitude and arrival time so that a decision could be made whether or not to re-position the sampling points.

A less optimal, but still improved, receiver would make





measurements on the skywave free portion of the signal - but at later times in the many cases in which skywave arrival times are much more than 30 microseconds after the beginning of the groundwave. In this case, the receiver requires only the knowledge of the skywave arrival time. More ambitious attempts have been made to implement a total power receiver. In this receiver, an attempt is made to digitally implement a scheme to measure skywave arrival times, magnitudes and phases, and then to subtract them from the received signal thereby greatly increasing the signal to noise ratio.

Another improvement that can be thought of would be allowed by a receiver capable of making precise measurements on the envelope of the groundwave. This would overcome the problems introduced by the different propagation speeds which might cause cycle ambiguity in the measurement. Even if a measurement based on the envelope might not have quite the precision of the rf measurement and therefore not be of use in a navigation receiver, it would be useful in calibrating regions in which the envelope - carrier phase shift is significant.

The investigation of an alternate method of accomplishing some of these goals is the subject of this report. The method - homomorphic deconvolution - will now be presented.

## 1.2 Homomorphic Deconvolution

In 1965, A.V. Oppenheim presented a theory of generalized superposition which could be applied to certain classes of non-linear systems.<sup>2</sup> A simplified description of the theory can be given via





an example. Consider processing a signal consisting of two or more components which have been combined in some non-linear fashion. By means of certain elementary operations, it may be possible to transform the non-linear combining operation into a linear one. If the components, when so transformed, show a certain distinctiveness, it may be possible to process them by conventional linear techniques. One of the components can be enhanced relative to the others, or the components can be separated. If the inverse transformation can be realized, the recovered signal has been obtained by what is referred to as generalized linear filtering.

The theory has been implemented with some success in what may be called multiplicative systems. If  $x$ , the signal to be processed, consists of components  $x_1$  and  $x_2$  combined as in:  $x = x_1^\alpha \cdot x_2^\beta$ , then the transformation employed might be the logarithm function (real or complex). What then results is,

$$\log x = \alpha \cdot \log x_1 + \beta \cdot \log x_2$$

so that the modified components,  $\log x_1$  and  $\log x_2$ , have been combined in the ordinary linear sense. Whether or not anything has been gained, as well as the form of the processing to follow, depends upon certain properties of  $x_1$  and  $x_2$ . Another class of systems to which the theory has been applied may be called convolutional.

If  $x$ , the signal to be processed, consists of components  $x_1$  and  $x_2$  which are combined by a convolution, denoted  $x = x_1 * x_2$ , the generalized linear filtering technique may be effective. The transformation might consist of, first, the evaluation of the Fourier Transform since it maps a convolution to a multiplication:



$$F[x] = F[x_1] \cdot F[x_2]$$

As before, this can now be followed by a logarithm function evaluation.

Here, the logarithm must, in general, be complex. What results is,

$$\log F[x] = \log F[x_1] + \log F[x_2]$$

Again, whether or not anything has been gained depends on the properties of  $x_1$  and  $x_2$ . Schafer<sup>4</sup> has examined a specific class of signals in which the  $x_1$  and  $x_2$  exhibit favorable properties. His presentation is closely followed herein. The signals may be described as echoed, i.e., of the form

$$(1.1) \quad x(t) = \sum_{i=0}^k a_i s(t-T_i)$$

Such a signal consists of a basic waveform with scaled, delayed versions of the same waveform superimposed. This is a reasonably approximate description of multipath signals which can arise in many applications. The components  $x_1$  and  $x_2$  are identified by re-writing equation (1.1) as a convolution of the basic waveform and an impulse train,

$$(1.2) \quad \begin{aligned} x(t) &= x_1(t) * x_2(t) \\ x_1(t) &= s(t) \\ x_2(t) &= \sum_{i=0}^k a_i \delta(t-T_i) \end{aligned}$$

where  $\delta(\cdot)$  represents the Dirac delta function

The important aspect of the identification made in equation (1.2)



is that  $\log F[x_1]$  is a slowly varying function of frequency while  $\log F[x_2]$  is, in many cases, a rapidly varying function. Consequently, the inverse Fourier Transforms of  $\log F[x_1]$  and  $\log F[x_2]$  are, in many cases, somewhat disjoint. A more important property is that  $F^{-1}[\log F[x_2]]$  is also an impulse train. Hence, by use of the operation  $F^{-1}[\log F[x]]$ , the convolved components are transformed to added components which exhibit properties that may make separation possible.

A similar operation was described by Bogert, Healy and Tukey<sup>5</sup> in which the power spectrum of the log of the power spectrum of the convolved signals was used. The result was called the cepstrum of the signal, denoted  $\hat{x}$ ,

$$\hat{x} = \left| F^{-1} \left[ \log |F[x]| \right] \right|$$

Many properties of both operations are similar. In particular, the impulse train is mapped to another impulse train in both methods. A major difference is that, with the cepstrum, the loss of the phase information precludes any inverse transformation. Although filtering and recovery are not possible, some parameters of the signal are measurable in the cepstrum so that the technique finds many applications. Due to the similarities involved, the transformation which retains the phase information has come to be known as the complex cepstrum while the other is sometimes referred to as the power cepstrum to maintain the distinction.

On the subject of terminology; it becomes awkward to speak of "rapidly varying functions of frequency," as above, when the



temptation is to say "high frequency components - in the frequency domain." In this regard, some phrases have been developed in the literature of this subject and will be used to avoid confusion. In this thesis, the term power cepstrum will be used to refer to the transformation of Bogert et al. The transformation developed by Schafer will be referred to as the complex cepstrum, or as simply the cepstrum. The cepstrum will be considered to be a function of quefrequency. Thus, if the complex logarithm of the Fourier Transform of a signal has a component which is a rapidly varying function of frequency, it has a high quefrequency component. Filtering operations on the cepstrum will be referred to as short pass (analogous to low pass but in the quefrequency domain), long pass (analogous to high pass), and comb (the usual - but in the quefrequency domain) operations.

With the advances in technology leading to high speed digital computation and fast A/D conversion, and, with the development of the Cooley-Tukey algorithm, realization of the various mathematical operations called for by the technique has become increasingly practical. Since the implementation is via digital computer, the theory has been developed in terms of sampled data versions of the convolved signals. An in-depth presentation of the theory is contained in Schafer<sup>4</sup> and only the relevant portions will be related herein. A brief overview of transform theory for sampled data signals is called for before the specifics are presented.

A continuous - time signal,  $f(t)$ , may be sampled every  $DT$  time units to produce a sequence,  $f(n) = f(n \cdot DT)$ . Such a sequence has a Z - Transform defined as,







$$F(z) = \sum_{n=-\infty}^{\infty} f(n) z^{-n}$$

The inverse operation is accomplished via:

$$f(n) = \frac{1}{2\pi j} \oint_C F(z) z^{n-1} dz$$

where C is some closed contour in the region of convergence of F(z)

By this operation, f(n), a function of a discrete variable is transformed into a function of a continuous complex variable. The Fourier Transform of a discrete sequence is defined as the Z-Transform evaluated around the unit circle in the z - plane,

$$F(e^{j\omega}) = \sum_{n=-\infty}^{\infty} f(n) e^{-j\omega n}$$

The inverse operation is,

$$f(n) = \frac{1}{2\pi} \int_{-\pi}^{\pi} F(e^{j\omega}) e^{j\omega n} d\omega$$

Both the Z-Transform and the Fourier Transform will be referred to in the development of the report since they allow easily accomplished evaluations of results. Neither, however, can be directly realized by a digital computer since they are functions of continuous variables. What is utilized is the so-called Discrete Fourier Transform (DFT) which is the Z-Transform evaluated at equally spaced points around the unit circle in the z - plane,

$$F(k) = \sum_{n=0}^{N-1} f(n) e^{-j \frac{2\pi kn}{N}}$$



and the associated inverse is

$$f(n) = \frac{1}{N} \sum_{k=0}^{N-1} F(k) e^{\frac{j2\pi kn}{N}}$$

All of these transforms may suffer from shortcomings referred to as aliasing and leakage. Additionally, the DFT is accompanied by the so-called picket fence effect. These effects and means of counter-acting them are developed by Cooley et al <sup>6</sup>, and will be discussed in this report only when they present problems. The DFT is evaluated via the Cooley-Tukey algorithm, or the Fast Fourier Transform (FFT).

In the case of interest, the Z-Transform of the sampled composite signal is,

$$X(z) = X_1(z) \cdot X_2(z)$$

The logarithm is taken to obtain,

$$\hat{X}(z) = \log X(z) = \log X_1(z) + \log X_2(z)$$

The complex cepstrum,  $\hat{x}(n)$ , is to be,

$$\hat{x}(n) = Z^{-1} \left[ \hat{X}(z) \right] = \frac{1}{2\pi j} \oint_C \hat{X}(z) z^{n-1} dz$$

Here the complex logarithm presents a problem since it branches at values of  $z$  for which  $\text{ARG } X(z) = \pm\pi$ . When this happens,  $\hat{X}(z)$  has a discontinuous imaginary part and is therefore not analytic. Since the cepstrum will be computed via the DFT, it is required that  $\text{ARG } X(z)$  be continuous for values of  $z$  along the unit circle. The problem is overcome via a so-called phase unwrapping technique which



identifies the proper branch of the arctangent function defining the phase. This technique is described in Appendix B.

More specifics of the computation will be presented in subsequent chapters. The important aspects of the technique can be summarized:

1. Convolutions are mapped to additions.
2. The mapping is continuous; the inverse mapping exists and is continuous - hence the term homomorphic deconvolution.
3. Deconvolution is accomplished via a subtraction (if it is known what to subtract).
4. The components of the original signal, in some cases, become somewhat distinctive in the complex cepstrum so that they may be identified and separated.

The technique has found many applications since it can deconvolve signals when the components are unknown. It is merely necessary that the signal be reasonably echoed in nature with reasonably spaced echo arrival times. The basic waveform, either as it is or with minor processing, will have a low quefrency nature and decrease in magnitude at least as fast as  $1/n$  in the cepstrum. The impulse train can be made to have its lowest quefrency component displaced from the zero quefrency line by a value corresponding to the first echo arrival time. In cases of large echo times, the echoes can be removed by a simple short pass or more involved comb filter. Conversely, the basic waveform can be removed and the impulse train recovered by use of a long pass filter. This approach is applied in cases in which the multipath response,  $x_2$ , is not strictly impulsive and it



is desired to see precisely what it is. In such a fashion, properties of the paths involved can be measured.

Some applications of the technique have been to speech processing by Schafer, Oppenheim and Stockham<sup>3</sup>, to seismology, where it is desired to recover and measure  $x_2$ , by Ulrich<sup>7</sup>, and to processing of measured brain waves evoked by visual stimuli by Senmoto and Childers<sup>8</sup>.

In this last application, the data is available via an electroencephalogram. There is some degree of control in that the echoed signal measured represents the composite response of the brain to a pulse-like visual stimulus. The stimulus can be re-applied, at fixed intervals, over a pulse repetition interval. A somewhat involved technique is used to average the responses obtained over a repetition interval so that improved signal to noise ratio is obtained before computing the cepstrum.

The similarities between this application and the Loran-C case lead to speculation on signal to noise ratio improvement which will be discussed in Chapter 6. Considerations such as the effects of interference, atmospheric noise, and signal stability must be taken into account. Before these are considered however, more specifics of the problem must be developed.





## Chapter 2

### PROBLEM FORMULATION

In order to apply the homomorphic deconvolution technique, a model of the Loran-C signal as described in Chapter 1 must be developed. From this model the signal processing tasks can be identified so that an appropriate solution scheme results. To this end, the waveform to be processed will be considered to be obtained from one pulse duration of the received signal, represented as follows:

$$(2.1) \quad F(t) = n(t) + \sum_{i=0}^k A_i s_i(t) \sin \left[ \omega_c (t - T_i) - \theta_i \right]$$

In equation (2.1), the zero subscripts identify parameters to be associated with the received groundwave. The subscripts 1 through  $k$  identify parameters of the first through  $k^{\text{th}}$  skywaves respectively.  $s_i(\cdot)$  denotes the normalized pulse envelope of the  $i^{\text{th}}$  component of the composite signal. The  $T_i$ 's and  $A_i$ 's refer to the envelope arrival times and magnitudes, respectively.  $\theta_i$  represents the phase shift between the envelope and the carrier of the  $i^{\text{th}}$  component.

With a known carrier frequency, an equivalent method of specifying the signal is by use of the complex envelope representation as in equation (2.2).

$$(2.2) \quad \hat{f}^*(t) = \hat{n}^*(t) + \sum_{i=0}^k A_i \exp \left[ j \left[ \omega_c T_i + \theta_i \right] \right] s_i(t)$$



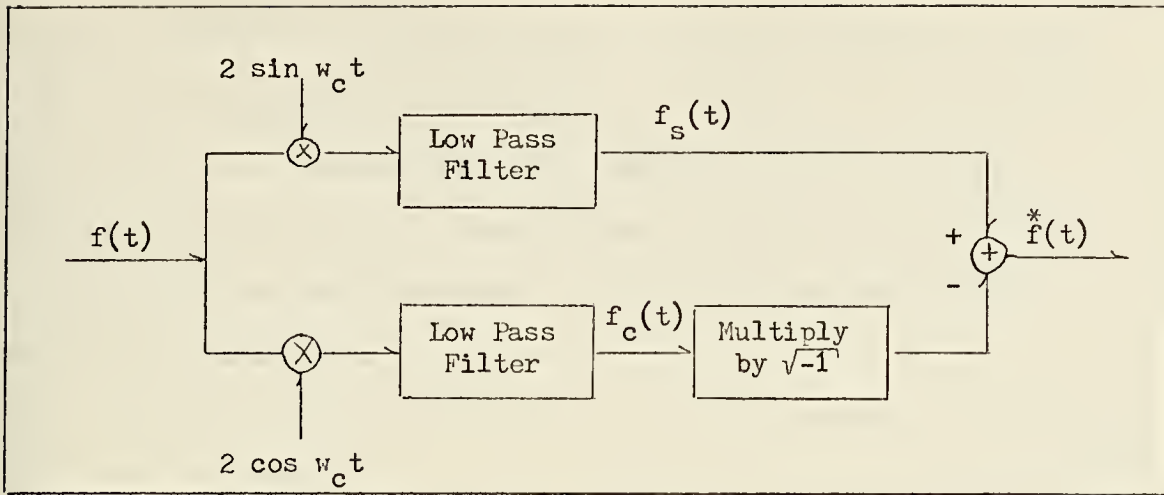


Figure 2-1 Generation of Complex Envelope

A common method of describing how the complex envelope is obtained is shown in figure 2-1. An analysis of the signal flow in the figure shows that,

$$f_c(t) = n(t) \cos w_c t - \sum_{i=0}^k A_i s_i(t) \sin [w_c T_i + \theta_i]$$

and,

$$f_s(t) = n(t) \sin w_c t + \sum_{i=0}^k A_i s_i(t) \cos [w_c T_i + \theta_i]$$

If the following definitions are made:

$$\tilde{n}(t) = n(t) \sin w_c t - j n(t) \cos w_c t$$

and

$$\tilde{f}(t) = f_s(t) - j f_c(t)$$

it follows that,

$$(2.3) \quad \tilde{f}(t) = \tilde{n}(t) + \sum_{i=0}^k A_i \exp \left[ j [w_c T_i + \theta_i] \right] s_i(t)$$



which is identical to equation (2.2). Clearly, the complex envelope representation for continuous signals is no more than a mathematical convenience. In a sampled data form however, it can be actually implemented and provides a compact means of handling the quadrature components of the baseband signal. The realization method is as depicted in figure 2-2.

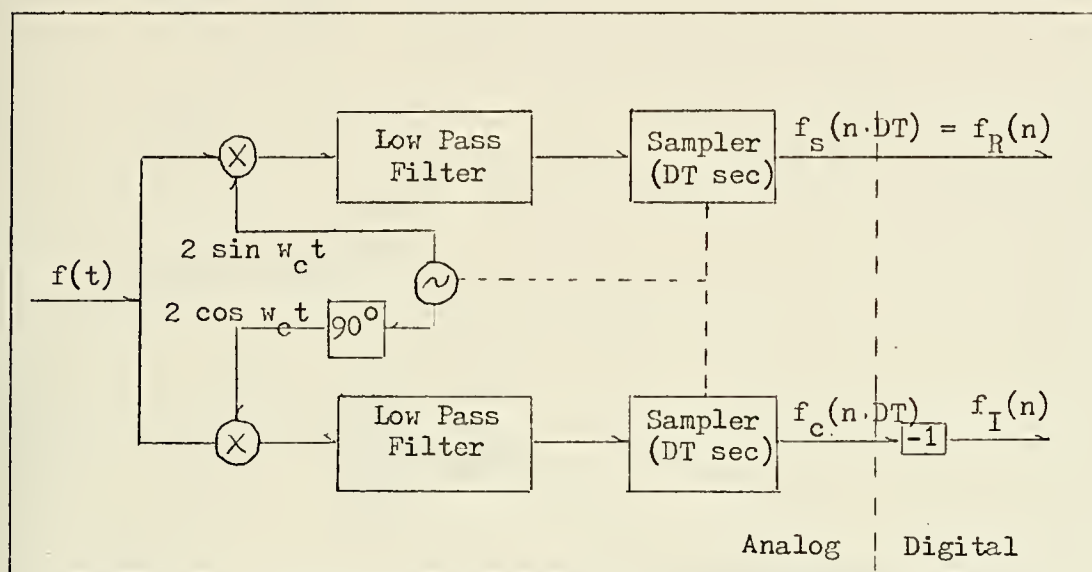


Figure 2-2 Realization of Sampled Complex Envelope

The component  $f_s(t)$  is sampled and stored in the real part of the sample word while  $f_c(t)$  is sampled, complemented, and stored in the imaginary part. What results is a sequence of the following form,

$$f(n) = s(n) + \sum_{i=0}^k A_i \exp \left[ j \left[ w_c T_i + \theta_i \right] \right] s_i(n)$$

For the remainder of the presentation in this chapter, the signal will be considered to be noise free. The theory of noisy signals is developed in Chapter 5. Consequently, the signal of interest is,



$$f(t) = \sum_{i=0}^k A_i \exp \left[ j \left[ w_c T_i + \theta_i \right] \right] s_i(t)$$

For notational convenience, and without loss of generality, the magnitudes will be normalized with respect to  $A_0$  and the phase notation will be simplified:

$$A'_i = \frac{A_i}{A_0}, \quad i = 0, 1, \dots, k$$

$$\phi_i = w_c T_i + \theta_i$$

$$B_i = A'_i e^{j\phi_i}$$

Hence,

$$(2.4) \quad f(t) = \sum_{i=0}^k B_i s_i(t)$$

In Chapter 4, distorted signals will be considered. Until then, it will be assumed that  $s_i(t) = s(t-T_i)$ . In this case, equation (2.4) becomes

$$f(t) = \sum_{i=0}^k B_i s(t-T_i)$$

This is the form of signals for which the homomorphic deconvolution technique has been developed. Additionally, it is possible to identify the tasks to be performed at this point. As presented in Chapter 1, it is desirable to measure  $\phi_0$ , the groundwave parameter from which time measurements are made, and  $T_0$ , to measure the difference in propagation speeds of the envelope and carrier. Additionally,





measurements of  $T_1$  and  $B_1$  would be helpful. Finally, measurements of all  $\phi_i$ 's,  $T_i$ 's, and  $|B_i|$ 's would be desirable since a total power receiver might then be feasible.

With the problem thus defined, solution techniques can be considered. To begin, consider the following to be a reasonable approximation to the received Loran-C pulse envelope:

$$s(t) = t^2 e^{-\alpha t} u_{-1}(t) \quad ; \quad \alpha = \left(\frac{2}{65}\right) \times 10^6 \text{ sec}^{-1}$$

where  $u_{-1}(t)$  is the Heaviside unit step function

Initially, make the following assumptions:

$$\phi_0 = 0$$

$$T_1 = n_i \cdot DT$$

$$n_i = \text{an integer}$$

$$DT = \text{the sampling time}$$

The sampled waveform in this case is:

$$f(n) = \sum_{i=0}^k B_i s(n-n_i) = s(n) \otimes \sum_{i=0}^k B_i \delta(n-n_i)$$

where  $\otimes$  denotes a discrete convolution and  $\delta(n-n_i)$  is a unit sample:

$$\delta(n-n_i) = \begin{bmatrix} 1 & n = n_i \\ 0 & n \neq n_i \end{bmatrix}$$



Therefore,

$$f(n) = s(n) \otimes p(n)$$

where

$$p(n) = \sum_{i=0}^k B_i \delta(n-n_i)$$

In the case of  $k = 1$ , i.e., in the case of a signal consisting of the groundwave and one skywave,

$$p(n) = \delta(n) + B_1 \delta(n-n_1)$$

If  $|B_1| < 1$ , the complex cepstrum of  $p(n)$  is (see Appendix A for the details of the computation):

$$\hat{p}(n) = \sum_{m=1}^{\infty} (-1)^{m+1} \frac{B_1^m}{m} \delta(n-mn_1)$$

whereas the cepstrum of  $s(n)$  is,

$$(2.5) \quad \hat{s}(n) = -\alpha \delta(n) + \sum_{m=1}^{\infty} \frac{3 + (-1)^{m+1}}{m} e^{-\alpha m} \delta(n-m)$$

Since the complex cepstrum operation has the property of mapping convolutions in the time domain to additions in the frequency domain, the composite cepstrum consists of  $\hat{s}(n) + \hat{p}(n)$ . In this case, a simple estimator can be made to scan the cepstrum sequence and determine  $n_1$  from the location of the components of the impulse train. A simple comb filter could then be employed to remove all traces of the echo from the cepstrum - only slightly affecting the component due to  $s(n)$ . Before filtering  $\hat{p}(n)$ , an estimate of  $|B_1|$  and  $\phi_1$  could be made from the components of the impulse train. In such a manner, estimates of  $T_1$ ,  $|B_1|$ , and  $\phi_1$  are obtained and all skywave contamination is removed.



When  $T_1$  is not an integer number of sampling times greater than  $T_0$ ,  $\hat{p}(n)$  no longer has such a simple form. The components of the impulse train become  $\frac{\sin x}{x}$  terms which spread throughout the cepstrum sequence as in equation (2.6) (See Appendix A).

$$(2.6) \quad \hat{p}(n) = \sum_{m=1}^{\infty} (-1)^{m+1} \frac{B_1^m}{m} \frac{\sin \left[ \pi [n-m(n_1+\Delta_1)] \right]}{\pi [n-m(n_1+\Delta_1)]}$$

where  $n_1 = \text{an integer}$

and  $T_1 = DT \cdot (n_1 + \Delta_1)$

$$- 0.5 < \Delta_1 < 0.5$$

In this case the filtering becomes less straightforward. A simple comb filter can not be effective. In the distortion free, noiseless case however, the cepstrum consists only of  $\hat{s}(n)$ , which is known, and  $\hat{p}(n)$ , which is known to within three parameters:  $B_1$ ,  $n_1$ , and  $\Delta_1$ , so that an estimator can be developed to identify  $\hat{p}(n)$ . When this identification is made, the deconvolution can be accomplished via a subtraction. The form of the estimator is developed in Chapter 3 and the effects of signal distortion and noise on its performance are presented in Chapters 4 and 5.

The problem is further complicated when  $T_0$  is not an integer multiple of the sampling time. In this case, the  $\hat{s}(n)$  of equation (2.5) has another term added to it, (Appendix A)

$$(2.7) \quad \hat{s}'(n) = \begin{bmatrix} \hat{s}(n) + (-1)^{n+1} \frac{\Delta_0}{n} & ; & n \neq 0 \\ \hat{s}(n) & ; & n = 0 \end{bmatrix}$$



The presence of this new term makes the estimation procedure described above suspect. Now, there are two unknown components in the computed cepstrum. Since the forms of the components are known however, a modified estimator can still be effective.

A summary of the problem as formulated thus far can be made via figure 2-3. The received signal is processed to produce quadrature baseband components. These are sampled and digitally combined to produce the sampled complex envelope. The complex cepstrum is computed. From the cepstrum, signal parameters are estimated. One of the uses of the estimated parameters is shown: the groundwave phase estimate provides feedback to the local oscillator to permit phase tracking. An important aspect of this particular use is that it provides a method of comparing the performance of the homomorphic filter with other receiver techniques.





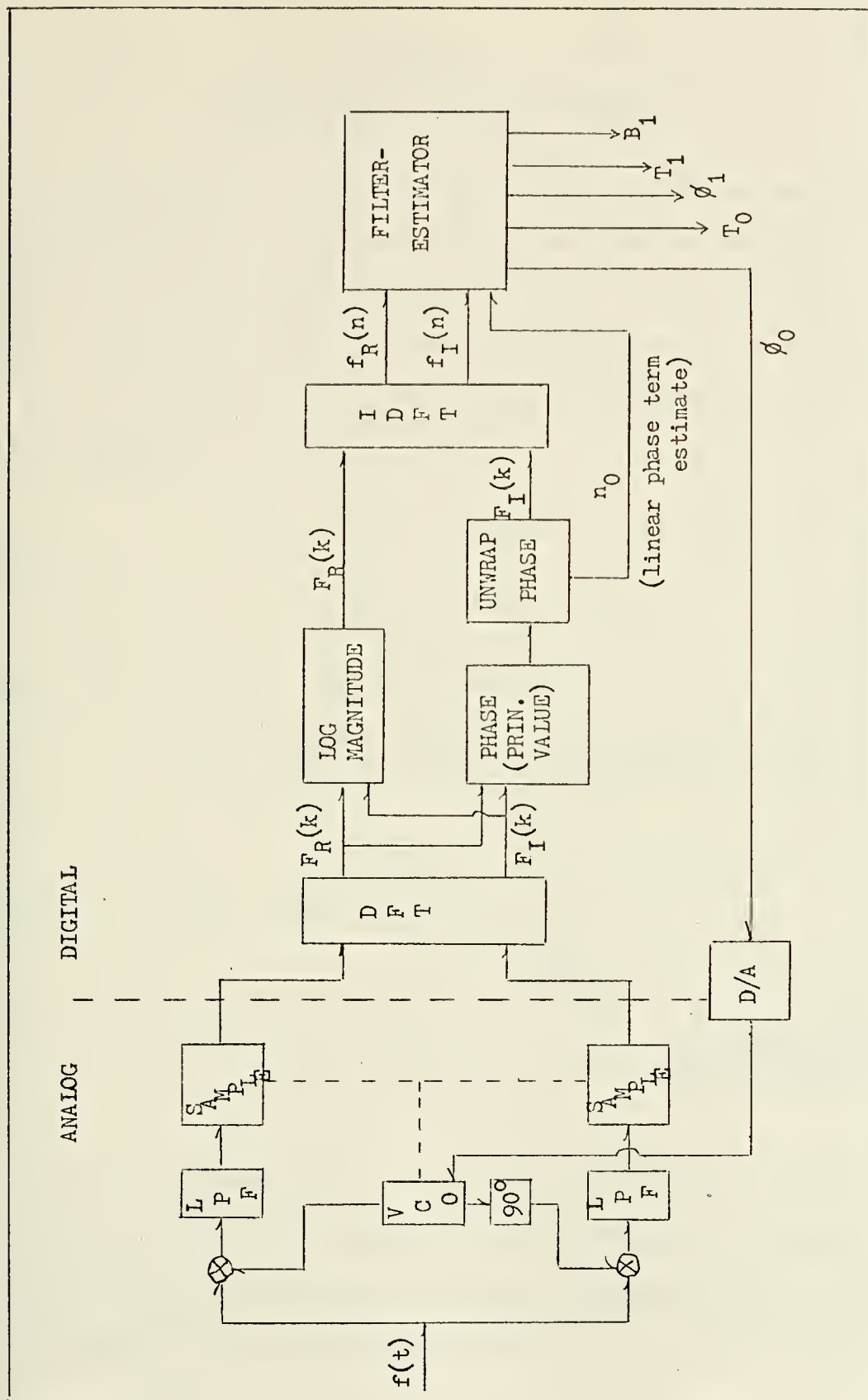


Figure 2-3 Homomorphic Filter Input-Output



## Chapter 3

## DECONVOLUTION OF NOISELESS SIGNALS

As developed in Chapter 2, it is desired to estimate waveform parameters from the cepstrum of the received signal so that the separation, or deconvolution, can be achieved. In the distortion free, noiseless case, the technique is as presented in this Chapter.

It is presumed that, with one skywave, the received signal will have a cepstrum of the following form:

$$\begin{aligned}
 \hat{f}(n) &= \hat{s}'(n) + \hat{p}(n) \\
 (3.1) \qquad &= \hat{s}(n) + \hat{g}(n) + \hat{p}(n)
 \end{aligned}$$

where, from equations (2.5), (2.6), and (2.7),

$$\begin{aligned}
 (a) \quad \hat{s}(n) &= -\alpha \delta(n) + \sum_{m=1}^{\infty} \frac{3 + (-1)^{m+1}}{m} e^{-\alpha m} \delta(n-m) \\
 (3.2) \quad (b) \quad \hat{g}(n) &= \begin{bmatrix} 0 & ; & n = 0 \\ (-1)^{n+1} \frac{\Delta_0}{n} & ; & n \neq 0 \end{bmatrix} \\
 (c) \quad \hat{p}(n) &= \sum_{m=1}^{\infty} (-1)^{m+1} \frac{B_1^m}{m} \frac{\sin \left[ \pi \left[ n-m(n_1+\Delta_1) \right] \right]}{\pi \left[ n-m(n_1+\Delta_1) \right]}
 \end{aligned}$$

In the estimation procedure it is desired to use the knowledge of the form of the above sequences in processing the received signal. Consequently, it will be necessary in the development to refer to the above sequences and corresponding components of the received signal



simultaneously. For clarity of presentation therefore, the notations  $s(n)$ ,  $g(n)$ ,  $p(n)$ , and  $f(n)$  will be used to refer to the predicted, or ideal, sequences as defined above whereas the received signal will be described as,

$$(3.3) \quad r(n) = s_a(n) \otimes g_a(n) \otimes p_a(n)$$

$$\text{or} \quad \hat{r}(n) = \hat{s}_a(n) + \hat{g}_a(n) + \hat{p}_a(n)$$

The subscript a signifies actual components of the signal as received. In the distortion free case, the only difference between the components of  $\hat{f}(n)$  in equation (3.2) and  $\hat{r}(n)$  in equation (3.3) is due to computation error.

A third set of sequences will also be referred to. Estimates of signal parameters  $\Delta_0$ ,  $\Delta_1$ ,  $n_1$ , and  $B_1$  will be made from the received signal. From these, estimated sequences will be generated. The estimated sequences will have the form of those in equation (3.2), but with parameters as estimated from the sequences of equation (3.3). Thus, the estimated sequence of  $\hat{g}(n)$  is:

$$\tilde{\hat{g}}(n) = \hat{g}(n) \Big|_{\Delta_0 = \tilde{\Delta}_0} = \begin{bmatrix} (-1)^{n+1} \frac{\tilde{\Delta}_0}{n} & ; & n \neq 0 \\ 0 & ; & n = 0 \end{bmatrix}$$

where  $\tilde{\Delta}_0$  is the estimate of  $\Delta_0$  obtained from  $r(n)$ .

### 3.1 Sequence of Estimation

The received signal consists of the terms  $\hat{s}_a(n)$ ,  $\hat{g}_a(n)$ , and  $\hat{p}_a(n)$  which are combined to produce the cepstrum sequence shown in figure 3-1.



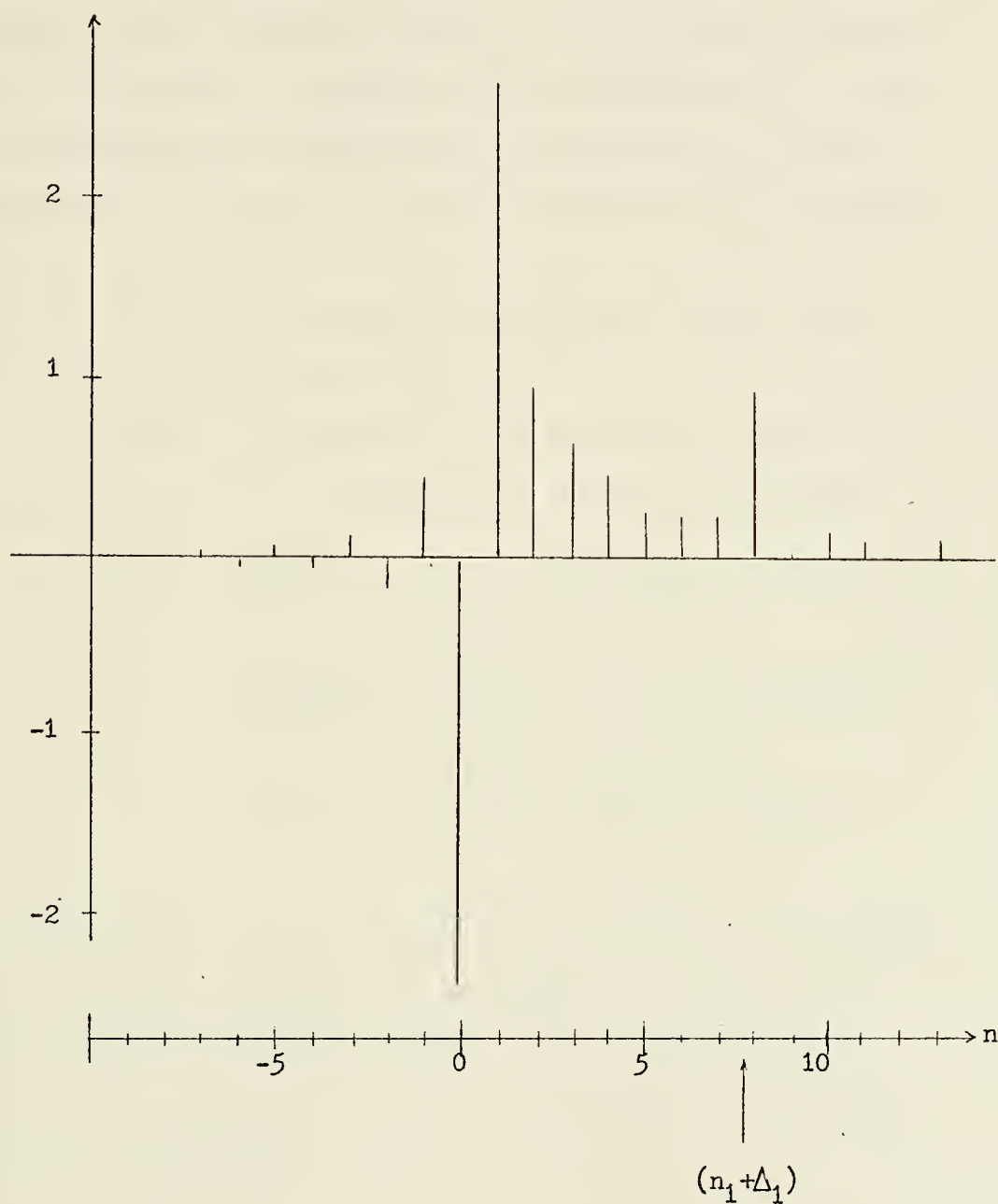


Figure 3-1 Cepstrum of Simulated Received Signal





It can be seen that there is insufficient separation between the sequences to allow for precise estimation of the various parameters directly. Consequently, the estimation is accomplished in a number of steps; systematically estimating the parameters one at a time. The procedure used herein is to make the estimates in the following order.

1.  $\tilde{\hat{s}}(n)$  - an estimate of the received signal basic waveform.
2.  $\tilde{\hat{g}}(n)$  - an estimate of the small linear phase term not removed before computing the cepstrum
3.  $\tilde{\hat{p}}(n)$  -
  - (a)  $\tilde{n}_1$  - a coarse measurement of the skywave arrival time
  - (b)  $\tilde{\Delta}_1$  - a precise measurement of the skywave arrival time
  - (c)  $\tilde{B}_1$  - skywave magnitude and phase

The procedure begins by utilizing the fact that a good a priori estimate of  $\hat{s}_a(n)$  is available, to wit:  $\hat{s}(n)$  of equation (3.2). Therefore the first estimate is  $\tilde{\hat{s}}(n) = \hat{s}(n)$ . This estimated sequence can be subtracted from the received cepstrum to generate a new sequence denoted  $\hat{x}(n)$ ,

$$\hat{x}(n) = \hat{r}(n) - \tilde{\hat{s}}(n) = \hat{g}_a(n) + \hat{p}_a(n) + \hat{c}_s(n)$$

where

$$\hat{c}_s(n) = \hat{s}_a(n) - \tilde{\hat{s}}(n)$$



In this chapter it can be assumed that this error sequence,  $\hat{\epsilon}_s(n)$ , is negligibly small. The procedure as thus far discussed was accomplished on a simulated received signal and the resulting  $\hat{x}(n)$  is shown in figure 3-2.

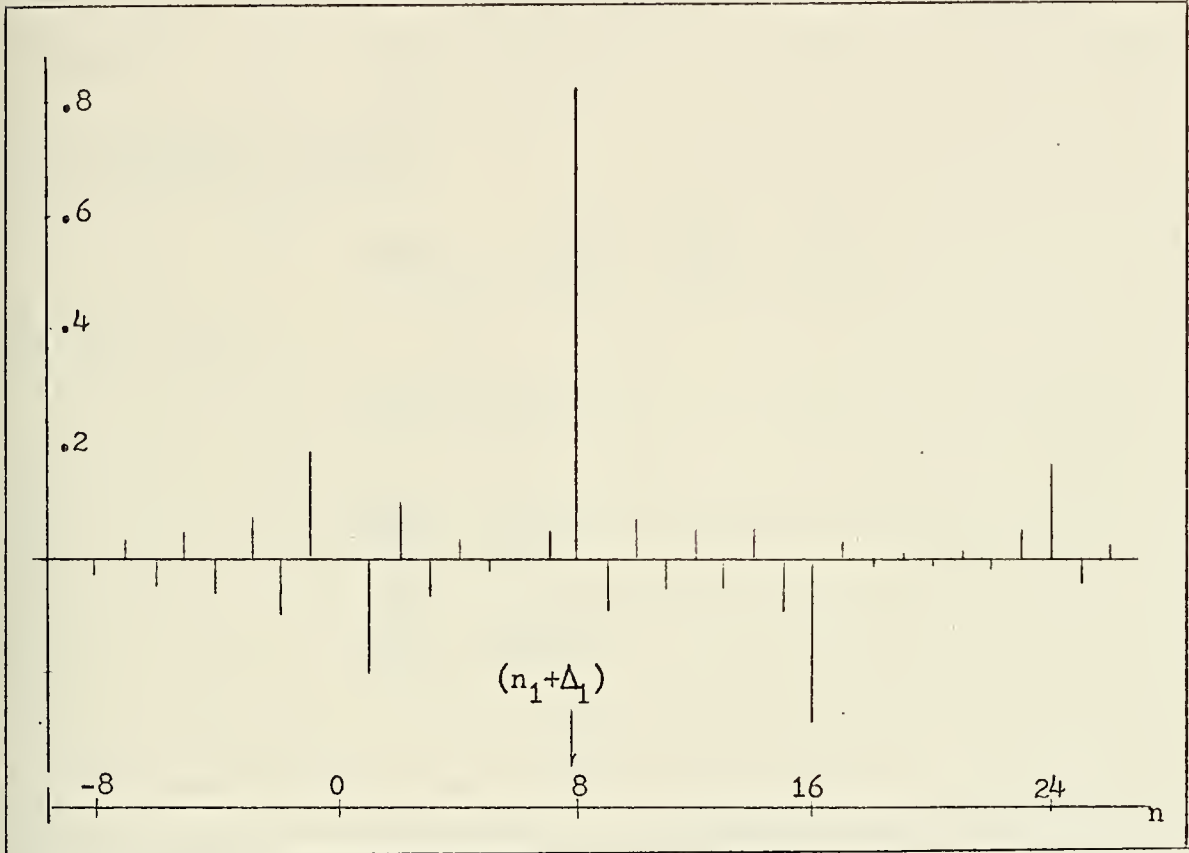


Figure 3-2 Simulated  $\hat{x}(n)$  Sequence

It can be seen that there is improvement over the situation shown in figure 3-1, but that the components of  $\hat{g}_a(n)$  and  $\hat{p}_a(n)$  still interfere so that the desired estimates are still not readily obtained. More precisely, it can be seen that for quefrency values greater than  $(n_1 + \Delta_1)$ , the various  $\frac{\sin x}{x}$  terms of  $\hat{p}_a(n)$  interfere with one another to some extent. For positive quefrencies less than  $(n_1 + \Delta_1)$ , there is



interference between  $\hat{g}_a(n)$  and the first  $\frac{\sin x}{x}$  term of  $\hat{p}_a(n)$ .

What makes the estimation possible is the fact that for small negative quefrencies,  $\hat{p}_a(n)$  is reduced enough so that it only slightly interferes with  $\hat{g}_a(n)$ . The next step in the procedure therefore will be to estimate  $\Delta_0$  from the negative quefreny portion of the cepstrum.

### 3.2 Estimation of $g_a(n)$

$$\text{Since} \quad \hat{g}(n) = (-1)^{n+1} \frac{\Delta_0}{n} ; \quad n < 0,$$

it follows that

$$\begin{aligned} \tilde{\Delta}_0 &= \hat{g}_a(-1) \\ -\frac{\tilde{\Delta}_0}{2} &= \hat{g}_a(-2) \\ \frac{\tilde{\Delta}_0}{3} &= \hat{g}_a(-3) \\ &\vdots \end{aligned}$$

where  $\tilde{\Delta}_0$  will be the estimate of  $\Delta_0$ . As described above, it is true that,

$$\begin{aligned} \hat{r}(-1) &= \hat{g}_a(-1) + \hat{p}_a(-1) + \hat{c}_s(-1) \approx \hat{g}_a(-1) \\ \hat{r}(-2) &= \hat{g}_a(-2) + \hat{p}_a(-2) + \hat{c}_s(-2) \approx \hat{g}_a(-2) \\ &\vdots \end{aligned}$$

since the  $\hat{p}_a(n)$  sequence is small for this range of quefrencies. The estimate of  $\Delta_0$  can therefore be obtained from,



$$(3.4) \quad \tilde{\Delta}_0 = \frac{\hat{r}(-1) - \hat{r}(-2) + \hat{r}(-3) - \hat{r}(-4)}{1 + \frac{1}{2} + \frac{1}{3} + \frac{1}{4}}$$

With  $\Delta_0$  so estimated, the sequence  $\tilde{\hat{g}}(n)$  can be generated and subtracted from  $\hat{x}(n)$  to produce the new sequence  $\hat{y}(n)$ :

$$\hat{y}(n) = \hat{x}(n) - \tilde{\hat{g}}(n)$$

where

$$\tilde{\hat{g}}(n) = \begin{cases} 0 & ; \quad n = 0 \\ (-1)^{n+1} \frac{\tilde{\Delta}_0}{n} & ; \quad n \neq 0 \end{cases}$$

The procedure was applied to the  $\hat{x}(n)$  in figure 3-2 to produce the  $\hat{y}(n)$  of figure 3-3.

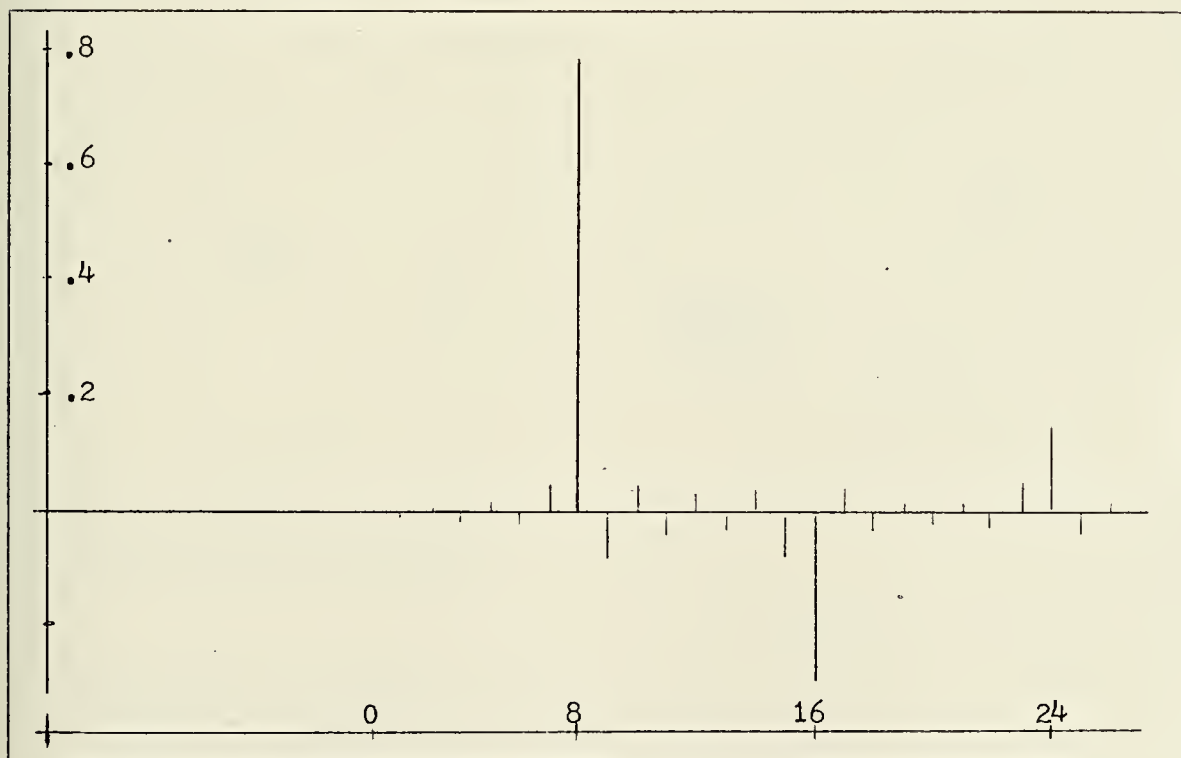


Figure 3-3 Simulated  $\hat{y}(n)$  Sequence





At this point in the procedure, since  $T_0 = DT (n_0 + \Delta_0)$ , the estimate of  $T_0$  can be made:

$$\tilde{T}_0 = DT (\tilde{n}_0 + \tilde{\Delta}_0)$$

where  $\tilde{n}_0$  is deduced in the phase unwrapping computation as described in Appendix C.

The reason for the particular estimator used in equation (3.4) can be seen from figure 3-4.

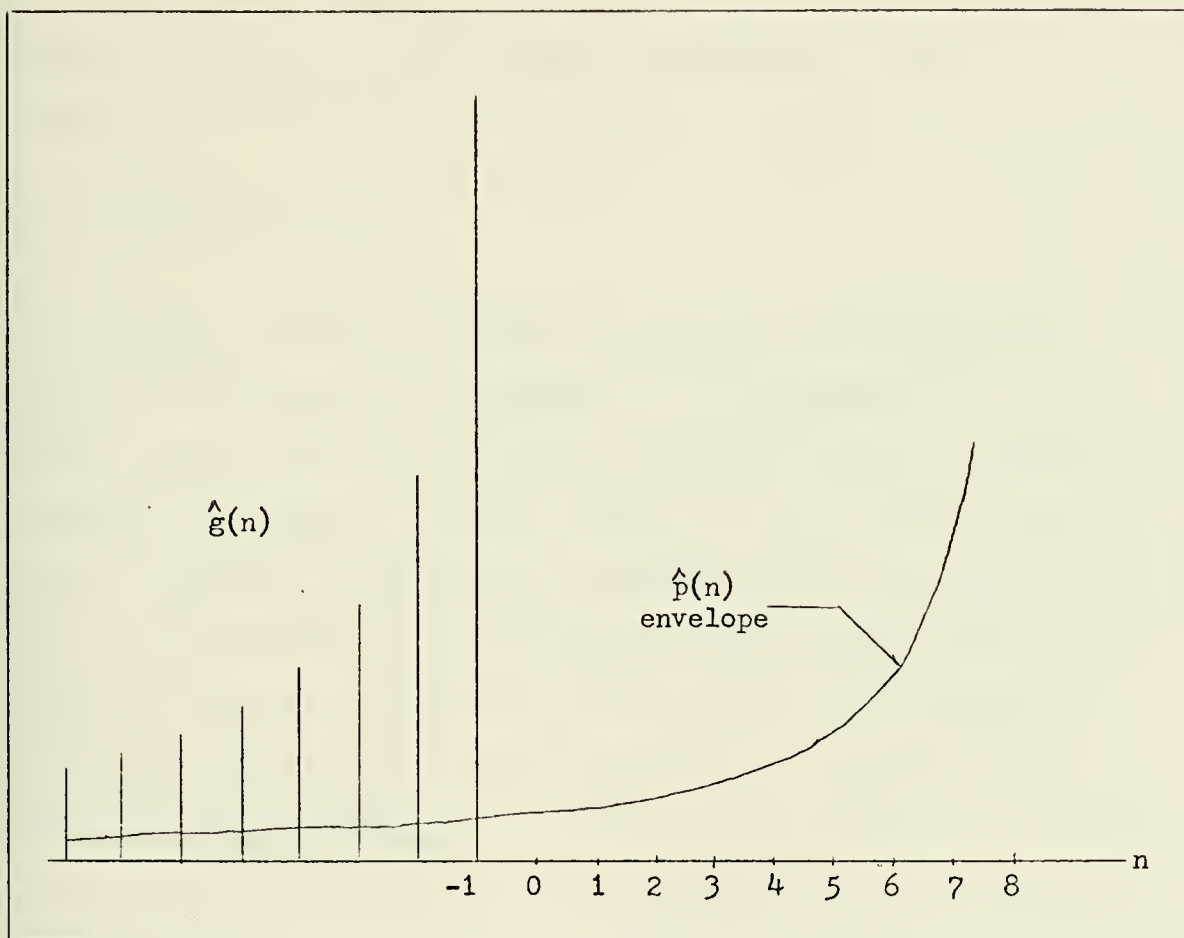


Figure 3-4 Comparison of  $\hat{g}(n)$  and  $\hat{p}(n)$



Both sequences  $\hat{g}_a(n)$  and  $\hat{p}_a(n)$  decrease essentially as fast as  $1/n$  for negative values of  $n$ . Near the zero quefrequency value, the  $\hat{g}_a(n)$  term clearly dominates the composite signal. As  $n$  becomes more negative however, the distinction between the two components is not as great. Consequently, only a few samples should be used to make the estimate and even among these few, the samples obtained from the more negative quefrequencies should be less heavily weighted. This is precisely what is accomplished in equation (3.4).

The next step in the procedure is to estimate the parameters of  $\hat{p}(n)$ , i.e.,  $\Delta_1$ ,  $n_1$ , and  $B_1$ , from the sequence  $\hat{y}(n)$ . This is accomplished in three steps, beginning with the estimation of  $n_1$ .

### 3.3 Estimation of $p_a(n)$

The values of  $\hat{y}(n)$  are examined for quefrequencies corresponding to times between about 30 microseconds and 60 microseconds. The largest value of  $\hat{y}(n)$  in this range of quefrequencies will be assumed to correspond to a sample in the main lobe of the first  $\frac{\sin x}{x}$  term in  $\hat{p}_a(n)$ . Consequently, the value of  $n$  at which this maximum occurs will be the estimate of  $n_1$ . The situation would typically be as depicted in figure 3-5. Since the values of  $\hat{y}(n)$  will, in general, be complex, the plot in the figure corresponds to either the real or imaginary part of  $\hat{y}(n)$ .



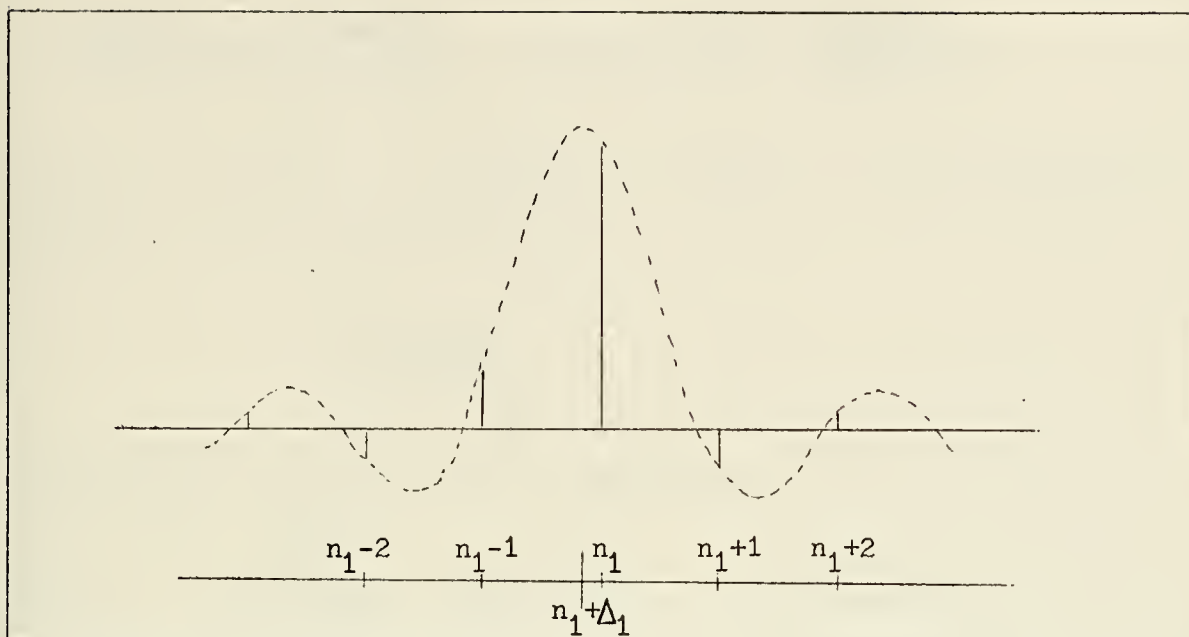


Figure 3-5 Expected Form of  $p_a(n)$

Once  $n_1$  is determined,  $B_1$  and  $\Delta_1$  can be estimated as follows. Consider the values of  $y(n)$  in the vicinity of  $n = n_1$  to be due only to the first  $\frac{\sin x}{x}$  function in the expansion of  $\hat{p}(n)$ . As an example of the validity of this assumption, consider the values of the first and second terms in the sum of equation (3.2b) for  $n = n_1$ :

$$\begin{aligned} \hat{p}(n_1) &= B_1 \frac{\sin \pi [n_1 - (n_1 + \Delta_1)]}{\pi [n_1 - (n_1 + \Delta_1)]} - \frac{B_1^2}{2} \frac{\sin \pi [n_1 - 2(n_1 + \Delta_1)]}{\pi [n_1 - 2(n_1 + \Delta_1)]} \\ &\quad + \dots \\ &= \frac{B_1 \sin \pi \Delta_1}{\Delta_1} - \frac{B_1^2 \sin \pi [(n_1 - 2\Delta_1)]}{2\pi \cdot (n_1 - 2\Delta_1)} + \dots \end{aligned}$$

The ratio of the magnitude of the second term to the magnitude of the first term will be,



$$\frac{|\Delta_1| |B_1|^2 |\sin 2\pi\Delta_1|}{2 |n_1 - 2\Delta_1| |B_1| |\sin \pi\Delta_1|} = \left| \frac{\Delta_1}{n_1 - 2\Delta_1} \right| |B_1| \left| \frac{\sin 2\pi\Delta_1}{2 \sin \pi\Delta_1} \right|$$

Exponential weighting , as described in Appendix A, ensures that  $|B_1|$  is less than 1. Additionally, the term

$$\left| \frac{\sin 2\pi\Delta_1}{2 \sin \pi\Delta_1} \right|$$

is less than 1 so that the ratio is less than

$$(3.5) \quad \frac{|\Delta_1|}{|n_1 - 2\Delta_1|} < \frac{1}{2 n_1 - 4\Delta_1} \quad , \quad \begin{array}{l} \text{for } n_1 > 1 \\ \text{since } |\Delta_1| < \frac{1}{2} \end{array}$$

Hence, for reasonably large values of  $n_1$ , the approximation is a good one and allows the following:

$$(3.6) \quad \begin{aligned} \hat{y}(n_1-2) &= \frac{B_1 \sin \pi [n_1 - 2 - (n_1 + \Delta_1)]}{\pi [n_1 - 2 - (n_1 + \Delta_1)]} = \frac{B_1 \sin \pi(2 + \Delta_1)}{\pi(2 + \Delta_1)} \\ \hat{y}(n_1-1) &= \frac{B_1 \sin \pi [n_1 - 1 - (n_1 + \Delta_1)]}{\pi [n_1 - 1 - (n_1 + \Delta_1)]} = \frac{B_1 \sin \pi(1 + \Delta_1)}{\pi(1 + \Delta_1)} \\ \hat{y}(n_1) &= \frac{B_1 \sin \pi [n_1 - (n_1 + \Delta_1)]}{\pi [n_1 - (n_1 + \Delta_1)]} = \frac{B_1 \sin \pi\Delta_1}{\Delta_1} \\ \hat{y}(n_1+1) &= \frac{B_1 \sin \pi [n_1 + 1 - (n_1 + \Delta_1)]}{\pi [n_1 + 1 - (n_1 + \Delta_1)]} = \frac{B_1 \sin \pi(1 + \Delta_1)}{\pi(1 + \Delta_1)} \\ \hat{y}(n_1+2) &= \frac{B_1 \sin \pi [n_1 + 2 - (n_1 + \Delta_1)]}{\pi [n_1 + 2 - (n_1 + \Delta_1)]} = \frac{B_1 \sin \pi(2 + \Delta_1)}{\pi(2 + \Delta_1)} \end{aligned}$$

The solution can proceed in two steps: estimate  $\Delta_1$ , then  $B_1$ . To





accomplish this, define the following variables:

$$\begin{aligned}
 d_1 &= \frac{\hat{y}(n_1-2)}{\hat{y}(n_1)} = \frac{\Delta_1}{2 + \Delta_1} \\
 d_2 &= \frac{\hat{y}(n_1-1)}{\hat{y}(n_1)} = \frac{-\Delta_1}{1 + \Delta_1} \\
 d_3 &= \frac{\hat{y}(n_1+1)}{\hat{y}(n_1)} = \frac{\Delta_1}{1 - \Delta_1} \\
 d_4 &= \frac{\hat{y}(n_1+2)}{\hat{y}(n_1)} = \frac{-\Delta_1}{2 - \Delta_1}
 \end{aligned}
 \tag{3.7}$$

It can be seen that four estimates of  $\Delta_1$  can be obtained from the  $d_i$ 's. The estimates obtained from  $d_2$  and  $d_3$  however, are made from values of  $\hat{y}(n)$  which are closer to, or in, the main lobe of the first  $\frac{\sin x}{x}$  term. They are therefore less sensitive to the effects of interference from other  $\frac{\sin x}{x}$  terms and the residuals of the  $\hat{g}_a(n)$  estimate than the estimates obtained from  $d_1$  and  $d_4$ . It is, however, desirable to base the estimate on as many measurements as possible so that a compromise would be to make a final estimate based on a weighted sum of the four individual estimates. The procedure is:

1. Compute the numbers  $d_1, d_2, d_3$ , and  $d_4$  as in equation (3.7)
2. Make four individual estimates as follows:

$$\begin{aligned}
 \tilde{\Delta}_{11} &= \frac{2d_1}{1 - d_1} \\
 \tilde{\Delta}_{12} &= \frac{-d_2}{1 + d_2}
 \end{aligned}$$



$$\tilde{\Delta}_{13} = \frac{d_3}{1 + d_3}$$

$$\tilde{\Delta}_{14} = \frac{-d_4}{1 - d_4}$$

where  $\tilde{\Delta}_{1k}$  denotes the estimate of  $\Delta_1$  based on the measurements which generated  $d_k$ .

3. Weight these estimates by the corresponding magnitudes of the measurements generating them and perform an appropriate scaling to arrive at the final estimate:

$$\tilde{\Delta}_1 = \frac{\sum_{k=1}^4 |d_k| \tilde{\Delta}_{1k}}{\sum_{k=1}^4 |d_k|}$$

When this estimate of  $\Delta_1$  is obtained, equation (3.6) can be re-applied to estimate  $B_1$ . To do this, make the following individual estimates.

$$\tilde{B}_{11} = \frac{\pi(2 + \tilde{\Delta}_1)}{\sin \pi(2 + \tilde{\Delta}_1)} \hat{y}(n_1-2)$$

$$\tilde{B}_{12} = \frac{\pi(1 + \tilde{\Delta}_1)}{\sin \pi(1 + \tilde{\Delta}_1)} \hat{y}(n_1-1)$$

$$\tilde{B}_{13} = \frac{\tilde{\Delta}_1}{\sin \pi \tilde{\Delta}_1} \hat{y}(n_1)$$

$$\tilde{B}_{14} = \frac{\pi(1 - \tilde{\Delta}_1)}{\sin \pi(1 - \tilde{\Delta}_1)} \hat{y}(n_1+1)$$

$$\tilde{B}_{15} = \frac{\pi(2 - \tilde{\Delta}_1)}{\sin \pi(2 - \tilde{\Delta}_1)} \hat{y}(n_1+2)$$



These are combined to produce the final estimate:

$$\tilde{B}_1 = \frac{\sum_{k=1}^5 |\hat{y}(n_1 + 3 - k)| \tilde{B}_{1k}}{\sum_{k=1}^5 |\hat{y}(n_1 + 3 - k)|}$$

With the estimates of  $n_1$ ,  $\Delta_1$ , and  $B_1$ , the estimated sequence  $\tilde{\hat{p}}(n)$  can be generated. This and  $\tilde{\hat{g}}(n)$  can be subtracted from the received signal cepstrum,  $\hat{r}(n)$ , to produce  $\tilde{\hat{s}}(n)$ . If the inverse DFT of  $\tilde{\hat{s}}(n)$  is computed, what would result would be an estimate of the complex log of the groundwave. From the zero frequency point in this sequence can be measured  $\phi_0$  - the phase of the groundwave.

If there are more than one skywaves present in the received waveform,  $\hat{p}_a(n)$  will have additional  $\frac{\sin x}{x}$  terms centered at quefrequencies of  $(n_2 + \Delta_2)$ ,  $2(n_2 + \Delta_2)$ , . . . ,  $(n_3 + \Delta_3)$  . . . , etc. and at various combinations of  $(n_1 + \Delta_1)$  and  $(n_2 + \Delta_2)$  as described in Appendix A. Once the terms due solely to the first skywave are removed however, the lowest quefrequency  $\frac{\sin x}{x}$  term that remains is due only to the second skywave so that the above estimation procedure can be re-applied to estimate  $n_2$ ,  $\Delta_2$ , and  $B_2$ . This can be done as often as necessary. The entire estimator can be described as in figure 3-6.



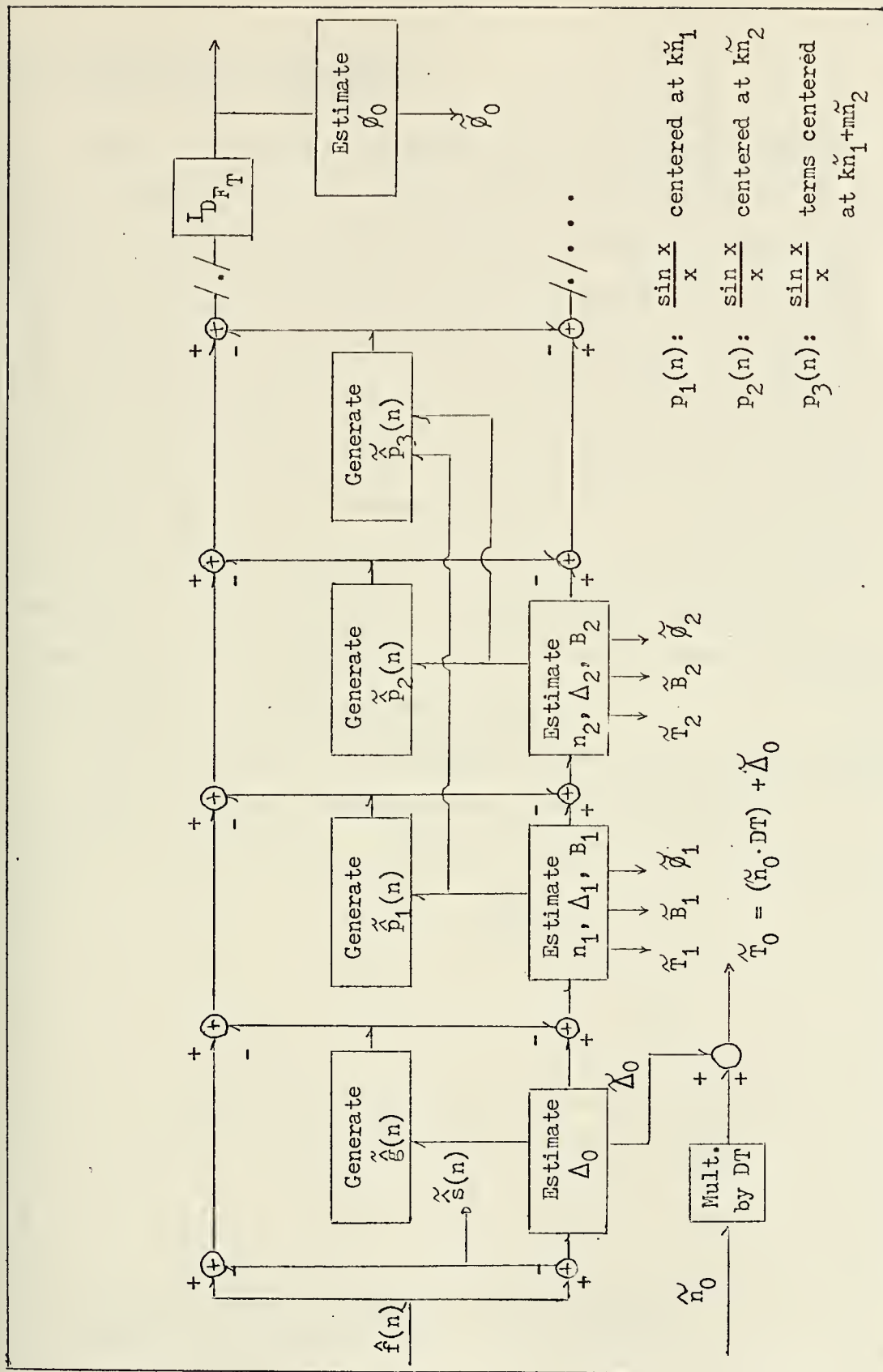


Figure 3-6 Homomorphic Filter-Estimator





### 3.4 Performance of Estimators

Before the results of applications of this technique are presented, a reason for the ad hoc nature of the estimators can be given. Due to the sequential nature of the estimation scheme and the manner in which the received signal is mapped to the cepstrum, the estimators are called upon to act in the presence of somewhat structured interference. As will be discussed, the interference structure can be anticipated so that the estimators can be designed to provide some degree of protection against it. To show this, it should not be necessary to work with the complicated estimators as developed. Instead, a similar, but much simpler, estimation situation can be considered. This will allow a clearer presentation of the important property of the estimators.

As a rough model of the sequence to which the  $\Delta_1$  and  $B_1$  estimators are applied, consider the sequence  $z(n)$  shown in figure 3-7.

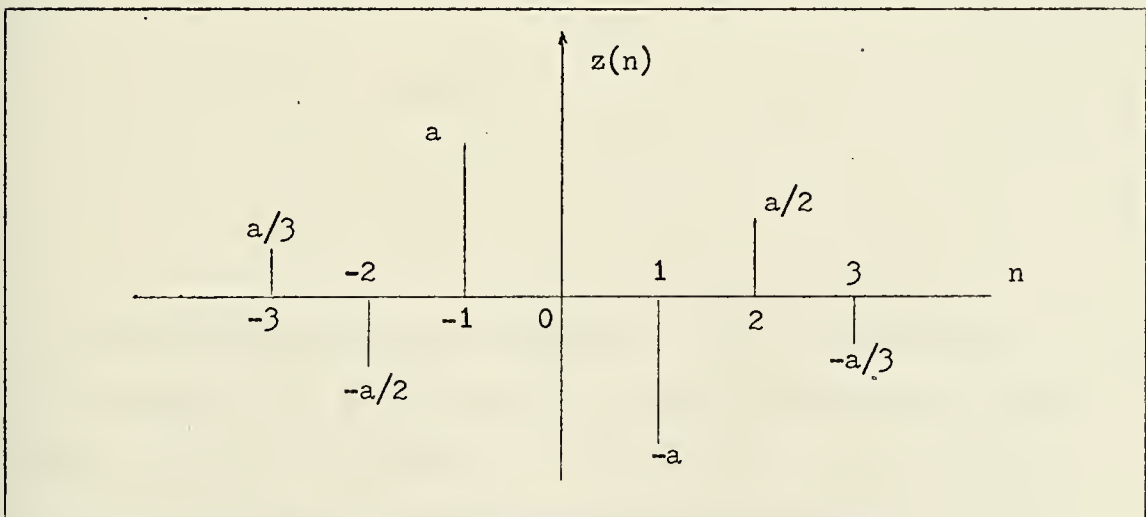


Figure 3-7 Simplified Signal to be Estimated



The sequence is known to be of the form shown, but the value of  $a$  is unknown and to be estimated. The important manner in which  $z(n)$  is similar to  $\hat{p}(n)$  is that the signs of the  $z(n)$  sequence values have a particular code to them: the values of  $z(n)$  are positive for odd negative values of  $n$  and even positive values of  $n$ . This code is similar to that encountered in  $\hat{p}(n)$  since, in  $\hat{p}(n)$ , there are two samples in the main lobe of the first  $\frac{\sin x}{x}$  term, causing a similar sign reversal. It is desired to consider the effects of the presence of structured interference on the estimation of  $a$ . To do this, consider first, the estimator of equation (3.8) which is of the form used for  $\Delta_1$  and  $B_1$ . In effect, the estimators are matched to, or instep with, the code of the  $z(n)$  sign reversals.

$$\begin{aligned}
 \tilde{a}_1 &= -2 z_a(-2) \\
 \tilde{a}_2 &= z_a(-1) \\
 \tilde{a}_3 &= -z_a(1) \\
 \tilde{a}_4 &= 2 z_a(2)
 \end{aligned}
 \tag{3.8}$$

Now suppose that the actual sequence,  $z_a(n)$ , consists of the anticipated  $z(n)$  as in figure 3-7, plus a constant interference sequence,  $w(n) = b$ . The sign code of  $w(n)$ , for  $n = -2, -1, 1, 2$ , is  $++++$ . This can be described as being orthogonal to the sign code of the estimators, which is  $+ - + -$ .



In this case,  $z_a(n) = z(n) + w(n) = z(n) + b$ , so that,

$$\tilde{a}_1 = -2 \left( -\frac{a}{2} + b \right) = a - 2b$$

$$\tilde{a}_2 = (a + b) = a + b$$

$$\tilde{a}_3 = -(-a + b) = a - b$$

$$\tilde{a}_4 = 2 \left( \frac{a}{2} + b \right) = a + 2b$$

Hence the individual estimates have complementary error. It should be assumed that  $|a| > 2|b|$  and  $a > 0$  in making the following argument about the combined estimate.

$$\tilde{a} = \frac{|z_a(-2)| \cdot \tilde{a}_1 + |z_a(-1)| \cdot \tilde{a}_2 + |z_a(1)| \cdot \tilde{a}_3 + |z_a(2)| \cdot \tilde{a}_4}{|z_a(-2)| + |z_a(-1)| + |z_a(1)| + |z_a(2)|}$$

Since  $a > |2b|$ , it follows that,

$$|z_a(-2)| = \left| \left( -\frac{a}{2} + b \right) \right| = \left( \frac{a}{2} - b \right)$$

$$|z_a(-1)| = |(a + b)| = (a + b)$$

$$|z_a(1)| = |(a - b)| = (a - b)$$

$$|z_a(2)| = \left| \left( \frac{a}{2} + b \right) \right| = \left( \frac{a}{2} + b \right)$$



From this, it also follows that,

$$\begin{aligned} \tilde{a} &= \frac{(\frac{a}{2} - b)(a - 2b) + (a + b)^2 + (a - b)^2 + (\frac{a}{2} + b)(a + 2b)}{(\frac{a}{2} - b) + (a + b) + (a - b) + (\frac{a}{2} + b)} \\ (3.9) \quad \tilde{a} &= \frac{3a^2 + 6b^2}{3a} = a + 2\frac{b^2}{a} \end{aligned}$$

As an example, suppose that  $b = a/5$ :

$$\tilde{a} = a + \frac{2a^2}{25a} = 1.08a$$

The estimate for this technique is  $0.08a$  whereas if only  $z_a(1)$ , for example, were used, the error would have been  $b = 0.2a$ . If  $b = .1a$ , the errors are  $0.02a$  and  $0.1a$  respectively. If it happens that the interference has the same code as the estimator, it can be shown that the error is  $0.36a$  for  $b = .2a$  and  $0.17a$  for  $b = .1a$ .

If  $w(n) = (-1)^n b$ , the individual estimates will be,

$$\tilde{a}_1 = -2(-\frac{a}{2} + b) = a - 2b$$

$$\tilde{a}_2 = (a - b) = a - b$$

$$\tilde{a}_3 = -(-a - b) = a + b$$

$$\tilde{a}_4 = 2(\frac{a}{2} + b) = a + 2b$$

Once again the errors are complementary and, it can be shown, the





total estimate will be as in equation (3.9). Figure 3-8 shows the variation of the estimate error as a function of  $b$  for an interference sequence of constant magnitude. The three plots are of: estimate from  $z_a(1)$  alone, four step estimate - interference in step with estimators, four step estimate - interference orthogonal to estimator.

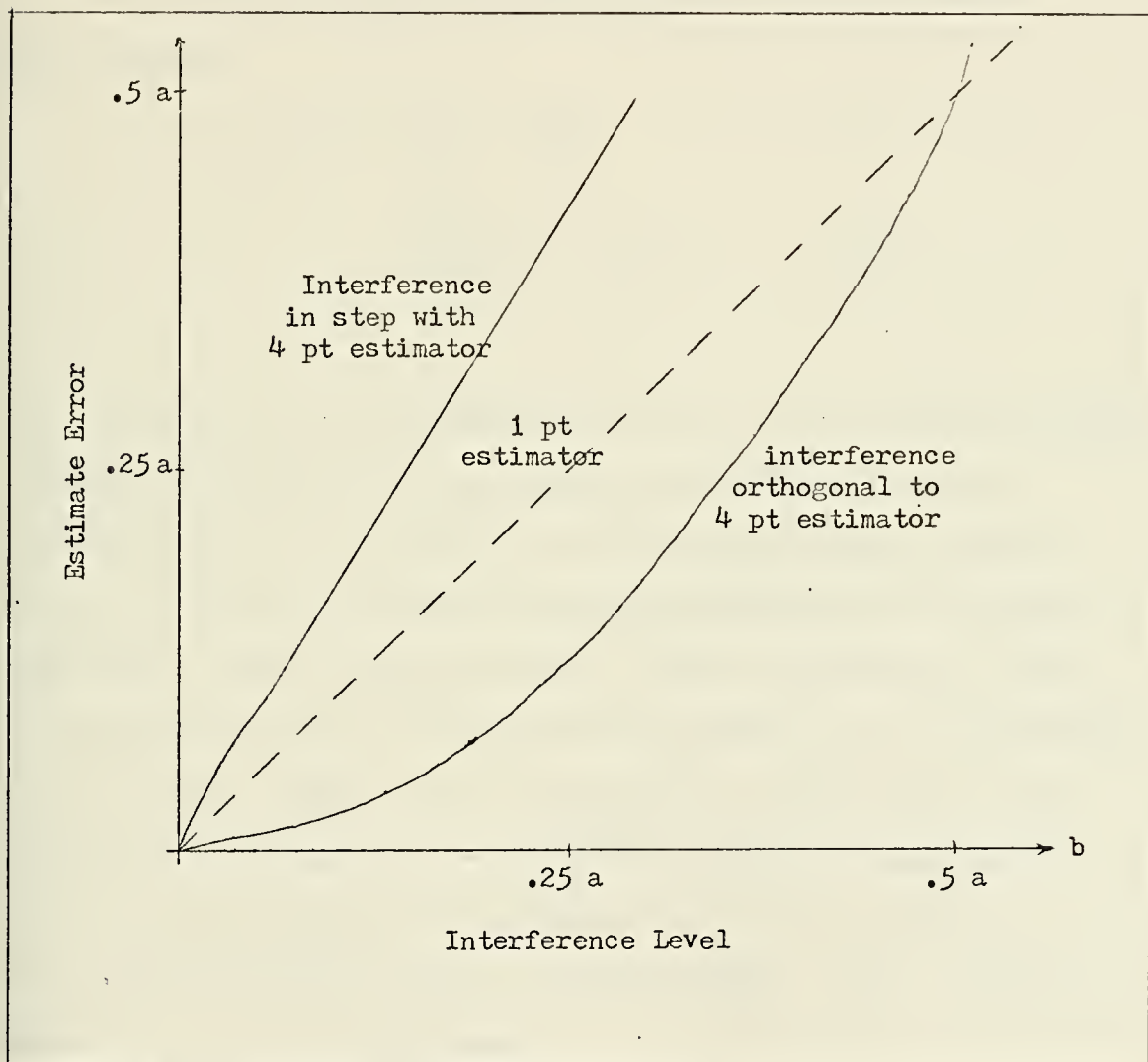


Figure 3-8 Estimator Performance Curve



In the actual case, the estimators are a bit more complicated than those of equation (3.7) and the symmetry is not quite complementary as described. The example does however, illustrate the improvement obtained by centering the measurements around the main lobe of the  $\frac{\sin x}{x}$  functions. Two cases wherein this property is helpful can be presented.

The use of the estimated sequence  $g(n)$  will generate some small residual:

$$\begin{aligned}\hat{\epsilon}_g(n) &= \hat{g}_a(n) - \tilde{g}(n) \\ &= \frac{(\Delta_0 - \tilde{\Delta}_0)}{n} (-1)^{n+1} = (-1) \frac{\epsilon_{\Delta 0}}{n}\end{aligned}$$

This is one source of interference when the  $\Delta_1$  and  $B_1$  estimates are made. Although the sequence is not of constant magnitude, the change is only from  $(\epsilon_{\Delta 0})/6$  to  $(\epsilon_{\Delta 0})/10$  in the quefreny range of interest for  $n_1 = 8$ . This is a reasonable enough approximation to a constant magnitude to produce some improvement. A more important case, since the magnitudes involved will typically be greater, is the interference from the second  $\frac{\sin x}{x}$  term. As developed in equation (3.5), the magnitude of this term will be fairly well reduced for quefrencies near  $n_1$ . The situation can be examined a little more closely to see that, if the largest value of the first  $\frac{\sin x}{x}$  term is denoted  $a$ , where

$$a = \frac{B_1 \sin \pi \Delta_1}{\pi \Delta_1},$$

then the interference sequence, denoted  $w(n)$ , due to the second



$\frac{\sin x}{x}$  function has values,

$$|w(n_1+2)| = \left| \frac{B_1^2 \sin \pi \Delta_1}{2\pi(n_1 + \Delta_1 - 2)} \right| = a |B_1| \frac{\Delta_1}{2(n_1 + \Delta_1 - 2)}$$

$$|w(n_1+1)| = \left| \frac{B_1^2 \sin \pi \Delta_1}{2\pi(n_1 + \Delta_1 - 1)} \right| = a |B_1| \frac{\Delta_1}{2(n_1 + \Delta_1 - 1)}$$

$$\vdots$$

$$|w(n_1-2)| = \left| \frac{B_1^2 \sin \pi \Delta_1}{2\pi(n_1 + \Delta_1 + 2)} \right| = a |B_1| \frac{\Delta_1}{2(n_1 + \Delta_1 + 2)}$$

If  $B_1 = 0.8$ ,  $n_1 = 8$ , and  $\Delta_1 = \frac{1}{2}$ , these values range from about 0.031a to about 0.019a. Once again, the symmetry is not perfect, but it is close enough so that some improvement can be gained.

### 3.5 Application to Simulated Signals

In the case of the generated received signal used for the example depicted in figures 3-1 through 3-3, the following parameters were used:

$$\begin{aligned} DT &= 5 && (\text{microseconds}) \\ T_0 &= 11.5 \\ T_1 &= T_0 + 39.5 ; && n_1 = 8, \quad \Delta_1 = -0.1 \\ B_1 &= 0.8 \\ \phi_0 &= 0 \end{aligned}$$

When the technique developed herein was applied to this signal, the resulting estimates were:



$$\begin{aligned}\tilde{T}_0 &= 11.48785 \\ \tilde{n}_1 &= 8 \\ \tilde{\Delta}_1 &= -0.096033 \\ \tilde{T}_1 &= T_0 + 39.5198 \\ \tilde{B}_1 &= (0.803417, -0.000881) = 0.803417 - j0.000881 \\ \tilde{\phi}_0 &= 0.0006864 \text{ radians}\end{aligned}$$

The phase error in this case,  $|\phi_0 - \tilde{\phi}_0| = \tilde{\phi}_0$ , is 0.039 in degrees. At a carrier frequency of 100 kHz, this corresponds to a time error of about 1.1 nanoseconds. The procedure was repeated for a variety of cases and the results are presented in Table 3-1.

$\phi_0$	$T_0$	$T_1$	$B_1$	$\tilde{T}_0$	$\tilde{T}_1$	$\tilde{B}_1$	$\tilde{\phi}_0$ (rad)	$\tilde{\phi}_0$ error nanoseconds
0	10.0	40.0	.8	10.0004	39.9996	(.800009, .000004)	-.000043	-.068
0	10.0	39.5	.8	9.9404	39.4404	(.810026, -.00015)	.000077	.044
0	10.0	38.0	.8	9.8091	37.9863	(.811575, -.00036)	.000251	.400
0	11.5	40.0	.8	11.5326	39.9815	(.791344, -.00017)	.000125	.195
0	11.5	39.5	.8	11.4878	39.5198	(.803417, -.00088)	.000686	1.095
0	11.5	38.0	.8	11.3366	37.9698	(.803411, .00019)	-.000227	-.361
0	8.5	40.0	.8	8.5685	39.9902	(.795314, .00024)	-.000239	-.380
0	8.5	39.5	.8	8.5189	39.5029	(.799695, .00054)	-.000464	-.740
0	8.5	38.0	.8	8.3650	37.9386	(.808735, .00013)	-.001570	-2.50

Table 3-1 Results of Simulation: No Distortion, One Echo, Zero Phase

(Note: For convenience, the  $T_1$  column in the tables actually represents skywave arrival time relative to the groundwave; i.e., (Table  $T_1$ ) =  $T_1 - T_0$ )





The results shown in the table reflect the performance of the estimators on signals which were purely real to begin with. The phase errors would therefore define the precision available in the loop shown in figure 2-3 in which the homomorphic filter-estimator serves as the phase sensitive detector.

The results of the simulation for non-zero phase cases are shown in Table 3-2. What can be seen in these cases is that the  $B_1$ 's are essentially  $-.19723$  radians out of phase with the true values. This can be explained by examining the Fourier Transform of  $p(n)$ :

$$P(e^{j\omega}) = B_0 + B_1 e^{-j\omega n_1} = B_0 \left(1 + \frac{B_1}{B_0} e^{-j\omega n_1}\right)$$

In other words, all magnitudes and phases in the complex cepstrum are measured relative to the groundwave magnitude and phase.

$\phi_0$	$T_0$	$T_1$	$B_1$	$\tilde{T}_0$	$\tilde{T}_1$	$\tilde{B}_1$	$\tilde{\phi}_0$ (rad)	$\tilde{\phi}_0$ error nanosec
.19723	8.5	40.0	.8	8.5687	39.9900	(.779802, -.155877)	.196285	-1.50
.19723	8.5	39.5	.8	8.5169	39.5030	(.783872, -.157803)	.197302	.112
.19723	8.5	38.0	.8	8.3671	37.9392	(.792381, -.160622)	.202399	8.08

Table 3-2 Results of Simulation: No Distortion, One Echo, Non-zero Phase

The cases in which the skywaves are larger than the groundwave are considered next. As discussed in Appendix B, exponential weighting must be used in these cases. The only thing that changes in the estimation procedure is that  $\hat{S}(n)$ , the a priori estimate, must also show the effects of the exponential weighting. This is easily



accomplished as shown in Appendix A. The results are presented in Table 3-3. The extra column,  $B_1'$ , gives the effective skywave coefficient relative to the groundwave after exponential weighting.

$\phi_0$	$T_0$	$T_1$	$B_1$	$B_1'$	$\tilde{T}_0$	$\tilde{T}_1$	$\tilde{B}_1$	$\tilde{\phi}_0$ (rad)	$\tilde{\phi}_0$ err
0	10.0	40.0	(2.0, 2.0)	(.51332, .51332)	10.0001	39.9999	(.513279, .513268)	.000024	.039
0	10.0	39.5	(2.0, 2.0)	(.52213, .52213)	9.9419	39.4499	(.523293, .533561)	-.00581	-9.30
0	10.0	38.0	(2.0, 2.0)	(.54945, .54945)	9.8493	38.0031	(.547588, .560679)	-.00357	-5.7
.78540	10.0	40.0	(2.0, 2.0)	.725	10.0000	39.9841	(.719902, .001483)	.784204	-1.90
.78540	10.0	39.5	(2.0, 2.0)	.74	9.9450	39.4468	(.748461, .001661)	.784109	-2.05
.78540	10.0	38.0	(2.0, 2.0)	.775	9.8156	37.9970	(.785317, .000722)	.784751	-1.02

Table 3-3 Results of Simulation: No Distortion, One Echo, Skywave Larger than Groundwave

In the cases presented thus far, either the groundwave and the skywave were in phase, or one of the two was at zero phase. For completeness, Table 3-4 presents the results for different, non-zero phases.

$\phi_0$	$T_0$	$T_1$	$B_1$	$B_1'$	$\tilde{T}_0$	$\tilde{T}_1$	$\tilde{B}_1$	$\tilde{\phi}_0$ (rad)	$\tilde{\phi}_0$ error
.19723	10.0	40.0	( $\frac{1}{2}$ , $-\frac{1}{2}$ )	(.39233, -.58828)	10.0002	39.9993	(.392375, -.58821)	.197271	.064
.19723	10.0	39.5	( $\frac{1}{2}$ , $-\frac{1}{2}$ )	(.39233, -.58828)	9.9412	39.4472	(.388902, -.59842)	.201864	7.36
.19723	10.0	38.0	( $\frac{1}{2}$ , $-\frac{1}{2}$ )	(.39233, -.58828)	9.8134	37.9994	(.38774, -.59804)	.199813	4.10

Table 3-4 Results of Simulation: No Distortion, One Echo, Skywave and Groundwave at Arbitrary Phases.



In all of the above cases, the final estimate of the groundwave cepstrum sequence,  $\hat{s}(n)$ , was short pass filtered after 150 microseconds before taking the inverse DFT to measure  $\phi_0$ . As discussed in Appendix A, this is done to facilitate filtering in the multiple skywave case. Table 3-5 shows the results of the estimation scheme when applied to a signal with two skywaves. The results are not quite as good as in the single skywave case. Nevertheless, it is felt that, if warranted, more elegant estimation algorithms can be developed. The point of the presentation thus far is to demonstrate that, in the distortion free, noiseless case, measurement precision on the order of a few nanoseconds is possible. The effects of signal distortion can now be examined.



$\phi_0$	$T_0$	$T_1$	$T_2$	$B_1'$	$B_2'$	$\tilde{T}_0$	$\tilde{T}_1$	$\tilde{T}_2$	$\tilde{B}_1$	$\tilde{B}_2$	$\tilde{\phi}_0$ (rad)	$\tilde{\phi}_0$ error
.19723	10.0	40.0	79.0	(.32977, -.49448)	(.16206, .10808)	9.9849	39.9404	78.8862	(.311999, -.48730)	(.16621, .12004)	.18616	-17.0
.19723	10.0	39.5	79.0	(.33627, -.50421)	(.16206, .10808)	9.9493	39.4443	78.9683	(.32803, -.51668)	(.16076, .10969)	.20170	7.1
.19723	10.0	38.0	79.0	(.35652, -.53458)	(.16206, .10808)	9.8380	38.0038	78.9587	(.34893, -.54411)	(.16648, .11093)	.19349	-5.9

Table 3-5 Results of Simulation: No Distortion, Two Echoes





## Chapter 4

### DISTORTED SIGNALS

The results of the preceeding chapter depend heavily on the assumption that the received signal is identical in form to the sequence  $\hat{f}(n)$  defined in equation (3.1):

$$\hat{f}(n) = \hat{s}(n) + \hat{g}(n) + \hat{p}(n)$$

In practice, it can be expected that  $\hat{g}_a(n) = \hat{g}(n)$  since this component is merely due to the small portion of the linear phase not removed before computing the cepstrum. There remain however, two sources of error since  $\hat{s}_a(n)$  and  $\hat{p}_a(n)$  may not be of the expected form. The sensitivity of the estimators to these errors will be examined in this chapter.

#### 4.1 Distorted Basic Waveform

In the estimation scheme of Chapter 3 it was assumed that a good a priori estimate of  $\hat{s}_a(n)$  was available. What is meant by good might be that some criterion such as equation (4.1) is met.

$$(4.1) \quad \left| \frac{\hat{\epsilon}_s(n)}{\hat{s}_a(n)} \right| = \left| \frac{\hat{s}_a(n) - \tilde{s}(n)}{\hat{s}_a(n)} \right| < \epsilon \quad \text{for all } n \text{ such that } \hat{s}_a(n) \neq 0$$

where  $\epsilon$  is some appropriate bound. Upon close examination however, it can be seen that what is of importance is the effect of the residual sequence,  $\hat{\epsilon}_s(n)$ , on the sequence  $\hat{x}(n)$ .



$$\begin{aligned}\hat{x}(n) &= \hat{r}(n) - \hat{s}(n) = \hat{s}_a(n) + \hat{g}_a(n) + \hat{p}_a(n) - \hat{s}(n) \\ &= \hat{g}_a(n) + \hat{p}_a(n) + \hat{\epsilon}_s(n)\end{aligned}$$

Consequently, what is of concern is the ratio,

$$(4.2) \quad \frac{\hat{\epsilon}_x(n)}{\hat{g}_a(n) + \hat{p}_a(n)} = \frac{\hat{\epsilon}_s(n)}{\hat{g}_a(n) + \hat{p}_a(n)} \quad ; \quad \text{for all } n \text{ of interest}$$

As an example of the distinction, the ratio of equation (4.1) might have a value of about 0.01 for some value of  $n$ . As this stands by itself,  $\hat{s}(n)$  might therefore be considered a reasonably good estimate. However, if  $\hat{s}_a(n)$  is 100 times greater than  $\hat{p}_a(n) + \hat{g}_a(n)$  at this value of  $n$ , the ratio of equation (4.2) would equal 1. The estimate might then not be considered so good - particularly if the value of  $n$  in question happened to be near  $n_1$ .

Conversely, if the ratio of equation (4.1) is quite large for some queffrequency value not considered in the estimation procedure, or, for some queffrequency at which  $\hat{p}_a(n) + \hat{g}_a(n)$  is much larger than  $\hat{s}_a(n)$ , there may be no problem. The criteria for judging the appropriateness of the a priori estimate would therefore be as in equation (4.3).

$$(4.3) \quad \begin{aligned}\hat{\epsilon}_s(n) &\ll \hat{g}_a(n) \quad ; \quad n = -1, -2, -3, -4 \\ \hat{\epsilon}_s(n) &\ll \hat{p}_a(n) \quad ; \quad n \approx n_1\end{aligned}$$

Distortion of  $\hat{s}_a(n)$  will be introduced by the propagation path and by the receiver processing. It may be assumed that the propagation



distortion of the groundwave is negligible. Not so negligible however, would be the effects of receiver filters. In addition to performing the low pass filtering in the demodulation scheme shown in figure 2-2, the filters are called upon to suppress atmospheric noise and interference from other navigation or communication systems operating in the low frequency portion of the spectrum. Since no general linear time invariant filter can be used to model the effects of these filters under all conditions of operation, what will be presented will be a method of analyzing the technique which could then be applied to any specific implementation.

Suppose the received signal is processed by a single pole low pass filter (similar arguments can be applied for double or triple pole filters). A model of the basic waveform, i.e., the signal without echoes, to be sampled would then be,

$$s_a(t) = s(t) * h(t)$$

where 
$$h(t) = e^{-\beta t} u_{-1}(t)$$

so that 
$$\hat{s}_a(n) = \hat{s}(n) + \hat{h}(n)$$

and 
$$\hat{\epsilon}_s(n) = \hat{s}_a(n) - \tilde{\hat{s}}(n) = \hat{s}_a(n) - \hat{s}(n) = \hat{h}(n)$$

In this case, the cepstrum of the filter response is easy to compute:

$$H(e^{j\omega}) = \sum_{n=0}^{\infty} e^{-\beta n} e^{-j\omega n} = \left[ 1 - e^{-(\beta + j\omega)} \right]^{-1}$$



$$\log H(e^{j\omega}) = \sum_{n=1}^{\infty} \frac{e^{-\beta n}}{n} e^{-j\omega n} \quad \text{for } \beta > 0$$

and

$$\hat{\epsilon}_s(n) = \hat{h}(n) = \begin{cases} 0 & ; \text{otherwise} \\ \frac{e^{-\beta n}}{n} & ; n > 0 \end{cases}$$

The fact that the cepstrum is zero for negative quefrequencies will be true for any minimum phase filter - any linear phase term being removed in the phase unwrapping procedure. Since the  $\Delta_0$  estimate is made from the negative quefreny values of the received signal, it can be seen that the accuracy of the estimated sequence  $g_a(n)$  will not be affected by the presence of the  $h(n)$  term. The values of  $\hat{\epsilon}_s(n)$  for quefrequencies near  $n_1$  however, will cause problems. The values of  $\hat{\epsilon}_s(n)$  and  $\hat{p}(n)$  in this region are given in Table 4-1 for comparison. The parameters of the signals in this case are:

$$\begin{aligned} \beta &= \alpha = 2/65 \\ n_1 &= 8 \\ 1 &= -0.1 \\ B_1 &= 0.8 \\ DT &= 5 \end{aligned}$$

n	$\hat{\epsilon}_s(n)$	$\hat{p}(n)$
$n_1-2$	.13857	-.0348
$n_1-1$	.11518	.0792
$n_1$	.09770	.7796
$n_1+1$	.08423	-.0791
$n_1+2$	.07351	.0472

Table 4-1 Comparison of A Priori Estimate Error and  $\hat{p}(n)$ .





Clearly,  $\left| \frac{\hat{\epsilon}_s(n)}{\hat{p}(n)} \right|$  is too large in this case to permit estimation of  $\Delta_1$  and  $B_1$ . The problem can be overcome if the response of the filter can be presumed to be known reasonably well. The a priori estimate of  $\hat{s}_a(n)$  can then be modified:

$$\tilde{\hat{s}}(n) = \hat{s}(n) + \tilde{\hat{h}}(n)$$

so that 
$$\hat{\epsilon}_s(n) = \hat{s}_a(n) - \tilde{\hat{s}}(n)$$

$$= \hat{s}(n) + \hat{h}(n) - \hat{s}(n) - \tilde{\hat{h}}(n)$$

$$= \hat{h}(n) - \tilde{\hat{h}}(n)$$

In this case, an estimate of the form

$$\tilde{\hat{h}}(n) = \begin{bmatrix} 0 & ; \text{otherwise} \\ \frac{e^{-\gamma n}}{n} & ; n > 0 \end{bmatrix}$$

where  $\gamma \approx \beta$  might be used. The error therefore would be,

$$\hat{\epsilon}_s(n) = \frac{1}{n} \left[ e^{-\beta n} - e^{-\gamma n} \right] \quad ; \quad n > 0$$

For  $\gamma = \frac{3}{2}\beta$ , with the other parameters as in the preceding example, the error values would then be as shown in Table 4-2.



n	$\hat{\epsilon}_s(n)$	$\hat{p}(n)$
$n_1-2$	.01222	-.0348
$n_1-1$	.01176	.0792
$n_1$	.01129	.7796
$n_1+1$	.01089	-.0791
$n_1+2$	.01048	.0472

Table 4-2 Comparison of Revised  
A Priori Estimate  
Error and  $\hat{p}(n)$

Within this range of quefrencies,  $\hat{\epsilon}_s(n) < \hat{p}_a(n)$ . Further notice should be taken of the fact that the  $\hat{\epsilon}_s(n)$  terms are of relatively constant value and of constant sign. As developed in Chapter 3, the individual estimates of  $\Delta_1$  and  $B_1$  will therefore have nearly complementary errors. Consequently, the total estimates of  $\Delta_1$  and  $B_1$  are relatively unaffected by the incorrect a priori estimate of  $\beta$ .

If the correct value of  $\gamma$  is used, i.e.,  $\gamma = \beta$ , but an incorrect filter form is assumed, the results are quite different. Suppose

$$h(t) = t e^{-\beta t} u_{-1}(t)$$

It can be shown that the resulting cepstrum is,

$$\hat{h}(n) = \begin{bmatrix} 0 & ; & n < 0 \\ -\beta & ; & n = 0 \\ 2 \frac{e^{-\beta n}}{n} & ; & n > 0 \end{bmatrix}$$



Therefore,

$$\hat{\epsilon}_s(n) = \begin{cases} 0 & ; n < 0 \\ -\beta & ; n = 0 \\ \frac{e^{-\beta n}}{n} & ; n > 0 \end{cases}$$

This will produce the same situation as that depicted in Table 4-1.

In summary, it can be said that the a priori estimate of  $\hat{s}_a(n)$  must be changed to reflect the effects of the responses of any filters used. The estimation procedure of Chapter 3 will be relatively insensitive to errors in filter parameters, e.g., pole locations, but fairly sensitive to errors in estimated filter form.

## 4.2 Distorted Echoes

If the received signal is processed by a linear time invariant filter, the effects will be as described above. Such a filter will not change the echoed property of the signal, i.e.,  $\hat{p}_a(n)$  will not be changed. Distortion of  $\hat{p}_a(n)$  can only be introduced by differences in the propagation paths. The distortion can be modelled as follows in a single skywave case.

$$r(t) = s_a(t) + B_1 s_a(t-T_1) * h(t)$$

$$R(e^{j\omega}) = S_a(e^{j\omega}) \cdot G_a(e^{j\omega}) \cdot \left[ 1 + \left[ B_1 e^{-j\omega(n_1 + \Delta_1)} \cdot H(e^{j\omega}) \right] \right]$$



$$\log R(e^{j\omega}) = \log S_a(e^{j\omega}) + \log G_a(e^{j\omega})$$

$$+ \sum_{k=1}^{\infty} (-1)^{k+1} \frac{B_1^k e^{-j\omega k(n_1 + \Delta_1)}}{k} \cdot H^k(e^{j\omega})$$

$$\text{for } |B_1 H(e^{j\omega})| < 1$$

$$\hat{r}(n) = \hat{s}_a(n) + \hat{g}_a(n) + \hat{p}_a(n)$$

$$\text{where } \hat{p}_a(n) = F^{-1} \left[ \sum_{k=1}^{\infty} (-1)^{k+1} \frac{B_1^k e^{-j\omega k(n_1 + \Delta_1)}}{k} \cdot H^k(e^{j\omega}) \right]$$

The resulting  $\hat{p}_a(n)$  can be anticipated by recognizing that its components are inverse Fourier Transforms of products. Hence, what was the first  $\frac{\sin x}{x}$  term in the expansion is now convolved with  $h(n) = h(t) \Big|_{t=n \cdot DT}$ . The second  $\frac{\sin x}{x}$  term is convolved with  $h(n)$  twice and the third term is convolved with  $h(n)$  three times, etc. The results of these convolutions are combined to form  $\hat{p}_a(n)$ . In the cases considered thus far,  $h(t)$  has been an impulse function so that the  $\frac{\sin x}{x}$  terms appeared intact. If  $h(t)$  is only approximately impulsive, the first  $\frac{\sin x}{x}$  term will be only slightly distorted. Higher order  $\frac{\sin x}{x}$  terms however, will be convolved with  $h(n)$  a number of times and will tend to spread out - only loosely resembling  $\frac{\sin x}{x}$  functions.

In the Loran-C case,  $h(t)$  is nearly impulsive. Additionally, since the cepstrum is short pass filtered, the effects of the many-fold convolutions which distort the high order  $\frac{\sin x}{x}$  terms will





only slightly be felt. The selection of an appropriate model for  $h(t)$  is confounded by the fact that it is so nearly impulsive that it has not been possible to measure its form. Perhaps the only correct model would be that the skywave and groundwave are identical to within 1% along the leading edges of the pulses.

Although an appropriate form of  $h(t)$  is not available, it is desired to test the sensitivity of the estimators to a possible 1% distortion. What will be used in this case is a groundwave of the form  $t^2 e^{-\alpha t}$  and a skywave of the form  $t^2 e^{-\beta t}$ . If  $\alpha = 2/65$  and  $\beta = 2/70$ , and if the signals are scaled to achieve a value of 1 at their respective peaks ( $2/\alpha$  and  $2/\beta$ ), the skywave will have a magnitude of about 76% of the magnitude of the groundwave at  $t = 65$ . (with both signals beginning in coincidence). While the  $h(t)$  that would produce such distortion, i.e.,  $L^{-1} \left[ \left[ (s+\alpha)/(s+\beta) \right]^3 \right]$ , is not claimed to be a particularly realistic model of what actually occurs, it does serve as a clearly large overbound on the amount of distortion to be expected.

The case described above was simulated and the results are presented in Table 4-3. While the errors are, understandably, higher than in the cases presented in Chapter 3, they are the results of distortion which is much more than can be expected to be introduced by the propagation path. As long as the propagation path filter is nearly impulsive, the effect on the cepstrum estimators is minimal.

The results presented in this chapter will be discussed further in Chapter 6. It can be said however, that, with the assumptions made in the presentation, signal distortion only slightly affects the



performance of the homomorphic filter as used in this application.

$\phi_0$	$T_0$	$T_1$	$B_1$	$B_1'$	$\tilde{T}_0$	$\tilde{T}_1$	$\tilde{B}_1'$	$\tilde{\phi}_0$ rad	$\tilde{\phi}_0$ error
.19723	10.0	40.0	(2., -2.)	(.32977, -.49448)	10.0016	39.875	(.31743, -.47539)	.16990	43.5
.19723	10.0	39.5	(2., -2.)	(.33627, -.50421)	9.9506	39.4662	(.34000, -.52213)	.18663	16.9
.19723	10.0	38.0	(2., -2.)	(.35652, -.53459)	9.8317	38.0789	(.35804, -.55027)	.18418	20.8

Table 4-3 Results of Simulation: Distorted Echo



## Chapter 5

## NOISY SIGNALS

In this chapter the effects of noise on the cepstrum estimators will be examined. Before quantitatively presenting the effects of the noise, an attempt should be made to develop a theory which outlines the results to be anticipated. The development begins with an explanation of a matrix notation which seems best suited to a clear presentation of the elementary aspects of the problem.

If a continuous-time function,  $x(t)$ , is sampled every  $DT$  time units, the resulting samples have values  $x(n \cdot DT)$ . These samples produce a sequence of values denoted  $x(n)$  as used in the preceeding chapters. The values can also be denoted  $x_n$  and used to define a vector  $\underline{x}$ :

$$\underline{x} = (x_0, x_1, x_2, \dots, x_{N-1})^T = (x(0), x(1), x(2), \dots, x(N-1))^T$$

The sequence  $x_n$  has a Discrete Fourier Transform, denoted  $\underline{x}_k$ :

$$\underline{x}_k = \sum_{n=0}^{N-1} x_n e^{-\frac{j2\pi kn}{N}}$$

The values of the DFT can also be represented as defining a vector

$\underline{x}_k$ :

$$\underline{x}_k = (\underline{x}_0, \underline{x}_1, \underline{x}_2, \dots, \underline{x}_{N-1})^T$$

In matrix notation, the DFT relation can be expressed as:



$$\underline{\tilde{x}} = \underline{W} \underline{x}$$

or,

$$(5.1) \quad \begin{bmatrix} \tilde{x}_0 \\ \tilde{x}_1 \\ \tilde{x}_2 \\ \vdots \\ \tilde{x}_{N-1} \end{bmatrix} = \begin{bmatrix} 1 & 1 & 1 & \dots & 1 \\ 1 & W & W^2 & \dots & W^{N-1} \\ 1 & W^2 & W^4 & \dots & W^{2(N-1)} \\ \vdots & \vdots & \vdots & \ddots & \vdots \\ 1 & W^{(N-1)} & W^{2(N-1)} & \dots & W^{(N-1)^2} \end{bmatrix} \cdot \begin{bmatrix} x_0 \\ x_1 \\ x_2 \\ \vdots \\ x_{N-1} \end{bmatrix}$$

where  $W = \exp(-\frac{j2\pi}{N})$ .

It is desired to trace the effects of the noise from the time domain to the quefrency domain. The first step therefore is to examine the behavior of the DFT of a noise sequence. To facilitate the derivation, the noise sequence to be encountered will be considered to consist of samples of a zero mean, complex, white gaussian random process. The appropriateness of this model is discussed in Appendix D. To proceed, make the following definition,

$$\underline{x} = \underline{v} ; \quad \underline{v} \text{ is a zero mean, complex, white gaussian random vector}$$

The sequence  $\underline{x}$  then has the following properties<sup>9</sup>:

$$E[\underline{x}] = E[\text{Re}(\underline{x})] = E[\text{Im}(\underline{x})] = \underline{0}$$





$$E \left[ \text{Re}(\underline{x}^T) \text{Re}(\underline{x}) \right] = \frac{\sigma^2}{2} \underline{I} ; \quad \underline{I} = N \times N \text{ identity matrix}$$

$$E \left[ \text{Im}(\underline{x}^T) \text{Im}(\underline{x}) \right] = \frac{\sigma^2}{2} \underline{I}$$

$$E \left[ \text{Re}(\underline{x}^T) \text{Im}(\underline{x}) \right] = \underline{0}$$

$$E \left[ \underline{x}^T \underline{x}^* \right] = \sigma^2 \underline{I} \quad \text{where } * \text{ denotes complex conjugate}$$

In short,  $\underline{x}$  is a vector of  $N$  complex random variables. The vector contains a total of  $2N$  uncorrelated zero mean gaussian random variables (GRV's). The uncorrelated property, for zero mean GRV's implies independence. The complex variables,  $x_i$ , can also be represented as,

$$x_i = |x_i| \cdot \exp \left[ \text{ARG}(x_i) \right]$$

where  $|x_i|$  is a Rayleigh distributed random variable and  $\text{ARG}(x_i)$  is a random variable uniformly distributed on  $(-\pi, \pi)$ .

One way to arrive at the statistics of  $\underline{x}$  is to argue along the following lines. From equation (5.1),

$$\begin{aligned} \underline{x}_k &= x_0 + W^k x_1 + W^{2k} x_2 + \dots + W^{k(N-1)} x_{N-1} \\ (5.2) \quad &= x'_0 + x'_1 + x'_2 + \dots + x'_{N-1} \end{aligned}$$

where  $x'_1 = W^{k1} x_1$ . The purpose of defining this new sequence  $x'_n$  is as follows:



$$|x'_i| = |W^{ki} x_i| = |W^{ki}| \cdot |x_i| = |x_i|$$

$|x'_i|$  is therefore Rayleigh distributed with statistics identical to those of  $|x_i|$ . Furthermore,  $\text{ARG}(x'_i) = \text{ARG}(W^{ki}) + \text{ARG}(x_i)$ . Since the phases are computed as principal values,  $\text{ARG}(x'_i)$  is also uniformly distributed on  $(-\pi, \pi)$ . Consequently,  $x'_i$  has Rayleigh magnitude and uniform phase values which are statistically identical to those of  $x_i$ . It follows that the real and imaginary parts of  $x'_i$  must also be statistically identical to those of  $x_i$ , i.e., independent zero mean, identically distributed GRV's. It is also true that the elements of the  $x'$  vector are independent:

$$\begin{aligned} E \left[ x'_m x'^*_n \right] &= E \left[ W^{mk} x_m W^{-nk} x_n^* \right] \\ &= W^{k(m-n)} E \left[ x_m x_n^* \right] = \sigma^2 \delta_{mn} \end{aligned}$$

By the zero mean GRV property, this implies independence. The result of this intermediate step can be seen by re-writing equation (5.2) as below.

$$(5.2) \quad x_k = x'_0 + x'_1 + x'_2 + \dots + x'_{N-1}$$

$$(5.3) \quad \text{Re}(x_k) = \text{Re}(x'_0) + \text{Re}(x'_1) + \dots + \text{Re}(x'_{N-1})$$

$$\text{Im}(x_k) = \text{Im}(x'_0) + \text{Im}(x'_1) + \dots + \text{Im}(x'_{N-1})$$



The right sides of equation (5.3) contain a total of  $2N$  independent zero mean GRV's. The two sums, i.e.,  $R(x_k)$  and  $\text{Im}(x_k)$ , are therefore independent. Additionally, they each are sums of  $N$  independent zero mean GRV's with variances  $\frac{\sigma^2}{2}$ . It follows then that  $\text{Re}(x_k)$  and  $\text{Im}(x_k)$  are independent zero mean, identically distributed, GRV's with variances  $N \frac{\sigma^2}{2}$  so that  $|x_k|$  is Rayleigh and  $\text{ARG}(x_k)$  is uniform.

It is also possible to show that the individual elements of the  $\underline{x}$ -vector are independent. This follows from the orthogonality of the rows of the  $\underline{W}$ -matrix, i.e.,  $x_k$  and  $x_m$  become orthogonal random variables. Since they are also zero mean and gaussian, they are independent. To see this more explicitly, consider:

$$E \begin{bmatrix} x_k & x_m^* \end{bmatrix} = E \left[ \begin{aligned} & \left[ x_0 + W^k x_1 + W^{2k} x_2 + \dots + W^{k(N-1)} x_{N-1} \right] \\ & \cdot \left[ x_0^* + W^{-m} x_1^* + \dots + W^{-m(N-1)} x_{N-1}^* \right] \end{aligned} \right]$$

Since  $E \begin{bmatrix} x_i & x_j^* \end{bmatrix} = \sigma^2 \delta_{ij}$ , it follows that

$$\begin{aligned} E \begin{bmatrix} x_k & x_m^* \end{bmatrix} &= E \left[ |x_0|^2 + W^{(k-m)} |x_1|^2 + \dots + W^{(N-1)(k-m)} |x_{N-1}|^2 \right] \\ &= \sigma^2 \sum_{n=0}^{N-1} W^{n(k-m)} \end{aligned}$$

For  $k = m$ , the value of the above sum is clearly  $N\sigma^2$ . For  $k \neq m$ , the sum consists of  $N$  terms, all with equal magnitudes and with phases equally spaced from  $-\pi$  to  $\pi$ . The resultant sum is therefore zero so that,



$$E \begin{bmatrix} \tilde{x}_k & \tilde{x}_m^* \end{bmatrix} = \sigma^2 \sum_{n=0}^{N-1} W^{n(k-m)} = N \sigma^2 \delta_{km}$$

Once again, together with the zero mean gaussian property, this implies independence.

In summary, a zero mean, complex, white gaussian noise sequence has a DFT which is also a zero mean, complex, white gaussian noise sequence. All that changes, statistically, is that the variances are changed from  $\sigma^2$  to  $N\sigma^2$ .

In computing a DFT, it is sometimes desired to add zeroes to the end of the sequence. Since the same DT is used, this does nothing to change the bandwidth of the DFT. However, since there are more samples of the time sequence, the DFT will have more samples in it. This has the effect of increasing the resolution of the DFT. The effect of this operation on the statistics of the noise DFT should be examined.

Suppose that  $M$  samples of the noise sequence,  $x_n$ , are available and that an  $N$  point DFT is computed:

$$\begin{bmatrix} \tilde{x}_0 \\ \tilde{x}_1 \\ \tilde{x}_2 \\ \tilde{x}_3 \\ \vdots \\ \vdots \\ \vdots \\ \vdots \\ \vdots \\ \vdots \\ \vdots \\ \tilde{x}_{N-1} \end{bmatrix} = \begin{bmatrix} 1 & 1 & 1 & \dots\dots\dots 1 & \\ 1 & W & W^2 & & W^{N-1} \\ 1 & W^2 & W^4 & & W^{2(N-1)} \\ \cdot & \cdot & \cdot & & \cdot \\ \cdot & \cdot & \cdot & & \cdot \\ \cdot & \cdot & \cdot & & \cdot \\ \cdot & \cdot & \cdot & & \cdot \\ \cdot & \cdot & \cdot & & \cdot \\ \cdot & \cdot & \cdot & & \cdot \\ \cdot & \cdot & \cdot & & \cdot \\ \cdot & \cdot & \cdot & & \cdot \\ 1 & W^{(N-1)} & W^{2(N-1)} & \dots\dots\dots W^{(N-1)^2} \end{bmatrix} \cdot \begin{bmatrix} x_0 \\ x_1 \\ x_2 \\ \vdots \\ \vdots \\ \vdots \\ x_{M-1} \\ 0 \\ \vdots \\ \vdots \\ \vdots \\ 0 \end{bmatrix}$$





The  $\underline{\tilde{x}}$ -vector will, in general, have  $N$  non-zero elements which, as above, can be shown to have real and imaginary parts which are independent, zero mean GRV's with variances  $M \frac{\sigma^2}{2}$ . Hence the magnitudes of each point are Rayleigh distributed and the phases are uniformly distributed. The sequence, however, is no longer white. In fact, the  $\underline{\tilde{x}}$ -vector will span the same  $M$  dimensional complex (or  $2M$  dimensional real) space as that generated by the original sequence  $\underline{x}$ . The autocorrelation function of the DFT can be computed in a straightforward manner. From this it can be shown that, for example, if  $N/M = 4$ , points in the DFT 4 samples apart are independent. If  $N/M$  is not an integer, all the points are correlated, although only loosely for separations of more than about  $2N/M$ .

If  $\underline{x} = \underline{s} + \underline{v}$ , where  $\underline{s}$  is a deterministic vector and  $\underline{v}$  is the noise vector as previously described, it follows from the linearity of the DFT operation that

$$E [\tilde{x}_k] = E [\tilde{s}_k + \tilde{v}_k] = \tilde{s}_k$$

and

$$\begin{aligned} E [\tilde{x}_k \tilde{x}_m^*] &= E [(\tilde{s}_k + \tilde{v}_k) (\tilde{s}_m^* + \tilde{v}_m^*)] \\ &= \tilde{s}_k \tilde{s}_m^* + N\sigma^2 \delta_{km} \end{aligned}$$

With this background, consider the DFT of the sequence

$x_n = s_n + v_n$  which may appear as in figure 5-1.



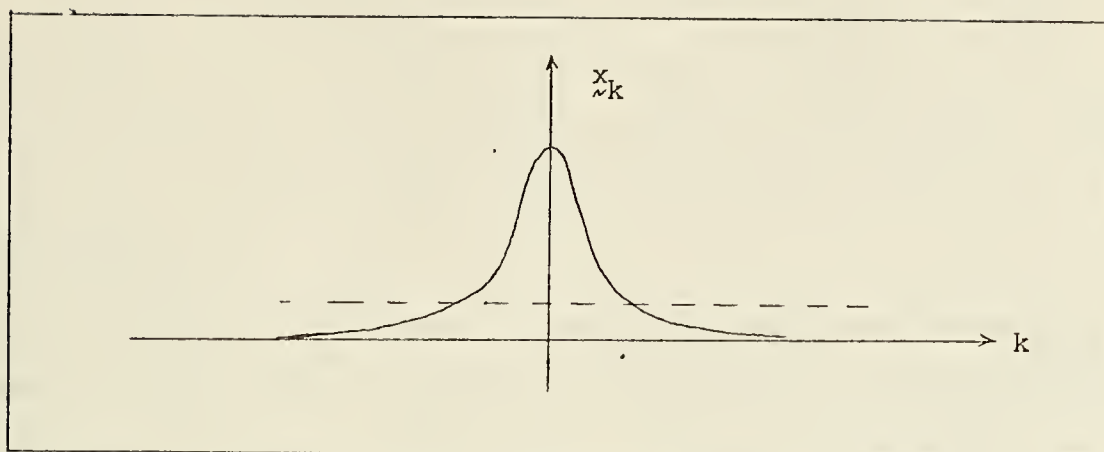


Figure 5-1 Frequency Plot of Signal and Noise

The solid line in the figure represents the magnitude of the DFT of the deterministic sequence. The dashed line represents some convenient probabilistic bound on the magnitude of the DFT of the noise as determined by its Rayleigh distribution. What must be considered is the effect of the noise on the phase of the composite signal. For values of  $k$  such that  $|s_k| > |v_k|$ , the vector sum may be as shown in figure 5-2(a).

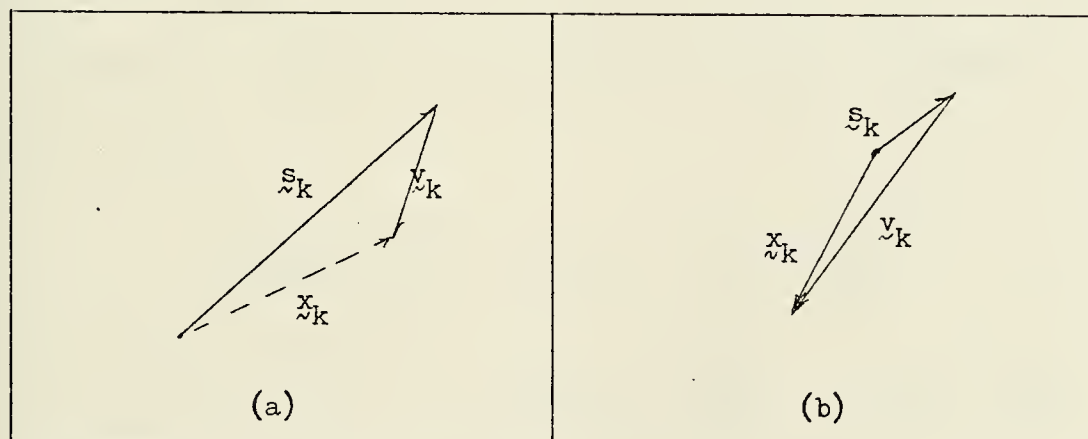


Figure 5-2 Vector Diagram of Signal and Noise



In this case, the composite phase will follow that of  $\tilde{s}_k$  reasonably closely. As an example, if  $|\tilde{s}_k| = 2|\tilde{v}_k|$ , the phase error, the difference between  $\arg(\tilde{s}_k)$  and  $\arg(\tilde{s}_k + \tilde{v}_k)$  is at most about  $31^\circ$ . The phase curve is therefore noisy; but the noise is small - less than  $\pi/2$  in magnitude.

For values of  $k$  such that  $|\tilde{s}_k| < |\tilde{v}_k|$ , the vector sum may be as shown in figure 5-2(b). The phase error in this case can be considered to produce a more noisy curve - errors as great as  $\pi$  in magnitude. However, the implications of this situation are more significant in view of the fact that the phase curve will now have the structure of the noise phase, i.e. white. This causes problems because it is presumed in the phase unwrapping algorithm that the phase has a smooth, or continuous, structure. If  $|\tilde{s}_k| > |\tilde{v}_k|$  for all  $k$ , every point in the DFT phase will be within  $\pm \frac{\pi}{2}$  of the correct value so that the measured number of branchings of the arctangent function defining the composite phase will be, at most, one different from the correct value. If  $|\tilde{s}_k| < |\tilde{v}_k|$  however, there can be any number of branchings of the phase so that a huge error can be expected in the corrected phase curve.

This can be summarized by considering the form of the complex log of the DFT.

$$\begin{aligned} \log [\tilde{s}_k + \tilde{v}_k] &= \log \tilde{s}_k + \log \left[ 1 + \frac{\tilde{v}_k}{\tilde{s}_k} \right] \\ &\approx \log \tilde{s}_k + \frac{\tilde{v}_k}{\tilde{s}_k} ; \quad |\tilde{s}_k| \gg |\tilde{v}_k| \end{aligned}$$



$$\log \left[ \tilde{s}_k + \tilde{y}_k \right] = \log \tilde{y}_k + \log \left[ 1 + \frac{\tilde{s}_k}{\tilde{y}_k} \right]$$

$$\approx \log \tilde{y}_k + \frac{\tilde{s}_k}{\tilde{y}_k} ; \quad |\tilde{y}_k| \gg |\tilde{s}_k|$$

If the phase of  $\tilde{y}_k$  is uniform and white, the phase of  $\frac{\tilde{y}_k}{\tilde{s}_k}$  will also be uniform and white, when measured via its principal value. Therefore,  $\frac{\tilde{y}_k}{\tilde{s}_k}$  is statistically equivalent to  $\frac{\text{Re}(\tilde{y}_k) + j \text{Im}(\tilde{y}_k)}{|\tilde{s}_k|}$ . Consequently, the effect of the log DFT operation for  $|\tilde{s}_k| \gg |\tilde{y}_k|$  is to filter the noise as in figure 5-3(a). The  $|\tilde{s}_k|$  used is that of the Loran-C signal.

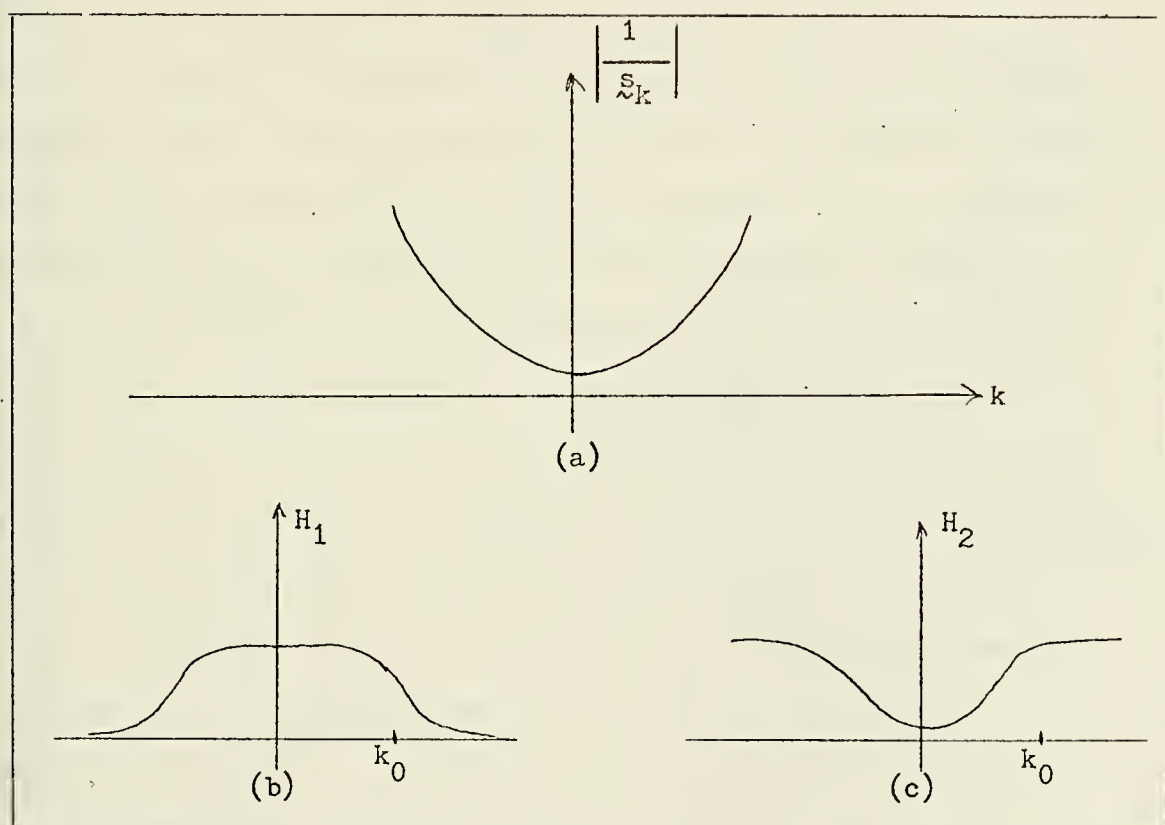


Figure 5-3 LOG DFT Filtering Effect





For  $|s_k| < |v_k|$ , the composite log DFT is essentially that of  $v_k$ . Consequently, the resultant log DFT can be approximated as:

$$\log [s_k + v_k] = [\log s_k] \cdot H_1 + [\log v_k + j\text{ARG}(v_k)] \cdot H_2$$

where  $H_1$  and  $H_2$  are as shown in figure 5-3 (b) and (c) and  $|v_k|$  and  $\text{ARG}(v_k)$  are the Rayleigh magnitude and uniform phase as previously derived. The equivalent operation is depicted in figure 5-4.

The implications of this problem can now be seen. The output of the phase unwrapping block of figure 5-4 will be grossly in error if the  $k_0$  of figure 5-3 corresponds to a frequency less than the sampling frequency,  $1/2DT$ . For a given signal to noise level therefore, sampling faster than a prescribed rate has dire consequences. It is, however, desired to sample the input signal as fast as possible, obtaining as many samples of the groundwave as possible before the first skywave arrives. The number of samples so obtained will define  $n_1$  in the complex cepstrum, the quefrency separation between the  $\frac{\sin x}{x}$  terms of  $\hat{p}_a(n)$ . If this number is reasonable, e.g., 4 or more, the estimators can be expected to perform well. If it is less than 4, there will be too much overlap between the terms of  $\hat{p}_a(n)$  to obtain the desired precision. If a greater bandwidth is necessary, some sort of smoothing would have to be applied to the log magnitude and phase curves to reduce the errors introduced by the false branchings due to noise. In such an operation, however, precision is lost in the cepstrum.



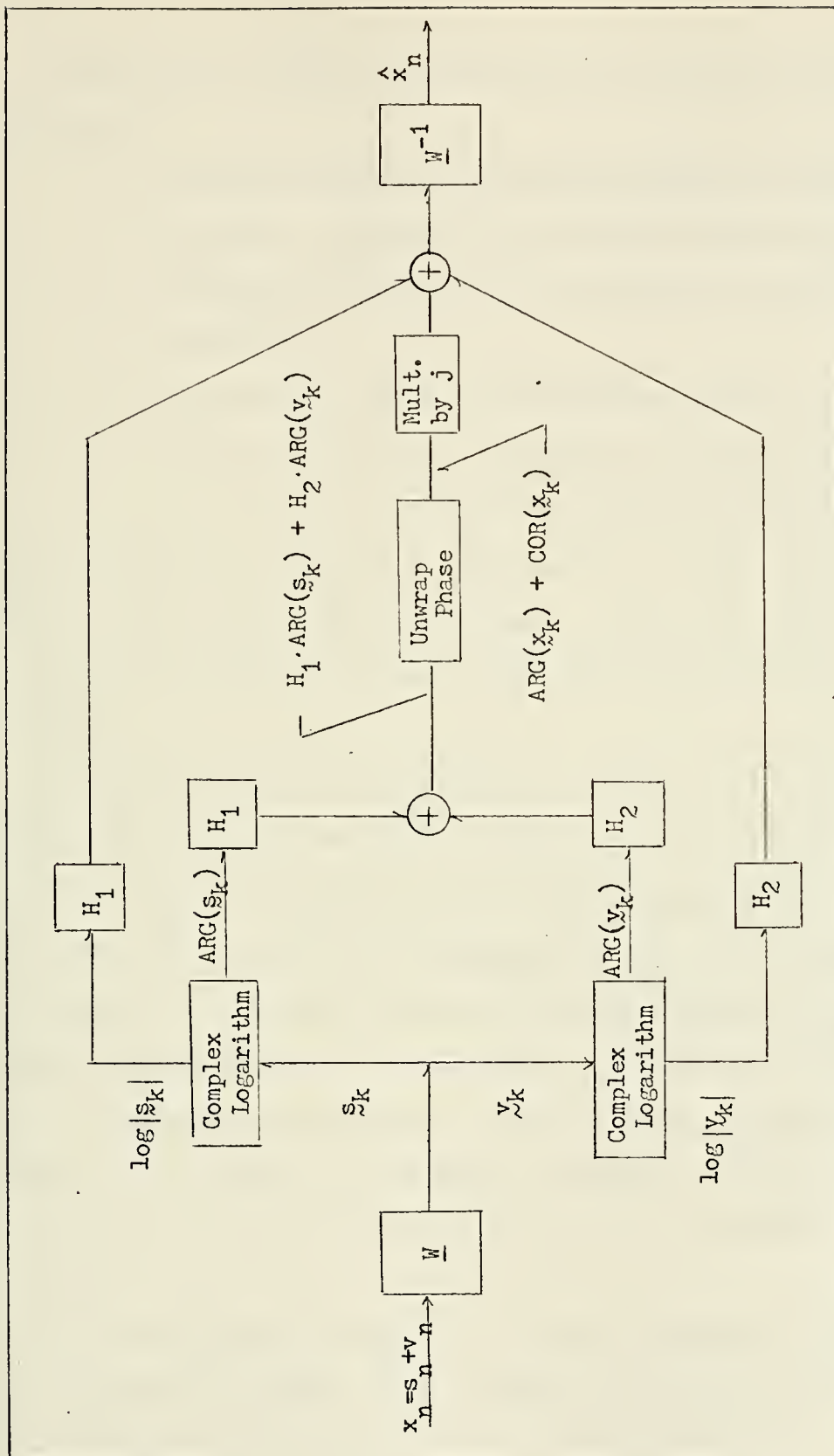


Figure 5-4 Development of Noisy Cepstrum



Consequently, a search for a compromise along the following lines must be made.

1. For high signal to noise ratio, determine the ranges of values of sampling rate and arrival times in which acceptable performance of the cepstrum estimators is achieved.
2. Corresponding to values within these ranges of sampling rate and arrival times, determine the lowest signal to noise ratio for which the estimators will function.

The minimum SNR will determine how many pulses will have to be sampled to obtain the desired performance. Through considerations such as signal stability, a means of evaluating the technique is available.

An example should now be considered to see how well the theory developed thus far fits the results. Signal power is typically defined in terms of the power at the 25 microsecond sampling point. As it turns out, this would be consistent with most other definitions of average power. Consider sampling every 10 microseconds for a 500 microsecond duration and then taking a 512 point DFT ( $N/M \approx 10$ ). Here, the normalized signal power is,  $s_n^2 \approx 0.26$ . For each component of 0 db noise, the variance is therefore,  $\sigma^2 = 0.13$ . For +40 db SNR,  $\sigma^2 = .000013$ . In the DFT,  $\tilde{g}^2 = 50 \sigma^2 = 0.00065$  so that  $\tilde{g} = .0245$ .

From the Rayleigh distribution, it can be determined that  $|s_k| > |y_k|$  with confidence levels .99 and .86 for  $[\log s_k] \approx -3.0$  and -2.6 respectively with  $y_k$  as above. From examination of a noise



free DFT it can be verified that these values are achieved at frequencies of about 27 kHz and 31 kHz. The case was simulated and the resulting magnitude and phase curves are presented in figure 5-5. From the phase curve it can be seen that the noise induced branching begins at about 36 kHz.

For a +30 db SNR, the same confidence levels correspond to frequencies of about 17 kHz and 19.5 kHz. The results of a simulation are shown in figure 5-6 where it can be seen that the first branching occurs at about 23 kHz. For +20 db, the predicted values are 11 kHz and 13 kHz while, as shown in figure 5-7, the branching occurs at about 18 kHz. If the magnitudes of these plots are considered, it can be seen that the frequencies at which branchings could have occurred are nearly exactly as predicted.

The cepstrum for the +40 db case was computed with the following signal parameters:  $\phi_0 = 0$ ,  $DT = 20 \mu\text{sec}$ ,  $T_0 = 20 \mu\text{sec}$ ,  $T_1 - T_0 = 80 \mu\text{sec}$ ,  $B_1 = (\frac{1}{2}, \frac{1}{2})$ . The resulting cepstrum is shown in figure 5-8. As can be seen, the error is small so that the estimators can work properly. As an indication of this, the estimate of the groundwave phase was -0.00822 radians, about a 13 nanosecond error.

In the +30 db case, the phase unwrapping presents problems since the 25 kHz point, i.e., the  $k = N/4$  point, is above the frequency at which  $|\tilde{y}_k| > |\tilde{s}_k|$ . The cepstrum is shown in figure 5-9.

These examples are felt to verify the theoretical limitations of the technique as presented earlier in this chapter. A discussion of the implications is included in the following chapter.





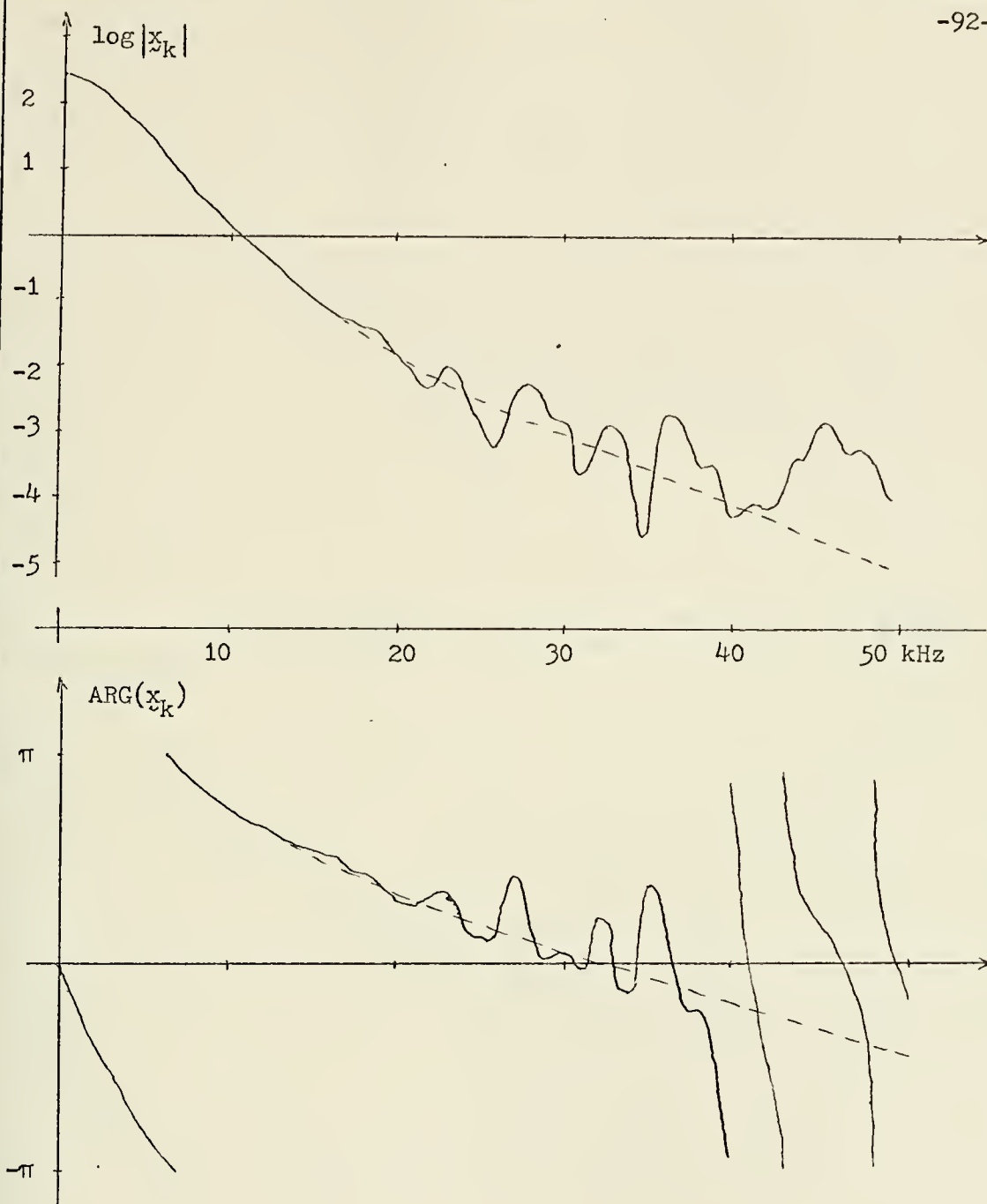


Figure 5-5 + 40 db SNR LOG DFT



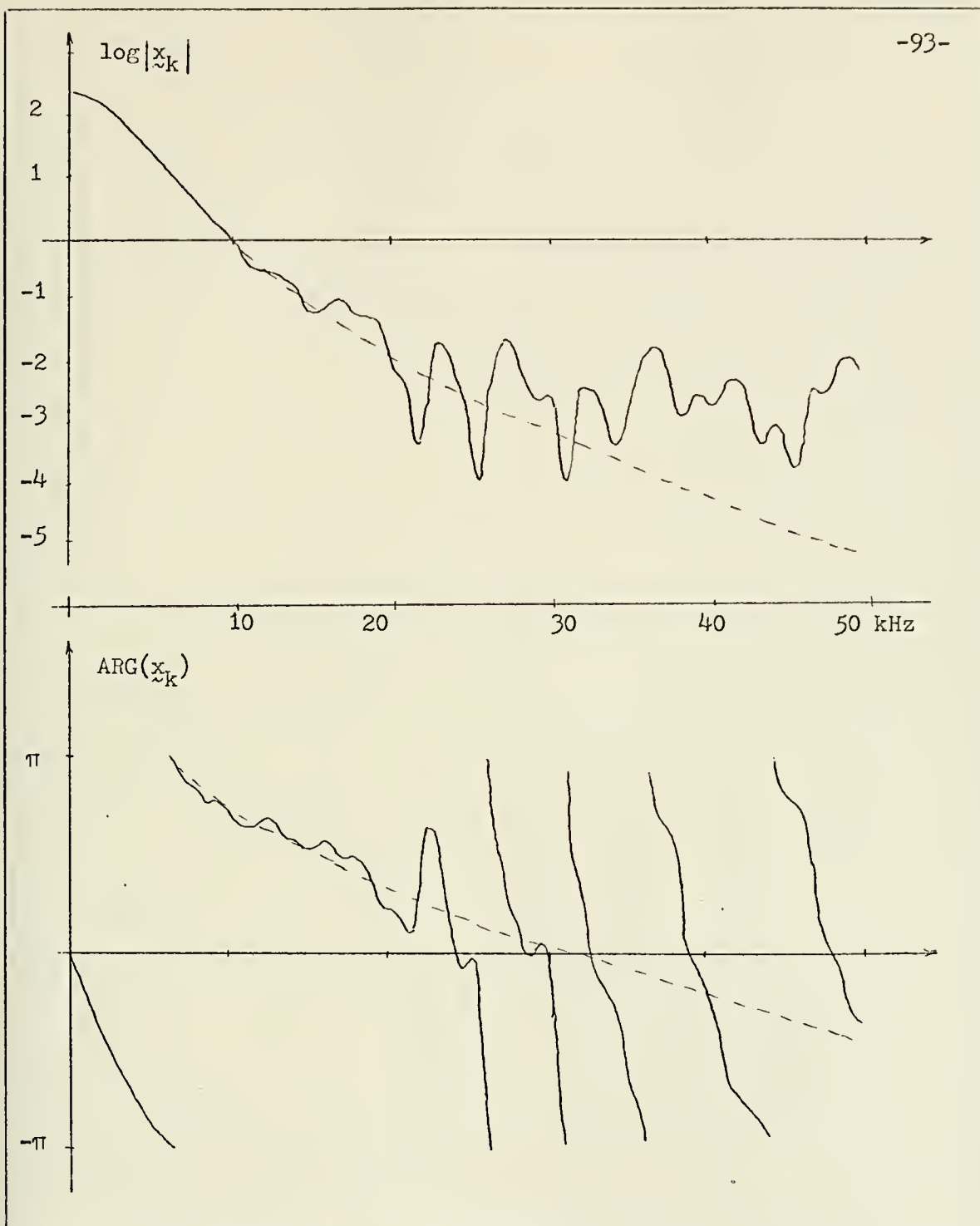


Figure 5-6 + 30 db SNR LOG DFT



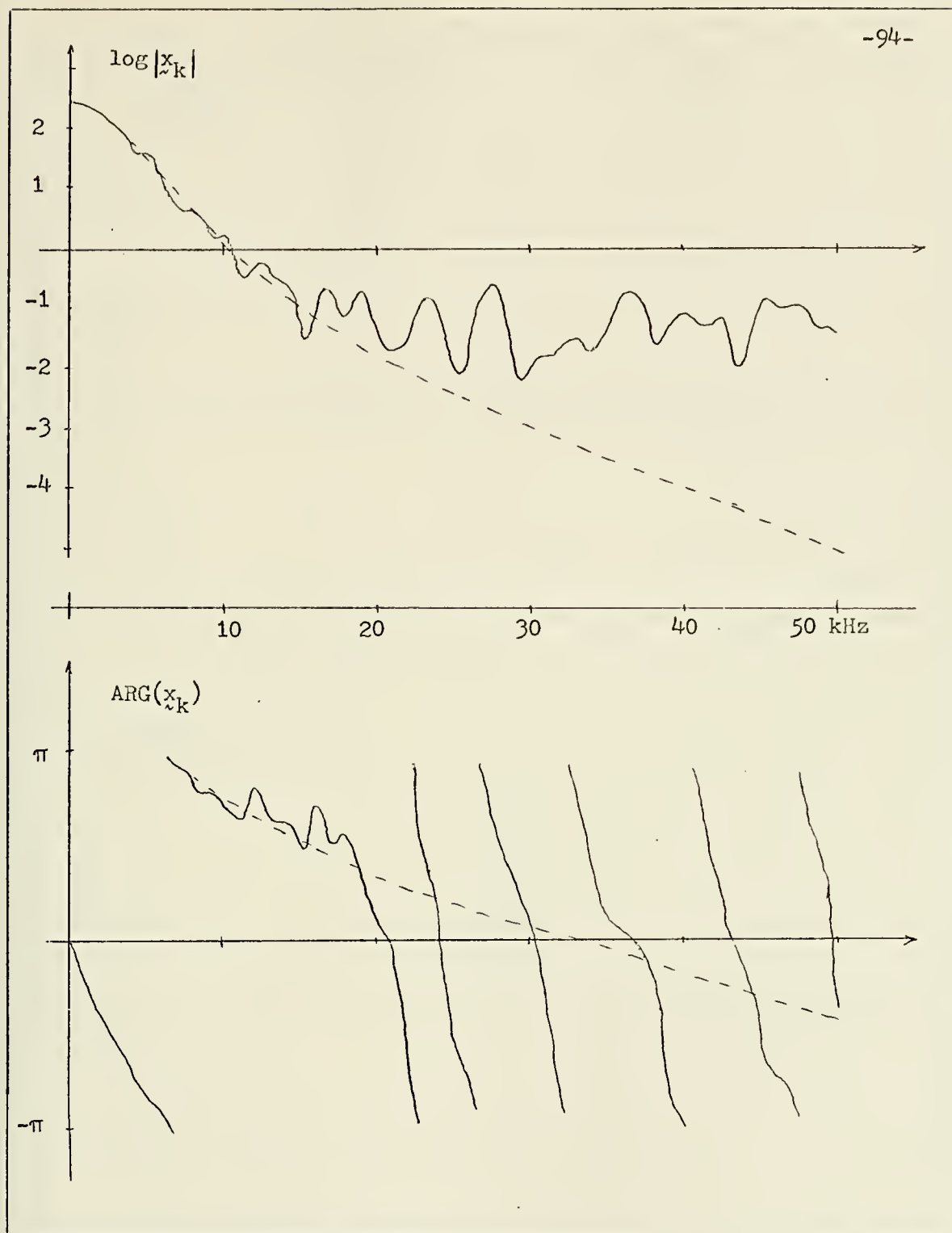


Figure 5-7 + 20 db SNR LOG DFT



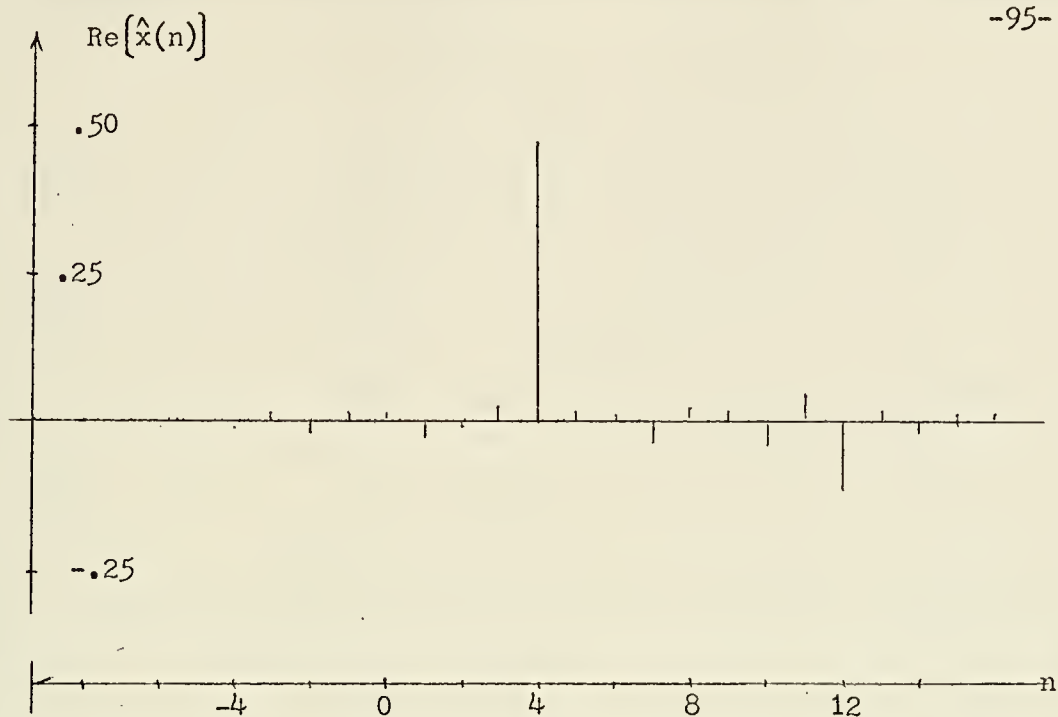


Figure 5-8 + 40 db SNR Cepstrum





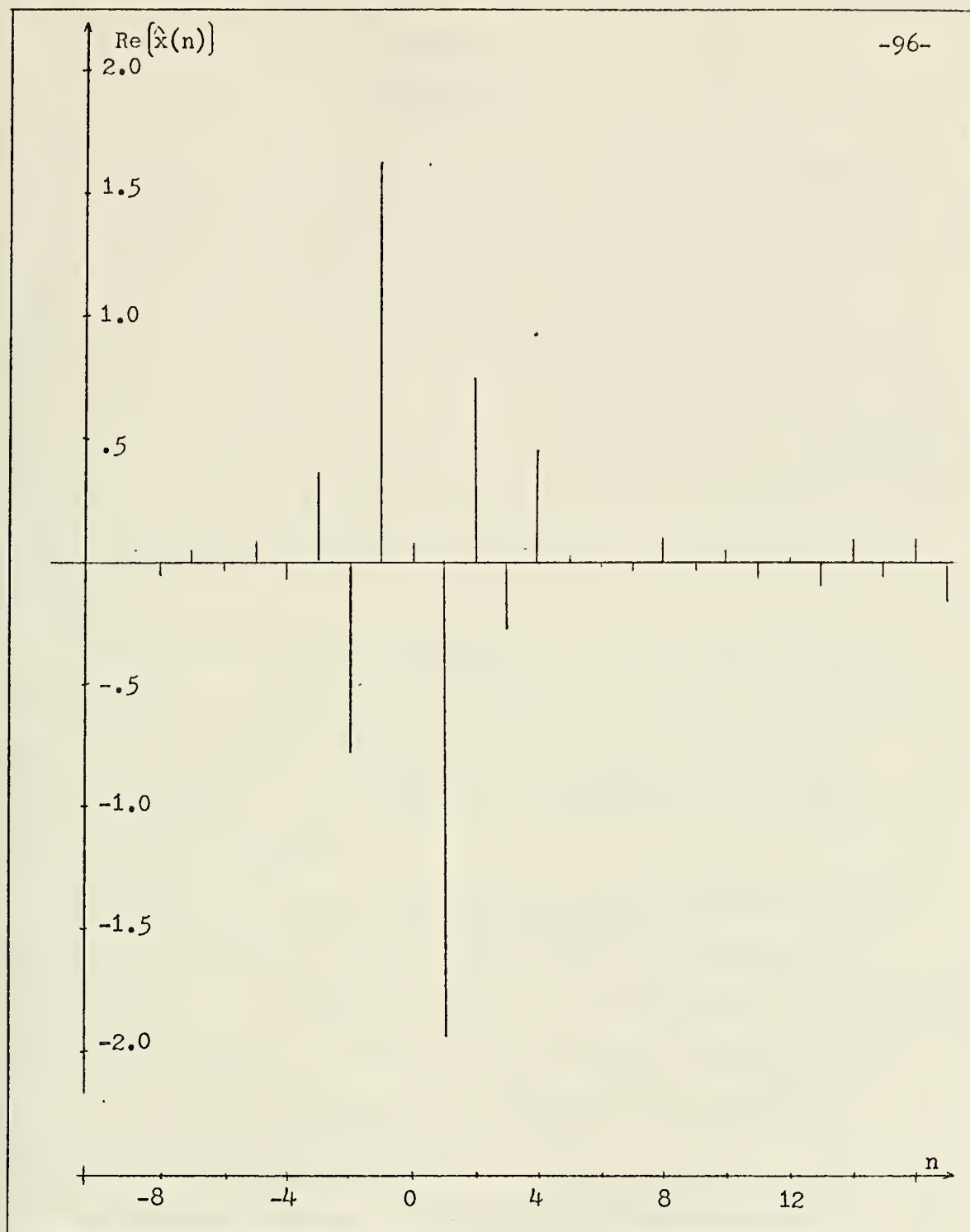


Figure 5-9 + 30 db SNR Cepstrum



## Chapter 6

### CONCLUSIONS

The results of the preceeding chapters will now be summarized.

The cepstrum of an undistorted received Loran-C signal consists of components which are known to within a few parameters. If the noise level is such that a sufficient sampling rate can be employed, the following condition ensues. While there is overlap and interference between the components in the cepstrum, there are ranges of quefrencies, albeit small, in which particular components dominate the sum. In these regions, parameters associated with the dominant component can be estimated.

The performance of the estimators under ideal noise conditions was demonstrated in Chapter 3. The technique estimates the groundwave phase as well as could be desired and has the added advantage of producing estimates of the various other parameters of the signal which could be of interest.

The results of Chapter 4 show that the signal distortion introduced by the propagation paths, of the amount to be anticipated in the Loran-C case, has negligible effect on the estimators. It was also shown that the distortion produced by the receiver filters could be accounted for so that performance is maintained - if the filter responses are reasonably well known.

The results of Chapter 5, although not conclusive, give an indication of the amount of processing time required by the scheme. In the +40 db SNR case, a bandwidth of about 36 kHz was usable. A



corresponding sampling rate of about 14 microseconds would produce values of about 3 and  $-.5$  for  $n_1$  and  $\Delta_1$  respectively in the case of a 35 microsecond skywave arrival time. Such a value of  $n_1$  is a limit for the type of estimators used here. This is due to the fact that the  $\Delta_1$  and  $B_1$  estimators can not make measurements on  $\hat{y}(n_1-2)$  if  $n_1 = 2$  since the zero frequency point is where all of the groundwave magnitude and phase information is mapped to.

It has been the purpose of this thesis to consider only the computational aspects of the application. Consequently, a conclusive statement on the feasibility of implementing the technique can not be made. What can be done however, is to cite some practical limitations of the Loran-C system and to review the results in light of them.

The major conclusion of the results is that a signal to noise ratio of about + 40 db is required. If each individual pulse was at a zero db power level, 10,000 pulses would have to be averaged to achieve the desired performance level. If all eight pulses of a group with a 100,000 microsecond repetition interval were used, this would require an averaging time of just over 2 minutes. Such long times require great signal stability and, of course, preclude use in a navigational application, i.e., on an aircraft or ship. The stability could be achieved in a stationary application, as in a calibration or monitoring receiver, but other effects must be considered.

The eight transmitted pulses are not actually identical. There is some degree of droop in signal power since it is difficult



for signal transmitters to recover from the effects of a large power pulse generated only 1000 microseconds earlier. The effects of such droop can be taken into account somewhat in the sampling-detection schemes presently employed. For a homomorphic filter receiver, however, it may be required that the averaging be accomplished on the first pulse of each group, thereby making the averaging time 16 minutes.

In addition, there are the effects of non-linear filters used to suppress the non-gaussian aspects of the atmospheric noise. These and other non-linearities involved in actual processing would have to be taken into account, especially with regard to whether they change the echoed nature of the signal drastically.

Speculation on the feasibility of the technique therefore leads to the following conclusions. The technique shows good results when applied to the most general signals that can be simulated. In view of the long averaging times and the more complex nature of an actual implementation however, the improvement in performance does not seem marked enough to conclude that it could be effectively implemented.





BIBLIOGRAPHY

1. "The Loran-C System of Navigation," Jansky and Bailey, Inc., Washington, D.C., 1962.
2. Oppenheim, A.V., "Superposition in a Class of Non-linear Systems," Massachusetts Institute of Technology, RLE Technical Report 432, March, 1965.
3. Oppenheim, A.V., Schafer, R.W., and Stockham, T.G., "Nonlinear Filtering of Multiplied and Convolved Signals," Proceedings of the IEEE, vol. 56, August, 1968.
4. Schafer, R.W., "Echo Removal by Discrete Generalized Linear Filtering," Massachusetts Institute of Technology, RLE Technical Report 466, February, 1969.
5. Bogert, B., M. Healy, and J. Tukey, "The quefrency analysis of time series for echoes," Proceedings of the Symposium on Time Series Analysis, M. Rosenblatt, Ed., New York, J. Wiley and Sons, 1963.
6. Cooley, J.W., P.A. Lewis, and P.D. Welch, "The FFT Algorithm: Programming Considerations in the Calculation of Sine, Cosine, and Laplace Transforms," Digital Processing of Signals, Rabiner and Rader, Eds., New York, IEEE Press, 1972.
7. Ulrich, T.J., "Application of Homomorphic Deconvolution to Seismology," Geophysics, Vol. 36, No. 4, August, 1971.
8. Senmoto, S., and D.G. Childers, "Adaptive Deconvolution of a Composite Signal of Identical Unknown Wavelets in Noise," IEEE Transactions on Systems, Man, and Cybernetics, Vol. SMC-2, No. 1, January, 1972.
9. Van Trees, H.L., Detection, Estimation, and Modulation Theory, Part III, J. Wiley and Sons, New York, 1968
10. Jolley, L.B.W., Summation of Series, Dover Publications, New York, 1961.



## Appendix A

### COMPLEX CEPSTRUM DERIVATIONS

This Appendix presents derivations of the complex cepstra of the various signals considered in this thesis. The complex cepstrum of the Loran-C signal, in its most general form, is somewhat complicated. It can, however, be arrived at in the following systematic fashion.

#### A-1 Basic Waveform, Arrival Time Coincident with Sampling Time

Consider first the basic waveform,  $s(t) = t^2 e^{-\alpha t} u_{-1}(t)$ , sampled so that:  $s(n) = n^2 e^{-\alpha n} u_{-1}(n)$ . The first step is to compute the Fourier Transform of this sequence. It can be most easily calculated by utilization of the following property.

$$\text{If,} \quad f(n) \xrightarrow{\quad} F(e^{j\omega}) = \sum_{n=-\infty}^{\infty} f(n) e^{-j\omega n}$$

$$\text{then,} \quad \frac{d}{d\omega} F(e^{j\omega}) = \sum_{n=-\infty}^{\infty} -jn f(n) e^{-j\omega n}$$

$$\text{and,} \quad \frac{d^2}{d\omega^2} F(e^{j\omega}) = \sum_{n=-\infty}^{\infty} -n^2 f(n) e^{-j\omega n}$$

The term on the right side of the above equation is, by definition, the Fourier Transform of  $-n^2 f(n)$ . It follows then that,

$$n^2 f(n) \xrightarrow{\quad} -\frac{d^2}{d\omega^2} F(e^{j\omega})$$

To utilize this property, let  $f(n) = e^{-\alpha n} u_{-1}(n)$ . Then,

$$F(e^{j\omega}) = \sum_{n=0}^{\infty} e^{-\alpha n} e^{-j\omega n} = \left[ 1 - e^{-(\alpha + j\omega)} \right]^{-1}$$



and,

$$\begin{aligned}
 -\frac{d^2}{dw^2} F(e^{jw}) &= -\frac{d^2}{dw^2} \left[ \left[ 1 - e^{-(\alpha+jw)} \right]^{-1} \right] \\
 &= \frac{e^{-(\alpha+jw)} \left[ 1 + e^{-(\alpha+jw)} \right]}{\left[ 1 - e^{-(\alpha+jw)} \right]^3},
 \end{aligned}$$

which is, therefore, the Fourier Transform of  $s(n)$ .

As described in Appendix B, the computation method used in the implementation will remove the linear phase term,  $e^{-jw}$ , thereby yielding a computed transform,

$$S(e^{jw}) = e^{-\alpha} \frac{1 + e^{-(\alpha+jw)}}{\left[ 1 - e^{-(\alpha+jw)} \right]^3}$$

The next step is to compute the complex natural logarithm of  $S(e^{jw})$ .

$$\log S(e^{jw}) = -\alpha + \log \left[ 1 + e^{-(\alpha+jw)} \right] + 3 \log \left[ \frac{1}{1 - e^{-(\alpha+jw)}} \right]$$

Since  $\alpha > 0$ , and therefore,  $\left| e^{-(\alpha+jw)} \right| < 1$ , the following logarithm expansions are appropriate:

$$\log(1+x) = \sum_{n=1}^{\infty} (-1)^{n+1} \frac{x^n}{n}, \quad |x| < 1$$

$$\log\left(\frac{1}{1-x}\right) = \sum_{n=1}^{\infty} \frac{x^n}{n}, \quad |x| < 1$$

Therefore,

$$\begin{aligned}
 \log S(e^{jw}) &= -\alpha + \sum_{n=1}^{\infty} \left[ (-1)^{n+1} \frac{e^{-\alpha n}}{n} e^{-jwn} \right] \\
 (A.1) \quad &+ 3 \sum_{n=1}^{\infty} \left[ \frac{e^{-\alpha n}}{n} e^{-jwn} \right]
 \end{aligned}$$

The final step is to evaluate the inverse Fourier Transform of  $\log S(e^{jw})$  and to denote it as  $\hat{s}(n)$ , the complex cepstrum of  $s(n)$ . In



this case, the form of the expression in equation (A.1) allows the inverse transform to be obtained by inspection since  $\hat{s}(n)$  is the coefficient of  $e^{-j\omega n}$  in its transform.

$$(A.2) \quad \hat{s}(n) = \begin{cases} 0 & , n < 0 \\ -\alpha & , n = 0 \\ \frac{3 + (-1)^{n+1}}{n} e^{-\alpha n} & , n > 0 \end{cases}$$

Two generalizations can be made on the results obtained thus far.

For any constant, B,

$$B s(n) \longrightarrow B S(e^{j\omega}) \longrightarrow \log B + \log S(e^{j\omega}) \longrightarrow (\log B) \delta(n) + \hat{s}(n)$$

so that any coefficient change, real or complex, in the original signal effects only the  $n = 0$  point in the cepstrum - in an additive fashion.

Additionally, consider the effects of sampling the continuous-time function,  $s(t) = t^2 e^{-\alpha t} u_{-1}(t)$ , at a rate  $(1/DT)$ . This yields,

$$\begin{aligned} s(n) &= (n \cdot DT)^2 e^{-\alpha(n \cdot DT)} u_{-1}(n \cdot DT) \\ &= (DT)^2 n^2 e^{-(\alpha \cdot DT)n} u_{-1}(n) \end{aligned}$$

Thus, there is a coefficient change and a virtual change in  $\alpha$ .

Therefore, to compute the cepstrum of  $s(n)$  for various values of  $DT$ , simply modify the expression in equation (A.2) by changing the exponent from  $\alpha$  to  $(\alpha \cdot DT)$  and adding the term  $(\log DT) \delta(n)$ .

## A-2 Basic Waveform Arrival Time Between Sampling Times

The notation in this case becomes a bit awkward and requires explanation. The expression  $\delta(n-x)$ , for non-integer  $x$  will be used. What is implied is that  $s(n) \otimes \delta(n-x)$  is a sampled version of  $s(t) * \delta(t-x)$ .





With this notation, consider

$$s'(n) = s(n) \otimes g(n)$$

$$\text{where } g(n) = \delta(n-\Delta), \quad -0.5 < \Delta < 0.5$$

$$S'(e^{j\omega}) = S(e^{j\omega}) G(e^{j\omega})$$

$S(e^{j\omega})$  will be as derived in the preceeding section and

$$G(e^{j\omega}) = e^{-j\omega\Delta}$$

$$\log G(e^{j\omega}) = -j\omega\Delta$$

The contribution to the cepstrum of  $s'(n)$  due to  $g(n)$  is,

$$\begin{aligned} \hat{g}(n) &= F^{-1} \left[ \log G(e^{j\omega}) \right] = \frac{1}{2\pi} \int_{-\pi}^{\pi} -j\omega\Delta e^{j\omega n} d\omega \\ &= \frac{j\Delta}{2\pi n^2} \left[ e^{jn\pi} (jn\pi - 1) + e^{-jn\pi} (jn\pi + 1) \right] \\ &= \frac{\Delta}{\pi n^2} \left[ -n\pi \frac{e^{jn\pi} + e^{-jn\pi}}{2} + \frac{e^{jn\pi} - e^{-jn\pi}}{2j} \right] \\ &= \frac{\Delta}{\pi} \left[ \frac{\sin n\pi}{n^2} - \frac{\pi n \cos n\pi}{n^2} \right] \end{aligned}$$

For  $n = 0$ ,

$$\hat{g}(n) = \frac{\Delta}{\pi} \left[ 0 - \frac{\pi}{n} \cos n\pi \right] = (-1)^{n+1} \frac{\Delta}{n}$$

For  $n \neq 0$ , consider  $n$  to be a continuous variable and consider the limit,

$$\begin{aligned} \lim_{n \rightarrow 0} \left[ \frac{\sin n\pi}{n^2} - \frac{\pi n \cos n\pi}{n^2} \right] \\ &= \lim_{n \rightarrow 0} \left[ \frac{\pi \cos n\pi - \pi \cos n\pi + \pi^2 n \sin n\pi}{2n} \right] \\ &= \lim_{n \rightarrow 0} \left[ \frac{\pi^2}{2} \sin n\pi \right] = 0 \end{aligned}$$



Consequently,

$$\hat{g}(n) = \begin{bmatrix} 0 & , n = 0 \\ (-1)^{n+1} \frac{\Delta}{n} & , n \neq 0 \end{bmatrix}$$

Since  $s'(n) = s(n) \otimes g(n)$ , so that  $\hat{s}'(n) = \hat{s}(n) + \hat{g}(n)$ , it follows that,

$$\hat{s}'(n) = \begin{bmatrix} (-1)^{n+1} \frac{\Delta}{n} & , n < 0 \\ -\alpha & , n = 0 \\ \frac{(-1)^{n+1} \Delta}{n} + \frac{3 + (-1)^{n+1}}{n} e^{-\alpha n} & , n > 0 \end{bmatrix}$$

### A-3 Multipath Impulse Train

The impulse train, denoted  $p(n)$ , consists of

$$(A.3) \quad p(n) = \delta(n) + B_1 \delta(n-n_1) + \dots + B_m \delta(n-n_m)$$

To begin the derivation, consider the case of  $m = 1$ ,  $|B_1| < 1$ ,

$$p(n) = \delta(n) + B_1 \delta(n-n_1)$$

$$P(e^{j\omega}) = \sum_{n=-\infty}^{\infty} p(n) e^{-j\omega n} = 1 + B_1 e^{-j\omega n_1}$$

$$\begin{aligned} \log P(e^{j\omega}) &= \log [1 + B_1 e^{-j\omega n_1}] \\ &= \sum_{k=1}^{\infty} \left[ (-1)^{k+1} \frac{(B_1 e^{-j\omega n_1})^k}{k} \right] \quad \text{since } |B_1| < 1 \end{aligned}$$

The cepstrum is then,

$$\begin{aligned} \hat{p}(n) &= F^{-1} [\log P(e^{j\omega})] \\ &= \frac{1}{2\pi} \int_{-\pi}^{\pi} \left[ \sum_{k=1}^{\infty} \left[ (-1)^{k+1} \frac{B_1}{k} e^{-j\omega k n_1} \right] e^{j\omega n} \right] d\omega \end{aligned}$$



$$\begin{aligned}
 \hat{p}(n) &= \sum_{k=1}^{\infty} \left[ (-1)^{k+1} \frac{B_1^k}{k} \int_{-\pi}^{\pi} \frac{e^{-j\omega(n-kn_1)}}{2\pi} d\omega \right] \\
 &= \sum_{k=1}^{\infty} \left[ (-1)^{k+1} \frac{B_1^k}{k} \cdot \frac{e^{-j\omega(n-kn_1)}}{j2\pi(n-kn_1)} \right]_{-\pi}^{\pi} \\
 (A.4) \quad \hat{p}(n) &= \sum_{k=1}^{\infty} \left[ (-1)^{k+1} \frac{B_1^k}{k} \frac{\sin \pi(n-kn_1)}{\pi(n-kn_1)} \right].
 \end{aligned}$$

If  $n_1$  is an integer, equation (A.4) becomes

$$\hat{p}(n) = \sum_{k=1}^{\infty} \left[ (-1)^{k+1} \frac{B_1^k}{k} \delta(n-kn_1) \right]$$

so that the echo contributes an impulse train to the cepstrum (for integer  $n_1$ ). In general, of course, the more involved  $\frac{\sin x}{x}$  behavior of equation (A.4) is encountered.

The more general form of equation (A.3) calls for more than one echo. In the case of  $m=2$ ,

$$p(n) = \delta(n) + B_1 \delta(n-n_1) + B_2 \delta(n-n_2).$$

In this case,

$$P(e^{j\omega}) = 1 + B_1 e^{-j\omega n_1} + B_2 e^{-j\omega n_2}$$

If  $|B_1| + |B_2| < 1$ , then

$$\begin{aligned}
 \log P(e^{j\omega}) &= \log \left[ 1 + B_1 e^{-j\omega n_1} + B_2 e^{-j\omega n_2} \right] \\
 &= \sum_{k=1}^{\infty} \left[ (-1)^{k+1} \frac{(B_1 e^{-j\omega n_1} + B_2 e^{-j\omega n_2})^k}{k} \right]
 \end{aligned}$$



This is the inverse Fourier Transform of the cepstrum,

$$\begin{aligned}
 F[\hat{p}(n)] = & B_1 e^{-j\omega n_1} - \frac{B_1^2}{2} e^{-j\omega 2n_1} + \frac{B_1^3}{3} e^{-j\omega 3n_1} - \dots \\
 & + B_2 e^{-j\omega n_2} - \frac{B_2^2}{2} e^{-j\omega 2n_2} + \frac{B_2^3}{3} e^{-j\omega 3n_2} - \dots \\
 & - B_1 B_2 e^{-j\omega(n_1+n_2)} + B_1 B_2 e^{-j\omega(2n_1+n_2)} \\
 & + B_1 B_2^2 e^{-j\omega(n_1+2n_2)} - B_1^3 B_2 e^{-j\omega(3n_1+n_2)} + \dots
 \end{aligned}$$

By a straightforward extension of the previous results, it can be seen that the cepstrum will consist of samples of  $\frac{\sin x}{x}$  functions centered at quefrequencies  $n_1, 2n_1, \dots, kn_1$  and  $n_2, 2n_2, \dots, kn_2$ . Additionally, there are samples of  $\frac{\sin x}{x}$  functions centered at all combinations of multiples of  $n_1$  and  $n_2$ .

Clearly, as the number of echoes increases, the cepstrum of the impulse train quickly becomes complicated and difficult to filter. To overcome some of the complications however, use can be made of the form of the signal information transfer between the time and quefrequency domains. As Schafer<sup>4</sup> has shown, if the cepstrum of a signal is short pass filtered with a cutoff quefrequency of, for example,  $m_0$ , the recovered waveform is identical to the original waveform for time values up to  $m_0$ . Additionally, for reasonably large values of  $m_0$ , the recovered waveform follows the original signal very closely for some time after  $m_0$ . Due to the pulse nature of the Loran signal, this fact makes a combination filter effective.





The cepstrum can be short pass filtered with a cutoff quefreny of about 150  $\mu$ sec. This will retain almost all of the groundwave information but remove much of the complicated impulse train contribution. A simple example can illustrate the effectiveness of this approach. Suppose  $n_1 \approx 40 \mu$ sec,  $n_2 \approx 80 \mu$ sec, and  $n_3 \approx 120 \mu$ sec. If a cutoff quefreny of 150  $\mu$ sec is used, sampled  $\frac{\sin x}{x}$  functions centered at the following quefrenies are retained:

$$n_1, 2n_1, 3n_1, 4n_1$$

$$n_2, 2n_2$$

$$n_3$$

$$n_1+n_2, 2n_1+n_2, 3n_1+n_2$$

Some of the above quefrenies are above the 150  $\mu$ sec cutoff, but close enough that their effects may be felt in the pass band. Other sampled  $\frac{\sin x}{x}$  functions are centered at quefrenies far enough removed from the cutoff that they may be considered removed by the short pass filter. Consequently only the quefrenies listed above have to be considered in the more elaborate filter-estimators of Chapter 3.

#### A-4 Cepstrum for Exponentially Weighted Signals

The multipath impulse train thus far has been considered to be

$$p(n) = \delta(n-n_0) + B_1 \delta(n-n_1) + B_2 \delta(n-n_2) + \dots + B_k \delta(n-n_k)$$

with the following condition met:

$$(A.5) \quad \sum_{m=1}^k |B_m| < 1$$



This ensured that the groundwave was the dominant component of the composite signal and allowed the expansion of  $\log P(e^{j\omega})$  in the manner presented. As will be shown in Appendix B, this is part of a set of conditions sufficient to ensure a complex cepstrum of the form desired for the methods of this thesis.

In the interesting Loran-C cases this condition is typically not met. The problems can be circumvented however, by exponentially weighting the signal in the manner to be described. Suppose

$$\begin{aligned} x(t) &= s(t) + B_1 s(t-T_1) \\ &= t^2 e^{-\alpha t} u_{-1}(t) + B_1 (t-T_1)^2 e^{-\alpha(t-T_1)} u_{-1}(t-T_1) \\ &\quad \text{with } |B_1| > 1 \end{aligned}$$

If the signal is multiplied by  $e^{-\beta t}$ , what results is

$$\begin{aligned} e^{-\beta t} x(t) &= t^2 e^{-(\alpha+\beta)t} u_{-1}(t) + B_1' (t-T_1)^2 e^{-(\alpha+\beta)(t-T_1)} u_{-1}(t-T_1) \\ &\quad \text{where } B_1' = B_1 e^{-\beta T_1} \end{aligned}$$

If  $\beta$  is such that  $|B_1'| < 1$ , the condition of equation (A.5) is satisfied. The resulting cepstrum will be as previously derived with  $\alpha$  replaced by  $(\alpha+\beta)$  and  $B_1$  replaced by  $B_1'$ . The cepstrum can then be computed and filtered in the manner developed in this thesis. If it is desired to recover the original signal after filtering, the filtered signal can be multiplied by  $e^{+\beta t}$  as a final step.



The results of the above argument can be generalized to the case of multiple echoes to obtain the requirement that

$$\sum_{m=1}^k |B_m| e^{-\beta T_m} < |B_0| e^{-\beta T_0}$$



## Appendix B

### PHASE UNWRAPPING CONSIDERATIONS

As mentioned in Chapter 1, the computation of the complex logarithm of the DFT of the signal presents problems. A computation on a point by point basis via an arctangent power series expansion will only provide the principle value of the desired phase. What would result in the case of a typical Loran-C signal might produce a phase plot as in figure B-1 (the dotted lines).

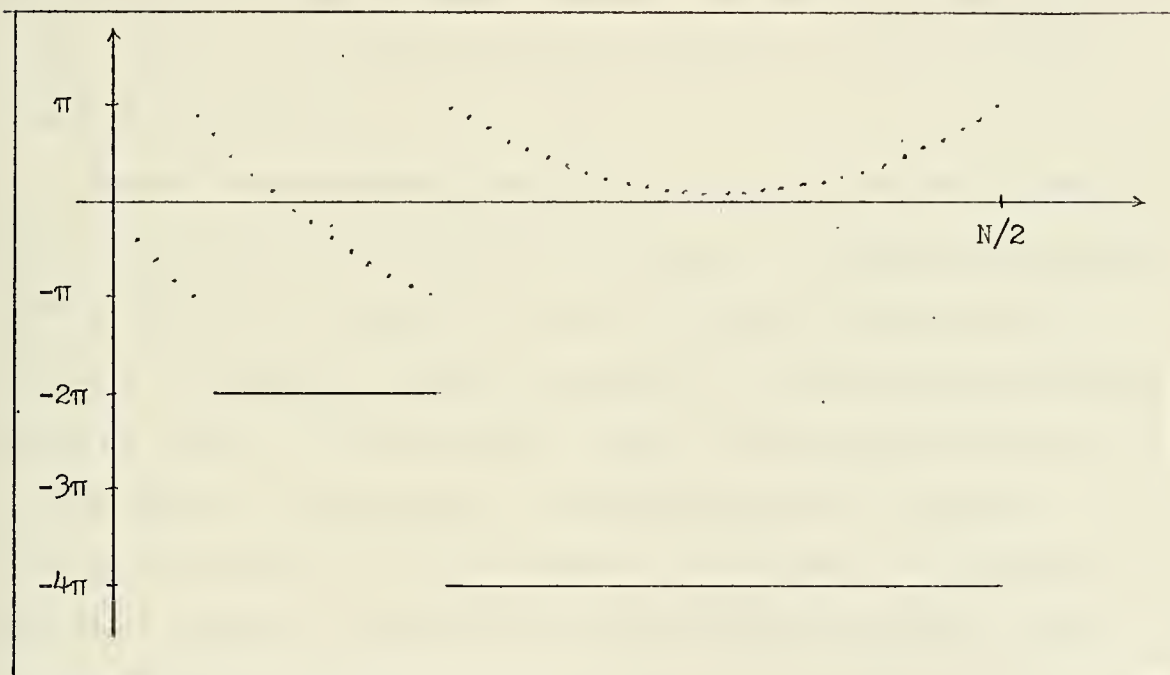


Figure B-1 Uncorrected Phase Curve

It is desired to remove the discontinuities induced by the branching of the arctangent function for the following reason. If  $x(n) = s(n) \otimes p(n)$ , then it is desired that

$$\log X(e^{j\omega}) = \log S(e^{j\omega}) + \log P(e^{j\omega})$$





In particular, the above equality must hold for both the real and imaginary parts of the expression. Thus,

$$\begin{aligned} \log X(e^{j\omega}) &= \log S(e^{j\omega}) + \log P(e^{j\omega}) \\ \text{and,} \\ \arg X(e^{j\omega}) &= \arg S(e^{j\omega}) + \arg P(e^{j\omega}) \end{aligned} \quad (B.1)$$

If, for example, there is some value of  $\omega$  for which  $\arg S(e^{j\omega})$  has a value  $3\pi/4$ , and  $\arg P(e^{j\omega})$  has a value  $\pi/2$ , then the right side of equation (B.1) equals  $5\pi/4$ . However,  $\arg X(e^{j\omega})$ , as evaluated by the arctangent power series will have a value of  $-3\pi/4$  so that the equality is violated.

Schafer<sup>4</sup> has described a method for removing the discontinuities. After the complex log of the DFT of the signal is computed, a sequence with imaginary part appearing as the dotted lines in figure (B-1) results. The imaginary part of the sequence is then scanned to detect jumps of almost  $2\pi$  in consecutive values. For appropriate values of  $k$  at which these jumps occur, a correction sequence is generated. This is represented by the heavy lines in the figure. The correction sequence is added to the originally computed phase sequence as shown in figure B-2.

As can be seen from the corrected phase, there is typically a large linear phase term involved. Since this term can easily dominate the phase plot, and the resulting complex cepstrum, it should be removed if it has no effect on the results. Schafer's method is to examine the value of the corrected phase curve for values of  $k$  near  $N/2$ .



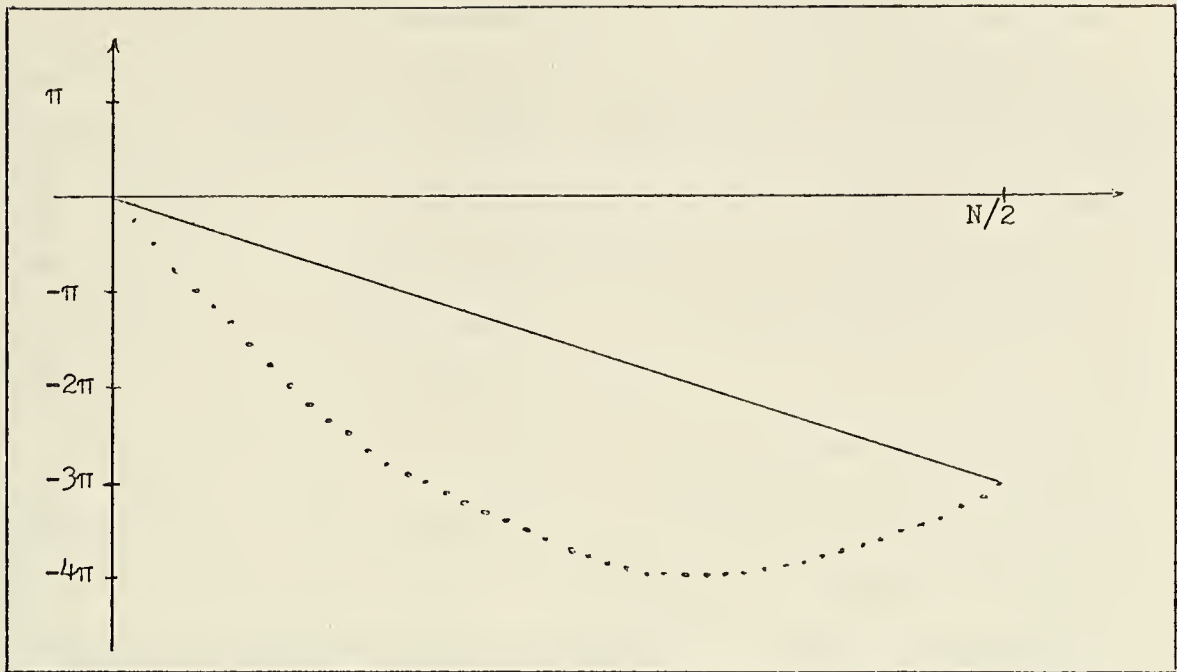


Figure B-2 Corrected Phase Curve

The integer multiple of  $\pi$  that is closest to this value is called the linear phase term. From this value, the straight line shown in figure B-2 can be generated. If this is subtracted from the corrected phase curve, a final version of the phase, as in figure B-3 results.

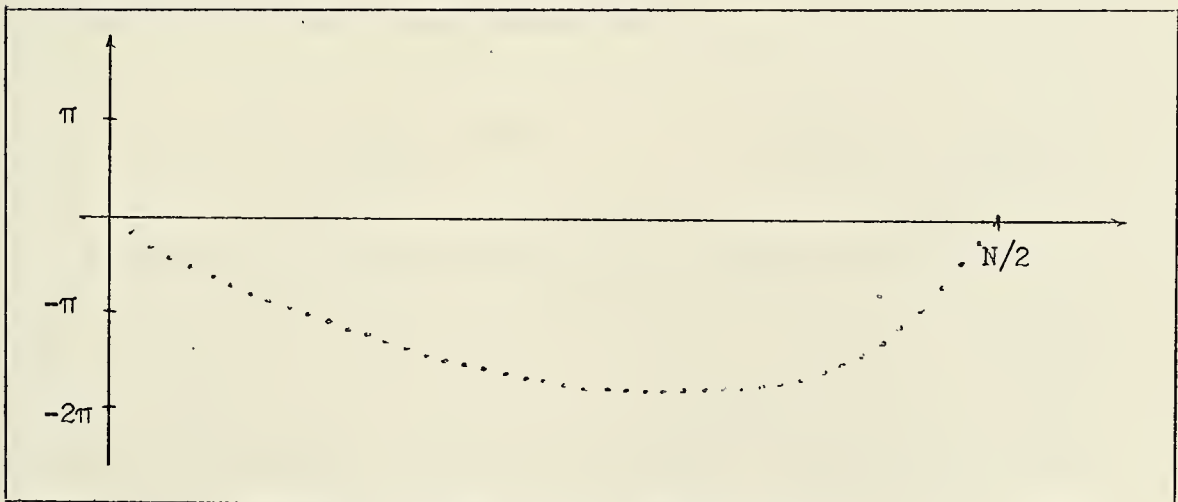


Figure B-3 Corrected Phase Curve - Final Version



The effect of this last operation is to multiply the DFT of the signal by  $e^{-j\omega m_0}$  where  $m_0$  is the integer linear phase term deduced in the manner described above. This is equivalent to convolving the signal with  $\delta(n-m_0)$  - or shifting the sequence  $m_0$  time samples. As a final step after the filtering is accomplished and the inverse operation is performed, the recovered signal can be re-shifted this amount to produce an output with a proper time base.

The corrected complex logarithm is now continuous and periodic, and the desired complex cepstrum can be computed from it. In effect, what is presumed here is that the branchings of the phase curve are caused, in a systematic fashion throughout the complex log sequence, by the same linear phase term. This presumption should be examined more closely. Consider the impulse train component of a typical echoed signal,

$$p(n) = \sum_{i=0}^k B_i \delta(n-n_i)$$

The Fourier Transform of this sequence is

$$P(e^{j\omega}) = \sum_{i=0}^k B_i e^{-j\omega n_i} \quad \text{where } B_i = |B_i| e^{j\phi_i}$$

The following analysis will consider the form of  $P(e^{j\omega})$  for various values of the  $|B_i|$ 's,  $\phi_i$ 's, and  $n_i$ 's. To begin the analysis, let  $B_0 = 1$ ,  $\phi_0 = 0$ ,  $n_0 = 0$ , and  $k = 1$ . Furthermore, let  $B_1$  be real, positive and less than 1 with  $n_1 = \text{an integer}$ . What results in this case is,



$$P(e^{jw}) = 1 + B_1 e^{-jwn_1}$$

$$0 < B_1 < 1$$

$$n_1 = \text{an integer}$$

A vector diagram representation of  $P(e^{jw})$  is as shown in figure B-4.

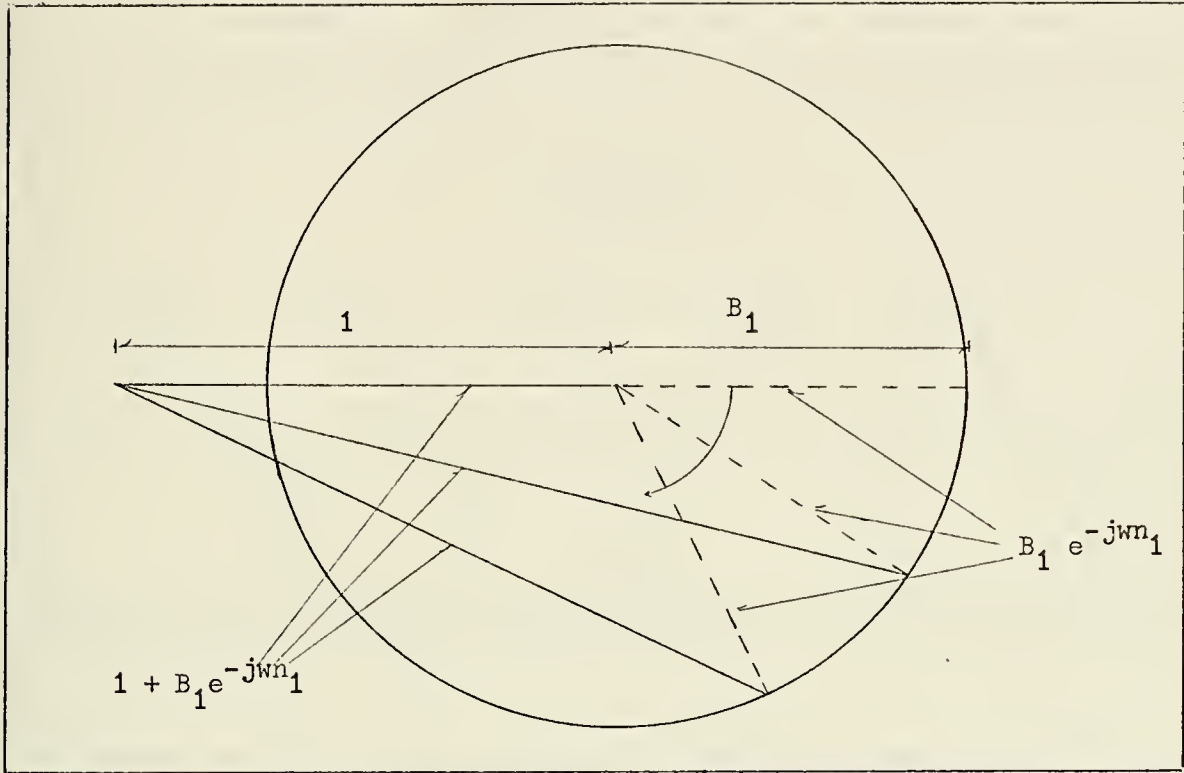


Figure B-4 Vector Representation of  $P(e^{jw})$

As  $w$  ranges from  $-\pi$  to  $\pi$ , the term  $B_1 e^{-jwn_1}$  traces out the circle  $n_1$  times. If  $B_1$  is complex, i.e.  $B_1 = |B_1| e^{j\phi_1}$ ,  $\phi_1 \neq 0$ , the dashed line of figure B-4 begins (for  $w = 0$ ) at an angle  $\phi_1$  with the line representing the vector 1. Importantly, as long as  $|B_1| < 1$ , the branch point at  $\pm\pi$  of the arctangent function defining the phase is avoided. Consequently the magnitude and phase of  $P(e^{jw})$  are as plotted in figure B-5.

For  $|B_1| < 1$ , A, the maximum value of the phase in figure B-5(b), is always less than  $\pi/2$ . If  $n_1$  is not an integer, the  $B_1 e^{-jwn_1}$  vector





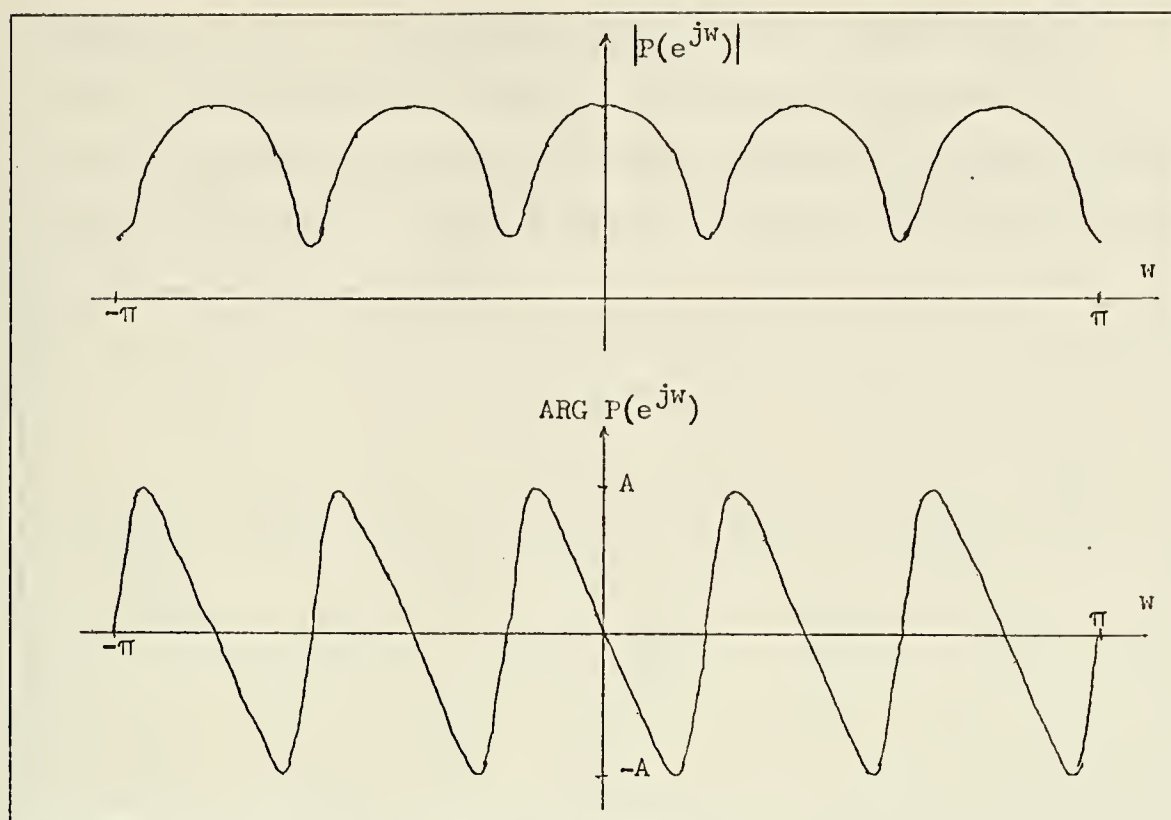


Figure B-5 Magnitude and Phase of  $P(e^{jw})$

in figure B-4 starts in line with the 1 vector but ends up, for  $w = \pi$ , at some arbitrary angle. In terms of figure B-5, this means the plot is essentially the same - except that the  $w = \pm\pi$  points are no longer nulls or peaks of the magnitude curve, nor zeroes of the phase curve. For  $B_1 = |B_1| e^{j\phi_1}$ ,  $\phi_1 \neq 0$ , the entire plot of figure B-5 is shifted to the right or left.

With these preliminaries, more general impulse trains can be considered. Suppose

$$p(n) = \delta(n-n_0) + B_1 \delta(n-n_1-n_0).$$

Consider first, the case wherein  $n_0 = 1$ ,  $B_1 =$  a real, positive



number less than 1. The magnitude of  $P(e^{j\omega})$  will be as in figure B-5(a). The phase however, will be as in figure B-6(a). When the two step correction procedure is employed as previously described, what results is presented in figure B-6(c) and is seen to be identical to the phase curve of figure B-5(b).

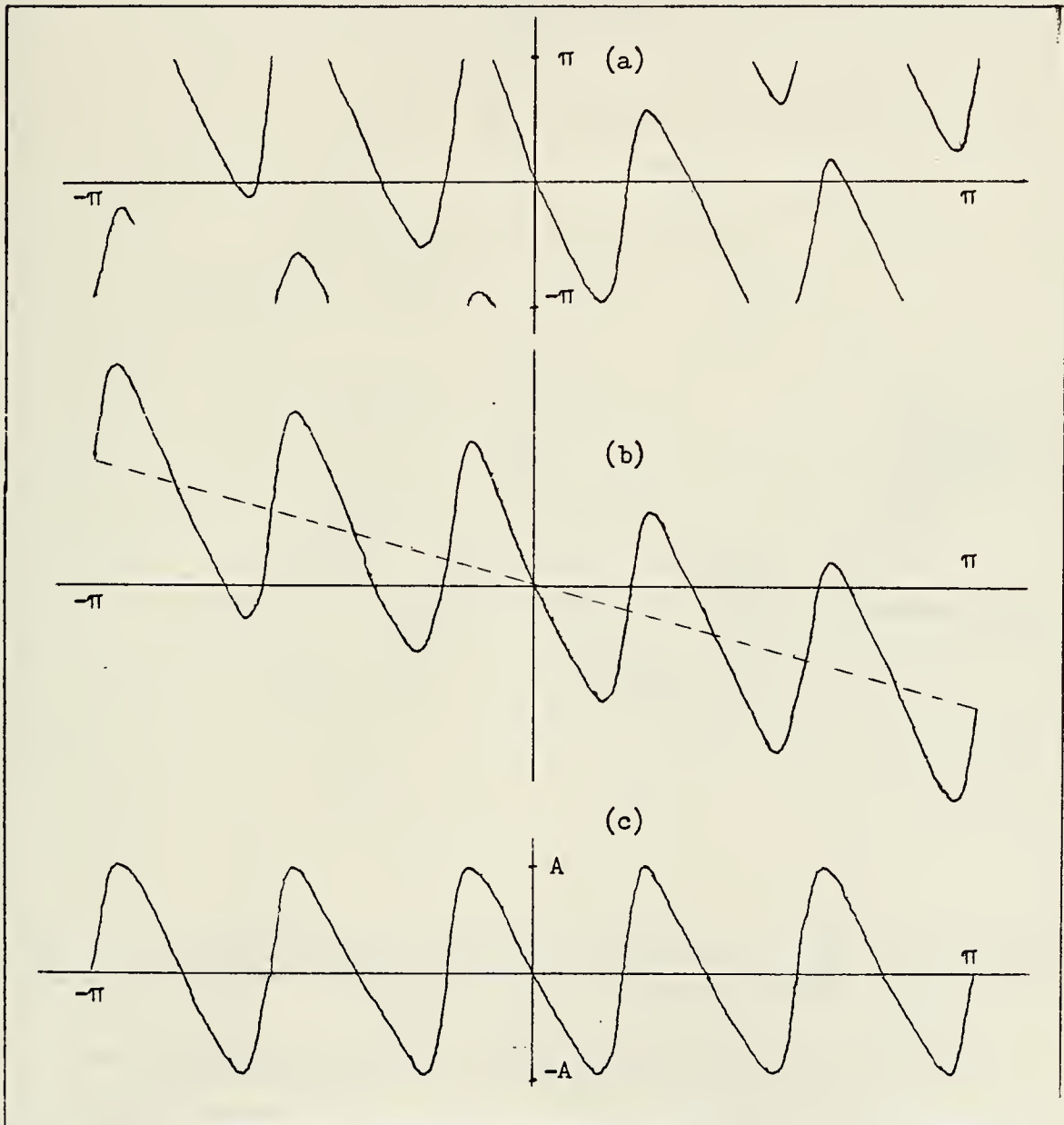


Figure B-6 Frequency Representation of  $P(e^{j\omega})$  With Linear Phase



A vector diagram of  $P(e^{jw})$ , parametric in  $w$ , is shown for this case in figure B-7. Notice that the total resultant number of crossings of the branch line is one, i.e.  $n_0$ . This is true independent of the orientation of the axes in the figure, i.e. for arbitrary  $\phi_0$ .

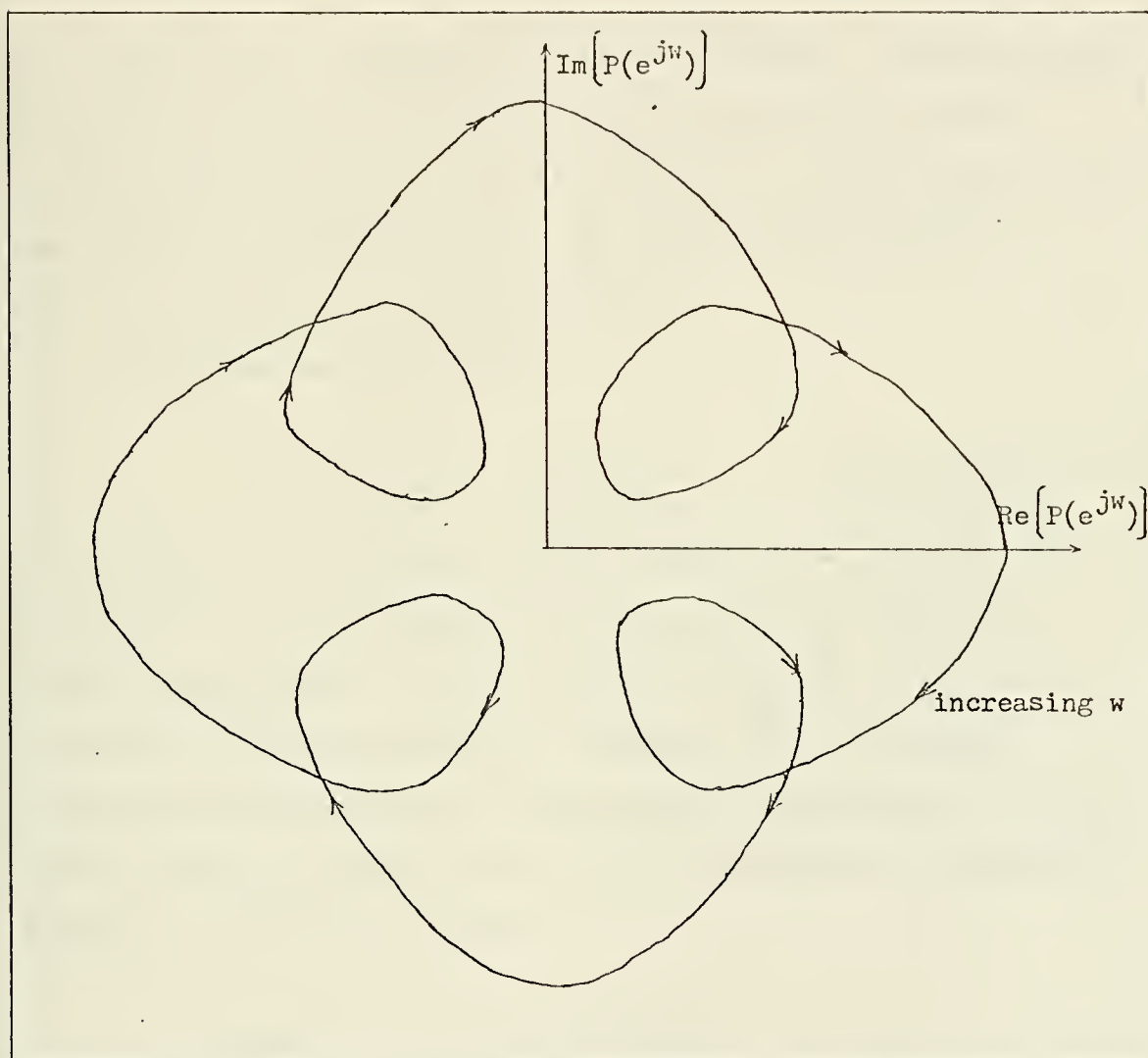


Figure B-7 Vector Representation of  $P(e^{jw})$  with Linear Phase

The following summary can be made of the results thus far. If

$$p_1(n) = \delta(n) + B_1 \delta(n-n_1)$$

$$|B_1| < 1$$



and,

$$p_2(n) = \delta(n-n_0) + B_1 \delta(n-n_1-n_0) \quad |B_1| < 1$$

$n_0 = \text{an integer}$

then,

$$p_2(n) = p_1(n) \times \delta(n-n_0),$$

i.e.,  $p_2(n)$  is  $p_1(n)$  shifted  $n_0$  samples to the right. Since any linear phase term is removed in the computation,  $p_1(n)$  and  $p_2(n)$  become identical signals beyond the complex log stage in the processing. It need merely be remembered to shift the recovered signal back  $n_0$  samples as a final step in the second case.

Now consider the case wherein

$$p(n) = \delta(n) + B_1 \delta(n-n_1) \quad B_1 = |B_1| > 1.$$

The resulting phase curve is as shown in figure B-8. What can be seen is that the linear phase term is due to  $n_1$ . The ripples in B-8(c) are as in figure B-5(b) but reversed in sense. This can be attributed to the fact that the 1 vector in  $P(e^{j\omega})$  is rotating counterclockwise relative to the linear phase term associated with  $n_1$ . Further light can be shown on the effect by considering the logarithm expansion of  $P(e^{j\omega})$  in this case.

$$\begin{aligned} \log P(e^{j\omega}) &= \log \left[ 1 + B_1 e^{-j\omega n_1} \right] \\ &= \log \left[ B_1 e^{-j\omega n_1} \right] + \log \left[ 1 + B_1^{-1} e^{+j\omega n_1} \right] \\ &= -j\omega n_1 + \log B_1 + \sum_{k=1}^{\infty} \left[ (-1)^{k+1} \frac{B_1^{-k}}{k} e^{j\omega k n_1} \right] \end{aligned}$$





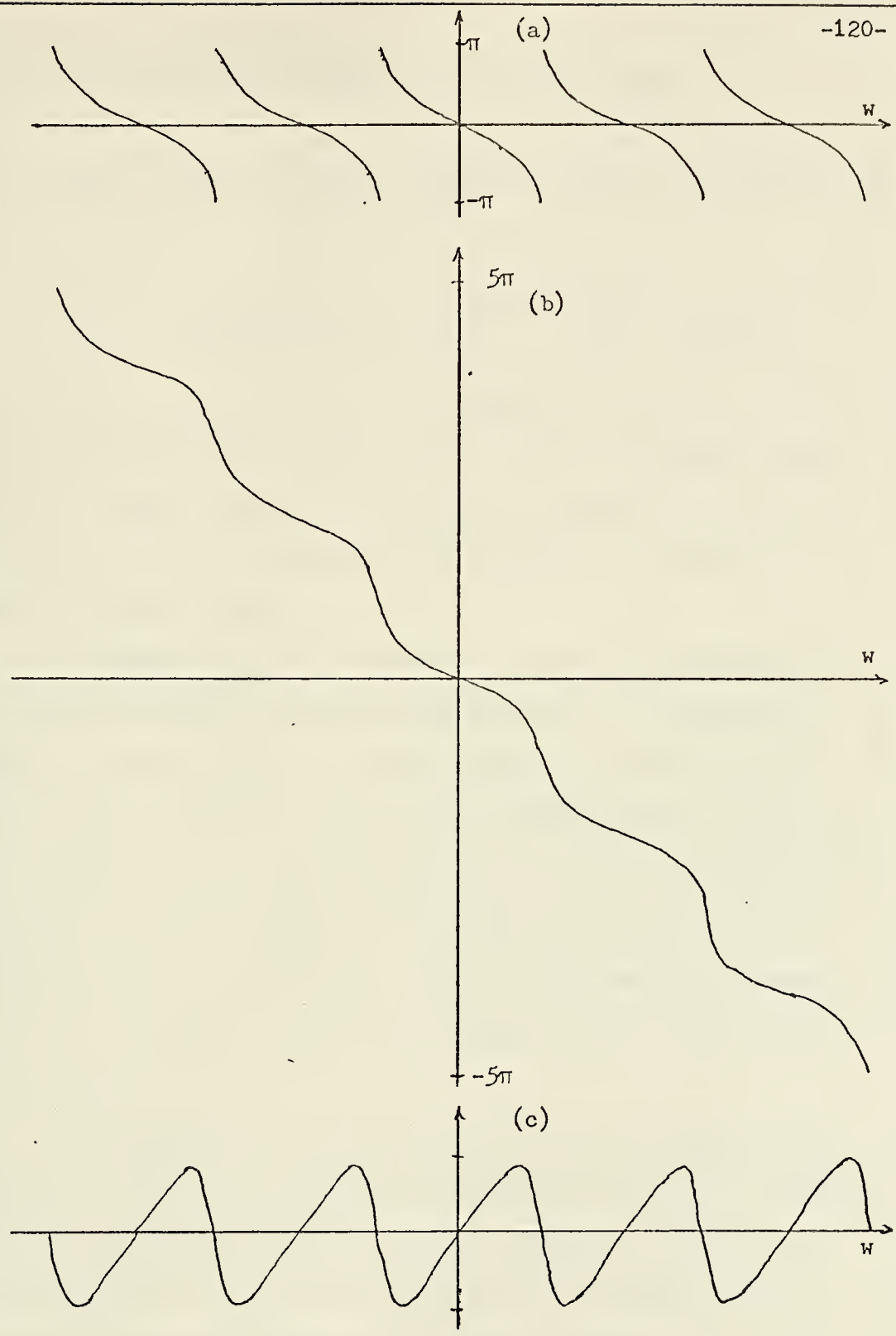


Figure B-8  $P(e^{j\omega})$  Phase,  $B_1 > 1$



With the linear phase term removed, the cepstrum becomes

$$\begin{aligned}\hat{p}(n) &= (\log B_1) \delta(n) + \sum_{k=1}^{\infty} \left[ (-1)^{k+1} \frac{B_1^{-k}}{2\pi k} \int_{-\pi}^{\pi} e^{jw(n+kn_1)} dw \right] \\ &= (\log B_1) \delta(n) + \sum_{k=1}^{\infty} \left[ (-1)^{k+1} \frac{B_1^{-k}}{k} \delta(n+kn_1) \right]\end{aligned}$$

for an integer  $n_1$ . This means that the impulse train appears in the negative quefrency portion of the cepstrum. What is further implied is that the largest component of the signal contributes to the low quefrency portion of the cepstrum while the smaller components produce the impulse trains.

In the Loran-C case, it is desired to recover the groundwave (or at least to treat it as the primary component). Consequently exponential weighting is used to ensure that the groundwave is the largest signal. This also simplifies the filtering process since, in a multiple echo case, in which a middle echo is the largest, impulses would appear in both the negative and positive quefrency regions. Additionally, various cross product terms in the logarithm expansion would produce impulses throughout the cepstrum (e.g., at  $n_2 - 2n_1$ ,  $n_3 - 3n_1$ , etc.)

From figure 8.8(b), it can be seen how easily the linear phase component can obscure the important information in the phase sequence. Clearly, it is important that this term be removed. However, in a multiple echo case, the discontinuities need not be caused merely by the linear phase component of the dominant signal. In terms of



the logarithm expansion,

$$\log P(e^{j\omega}) = \log \left[ \sum_{i=0}^k B_i e^{-j\omega n_i} \right]$$

the requirement can be seen to be

$$(B.2) \quad |B_0| > \left| \sum_{i=1}^k B_i e^{-j\omega n_i} \right|$$

to ensure that branching is due only to the linear phase term associated with  $n_0$ .

Schafer states that, after low pass filtering to avoid aliasing, the condition,

$$(B.3) \quad \sum_{i=1}^k |B_i| < |B_0|$$

is sufficient to meet the requirement of equation (B.2). This is certainly consistent with everything presented thus far and would be true if an ideal analog low pass filter were employed. In such a case, the condition of equation (B.3) could be met via exponential weighting as presented in Appendix A. However, for an analog filter with a finite passband to stopband transition width, the effects of aliasing should be examined more closely.

As it develops, for transforms with ripples as in figure B-5(a), the effects of aliasing can cause large amounts of distortion in the phase which can not be overcome by analog filtering. To show this, a more in-depth development of the DFT must be presented. As an example, the DFT of a sequence is represented by the dotted lines in figure B-9 (the sequence is  $e^{-n} u_{-1}(n)$ ). The solid lines in the figure



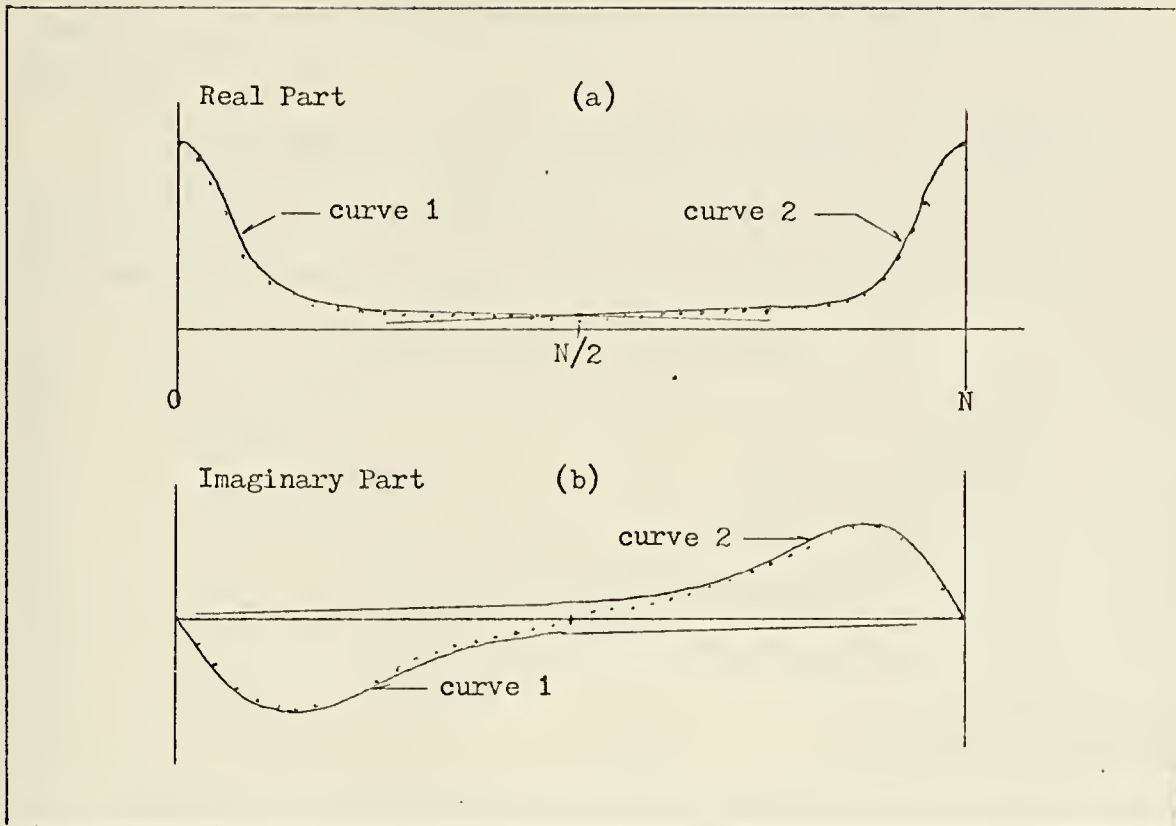


Figure B-9 Real and Imaginary Part of  $e^{-n}u_{-1}(n)$  DFT

represent the continuous Fourier Transform of the corresponding continuous time function depicted in a manner appropriate for comparison with the DFT, i.e., with the negative frequencies shown to the left of  $k = N$ .

It would, of course, be desired that the DFT would consist of samples of the appropriate solid lines, i.e., samples of curve 1 for  $k < N/2$  and samples of curve 2 for  $k > N/2$ . As is the case however, the DFT is actually samples of the sum of the two curves for all values of  $k$ . Due to the bandwidth of the signal and the sampling rate employed in this case, it appears that the aliasing has a negligible effect. The only errors that appear remotely discernible are in the





imaginary part of the DFT for values of  $k$  near  $N/2$ , and even these are small.

If the DFT is shown via its magnitude and phase as in figure B-10 however, the evaluation changes. There is a large error in the phase for a wide range of values of  $k$  in the vicinity of  $N/2$ .

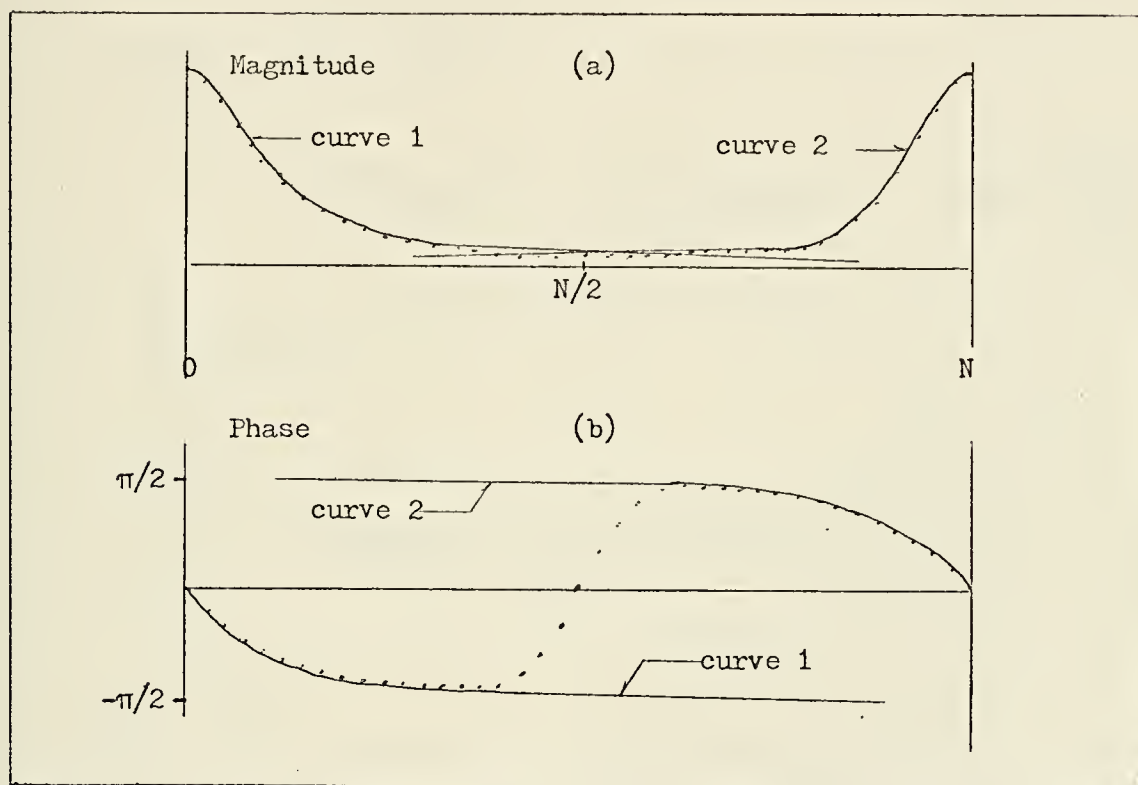


Figure B-10 Magnitude and Phase of  $e^{-n} u_{-1}(n)$  DFT

What can be seen is that for  $k < N/2$ , the composite phase is in the same quadrant as that of curve 1. For  $k > N/2$ , the composite phase is in the same quadrant as the phase of curve 2. This is due to the fact that the magnitude of the continuous Fourier Transform of  $e^{-t} u_{-1}(t)$  decreases monotonically with frequency. Consequently the aliased signal (curve 1 for  $k > N/2$ , curve 2 for  $k < N/2$ ) is always



smaller than the desired signal so that the sum is dominated by the correct signal and the resulting phase is of the correct sign.

With this background, the actual signals treated in this thesis should be considered to show what can possibly go wrong. Suppose

$$x(n) = s(n) \otimes p(n)$$

so that

$$\begin{aligned} X(e^{j\omega}) &= S(e^{j\omega}) P(e^{j\omega}) \\ &= |S(e^{j\omega})| \cdot |P(e^{j\omega})| \exp \left[ j \left[ \arg S(e^{j\omega}) + \arg P(e^{j\omega}) \right] \right] \end{aligned}$$

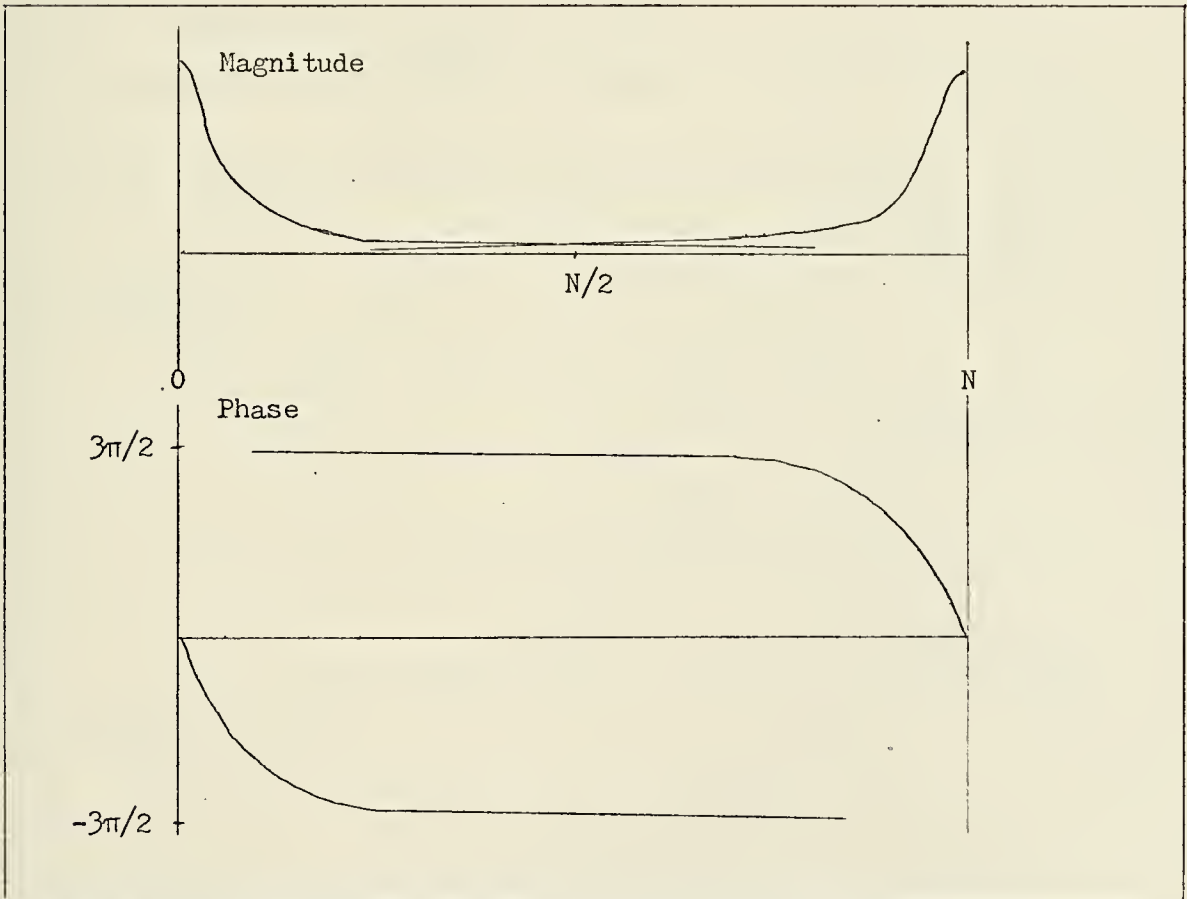


Figure B-11 Magnitude and Phase of Loran-C Signal Transform



The magnitude and phase of the continuous Fourier Transform of  $s(t)$ , the Loran-C signal, are shown in figure B-11. What is important to notice is that, for values of  $k$  less than, but nearly equal to,  $N/2$ , curves 1 and 2 are nearly  $180^\circ$  out of phase (modulo  $2\pi$ ).

Now suppose that

$$p(n) = \delta(n) + B_1 \delta(n-n_1-\Delta_1)$$

$$\text{where } B_1 = 0.8$$

$$n_1 = \text{an integer}$$

$$\Delta_1 = -.5$$

so that

$$P(e^{j\omega}) = 1 + .8 e^{-j\omega(n_1+\Delta_1)}$$

The vector plot of this  $P(e^{j\omega})$  is as shown in figure B-12.

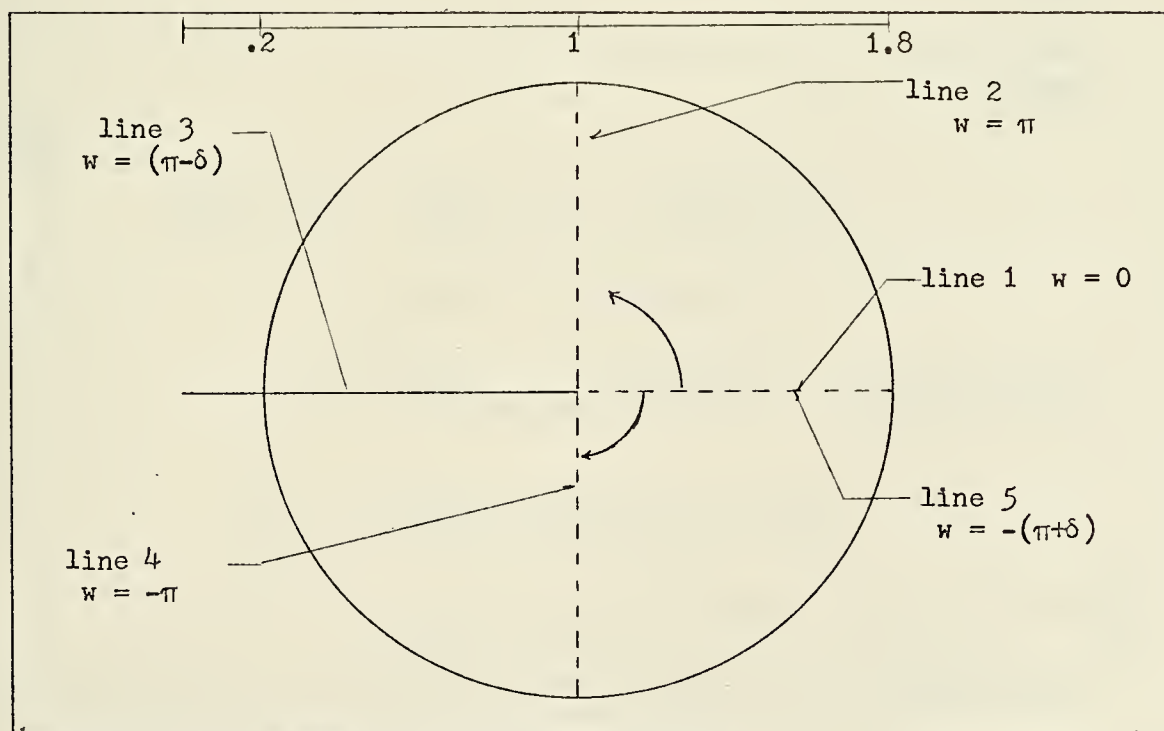


Figure B-12 Vector Representation of  $P(e^{j\omega})$



The rotating vector begins, for  $w = 0$ , at the position shown as line 1. As  $w$  increases to  $+\pi$ , the rotating vector moves in a clockwise direction to the position shown as line 2. When  $w$  is at a value of  $+(\pi-\delta)$ , the vector is at the position of line 3 - where the resultant magnitude of  $P(e^{jw})$  is 0.2. As  $w$  decreases to a value of  $-\pi$ , the rotating vector moves in a counterclockwise direction to the position of line 4. As  $w$  continues to decrease, the vector arrives at the position of line 5 when  $w = -(\pi+\delta)$  - where the resultant magnitude of  $P(e^{jw})$  is 1.8.

The implications of all of this is as follows. Let

$$\tilde{X} = X_1 + X_2$$

where  $\tilde{X}$  = DFT

$X_1$  = desired  
signal

$X_2$  = aliased  
signal

Then,

$$\begin{aligned} \tilde{X}\left(\frac{N}{2} - \delta\right) &= X(e^{j(\pi-\delta)}) + X(e^{j(-\pi-\delta)}) \\ &= \left|S(e^{j(\pi-\delta)})\right| \cdot \left|P(e^{j(\pi-\delta)})\right| \\ &\quad \cdot \exp \left[ j \left[ \arg S(e^{j(\pi-\delta)}) + \arg P(e^{j(\pi-\delta)}) \right] \right] \\ &\quad + \left|S(e^{j(-\pi-\delta)})\right| \cdot \left|P(e^{j(-\pi-\delta)})\right| \\ &\quad \cdot \exp \left[ j \left[ \arg S(e^{j(-\pi-\delta)}) + \arg P(e^{j(-\pi-\delta)}) \right] \right] \end{aligned}$$

To evaluate this, the following values should be used in this case:

$$\arg S(e^{j(\pi-\delta)}) \approx -\frac{3\pi}{2}$$





$$\arg S(e^{j(\pi-\delta)}) \approx + \frac{3\pi}{2}$$

$$\arg P(e^{j(\pi-\delta)}) = \arg P(e^{j(-\pi-\delta)}) = 0$$

$$P(e^{j(\pi-\delta)}) = .2$$

$$P(e^{j(-\pi-\delta)}) = 1.8$$

It follows then that

$$\begin{aligned} X_v\left(\frac{N}{2} - \delta\right) &\approx .2 \left[ S(e^{j(\pi-\delta)}) e^{-j\frac{3\pi}{2}} \right] + 1.8 \left[ S(e^{j(-\pi-\delta)}) e^{j\frac{3\pi}{2}} \right] \\ &\approx e^{-j\frac{3\pi}{2}} \left[ .2 S(e^{j(\pi-\delta)}) - 1.8 S(e^{j(-\pi-\delta)}) \right] \end{aligned}$$

The desired value of the phase is about  $-\frac{3\pi}{2}$  (or  $\frac{\pi}{2}$ ). If the term in the brackets is greater than zero, this is what will result. If the term in the brackets is negative, the phase will be  $-\frac{3\pi}{2} + \pi = -\frac{\pi}{2}$  (or  $-\frac{3\pi}{2} - \pi = -\frac{5\pi}{2} = -\frac{\pi}{2}$ ). In other words a branching will have occurred - not caused by the linear phase term of the groundwave.

For the term in the brackets to be positive, it is required that

$$S(e^{j(\pi-\delta)}) > 9 S(e^{j(-\pi-\delta)})$$

The value of  $\delta$  was such that  $\delta(n_1 + \Delta_1) = \pi/2$  or,  $\delta = \frac{\pi}{2(n_1 + \Delta_1)}$ .

For a Fourier Transform of a discrete sequence,  $\pi$  corresponds to  $N/2$  in the DFT. This can be represented as a frequency  $w_c$  so that



$$\delta = \frac{w_c}{2(n_1 + \Delta_1)}$$

If  $n_1 = 40$  (in many applications it can be much larger),  $\delta \approx \frac{w_c}{80}$ .

What is required therefore is that

$$\left| S(e^{j(\frac{79}{80} w_c)}) \right| > 9 \left| S(e^{j(-\frac{81}{80} w_c)}) \right|$$

Since  $|S(e^{jw})|$  has even symmetry, what is required is that the signal Fourier Transform magnitude decrease by a factor of more than 9 as  $w$  goes from  $.9875 w_c$  to  $1.0125 w_c$ . The Loran-C signal, by itself, decreases by a factor of about 1.07 in this band. Consequently, an analog filter which introduces an additional factor of about 9 decrease is needed.

It can be seen that if the  $B_1$  used in the example were 0.9, the decrease would have had to be by a factor of  $\frac{1 + .9}{1 - .9} = 19$ . If  $n_1$  were greater than 40, the transition band would be narrower. Additionally, greater values of  $\delta$ , i.e.,  $\delta = \frac{5\pi}{2(n_1 + \Delta_1)}$ , etc., will also cause this problem so that huge errors can accumulate.

Before considering possible solutions to this problem, a few examples of the phenomenon should be presented. A 2048 pt FFT was computed for a simulated Loran-C pulse. The complex logarithm of the results are shown in the following figures.

Figure B-13 shows an uncorrected phase curve for  $0 < k < N/2$  with  $n_0 = 0$ , no echo. Figure B-14 shows the same for  $n_0 = 4$ . Figure B-15 shows the log magnitude and phase for  $n_0 = 4$ ,  $n_1 = 20$ ,  $B_1 = .8$ . Notice that for values of  $k$  near  $N/2$  (corresponding to  $w \approx \pi$ ) there is a small amount of distortion. This represents the effects of aliasing as in figure B-10 - not enough to cause branchings.



Figure B-16 shows the log magnitude and phase curves for  $n_0 = 4$ ,  $(n_1 + \Delta_1) = 19.5$ . Here the problem can be seen (compare the last portion of the phase curve with figure B-6. Figure B-17 shows a corrected phase curve for  $n_0 = 0$ ,  $n_1 = 10$ ,  $B_1 = 0.8$ . The phase unwrapping and linear phase term removal have been done properly. Figure B-18 shows the corrected phase for  $n_0 = 0$ ,  $(n_1 + \Delta_1) = 9.5$ ,  $B_1 = 0.8$ . The large error is apparent.

A method of overcoming this problem is discussed in Appendix C.



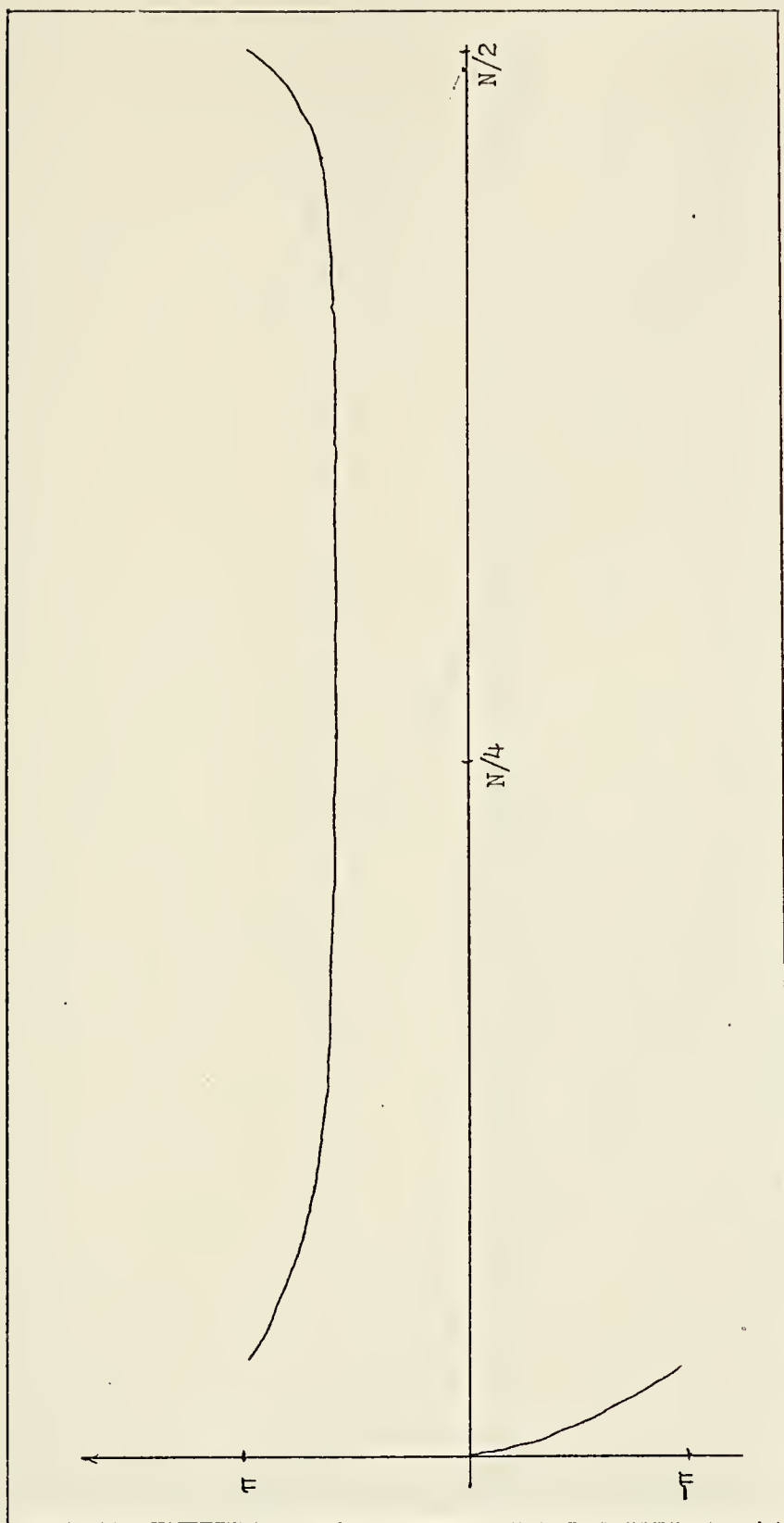


Figure B-13 Uncorrected Phase Curve, No Echo, No Linear Phase Term





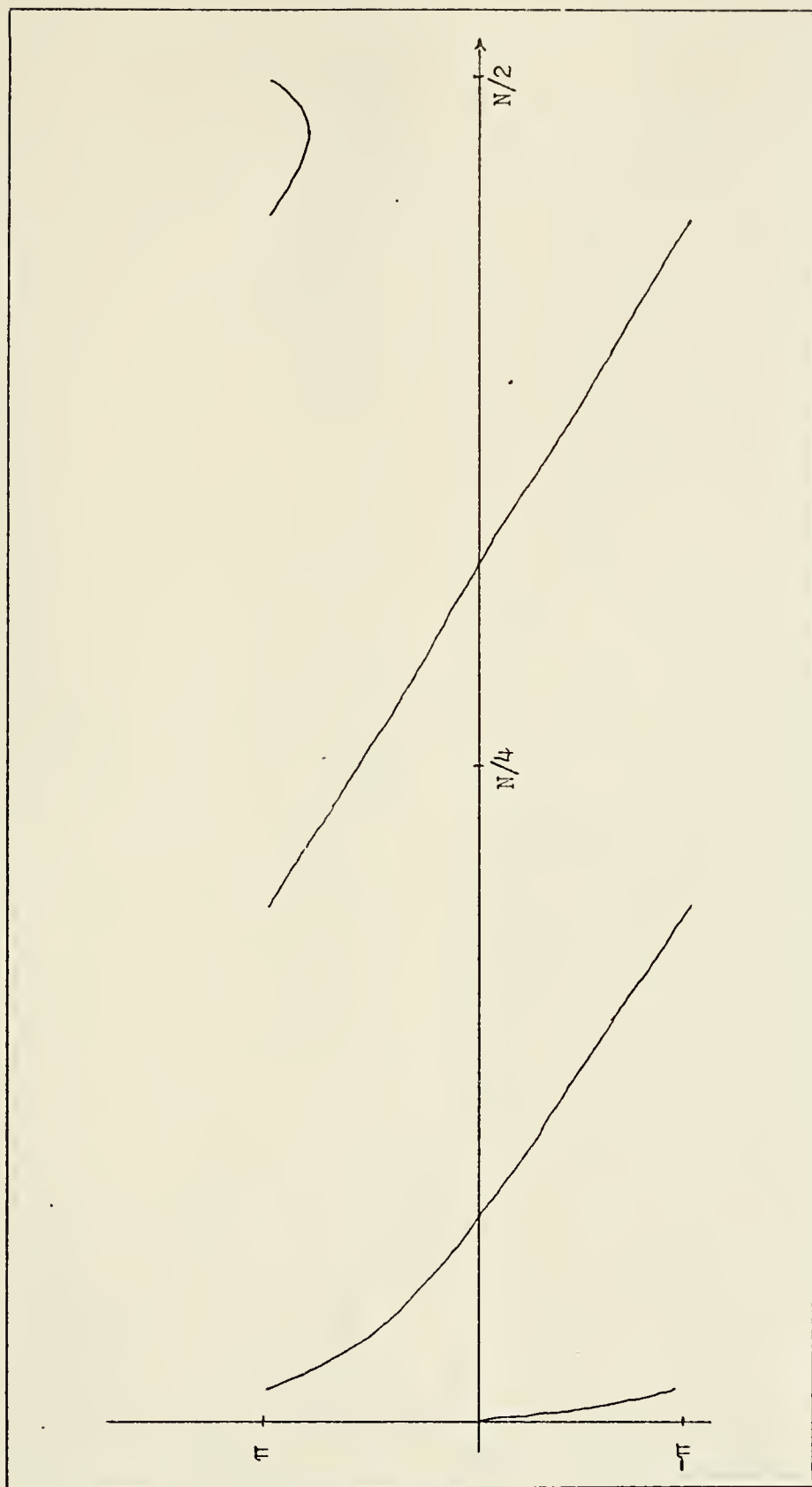


Figure B-14 Uncorrected Phase Curve, No Echo, With Linear Phase Term



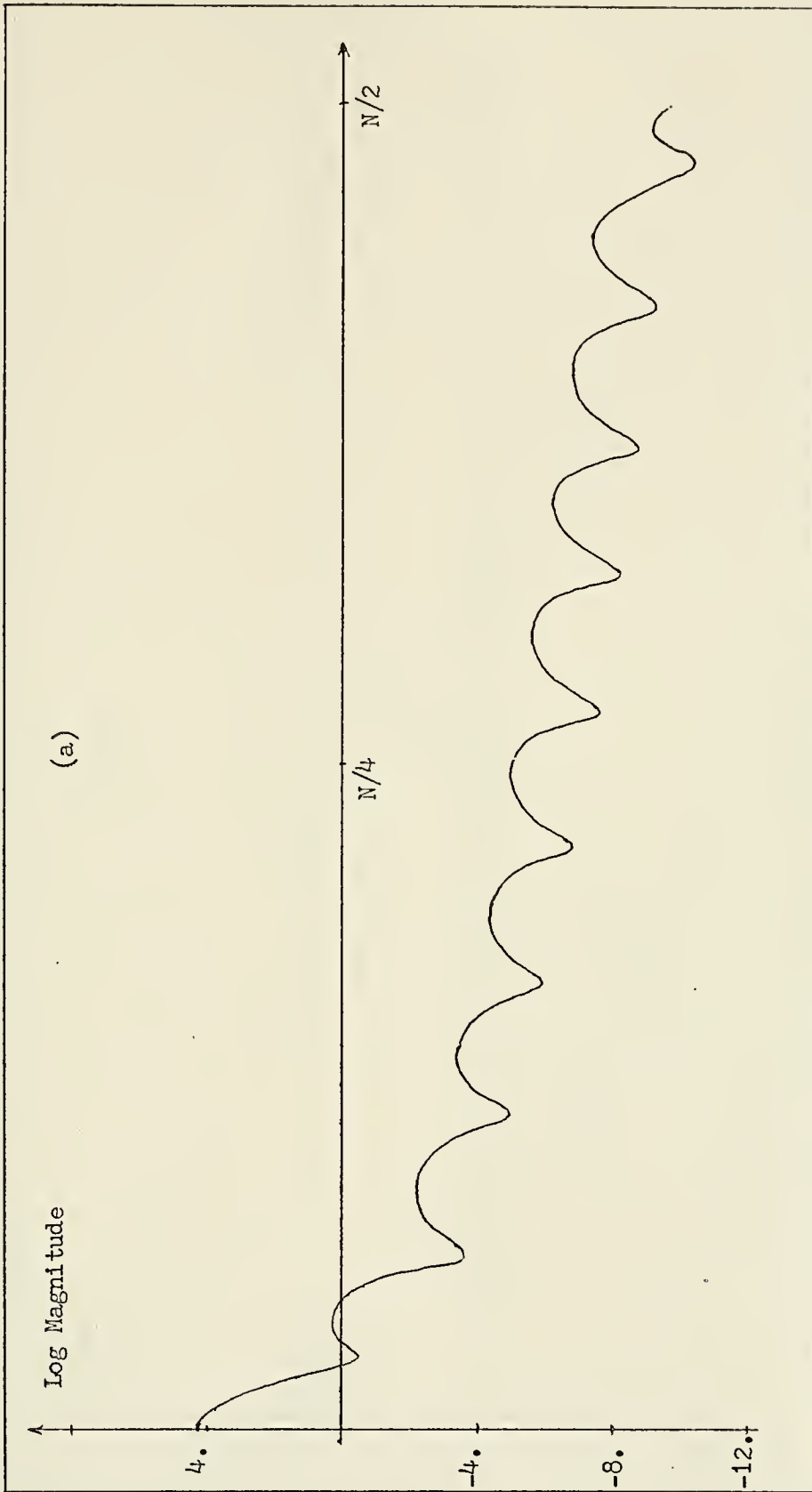


Figure B-15 Log Magnitude and Uncorrected Phase Curves: One Echo, No Aliasing



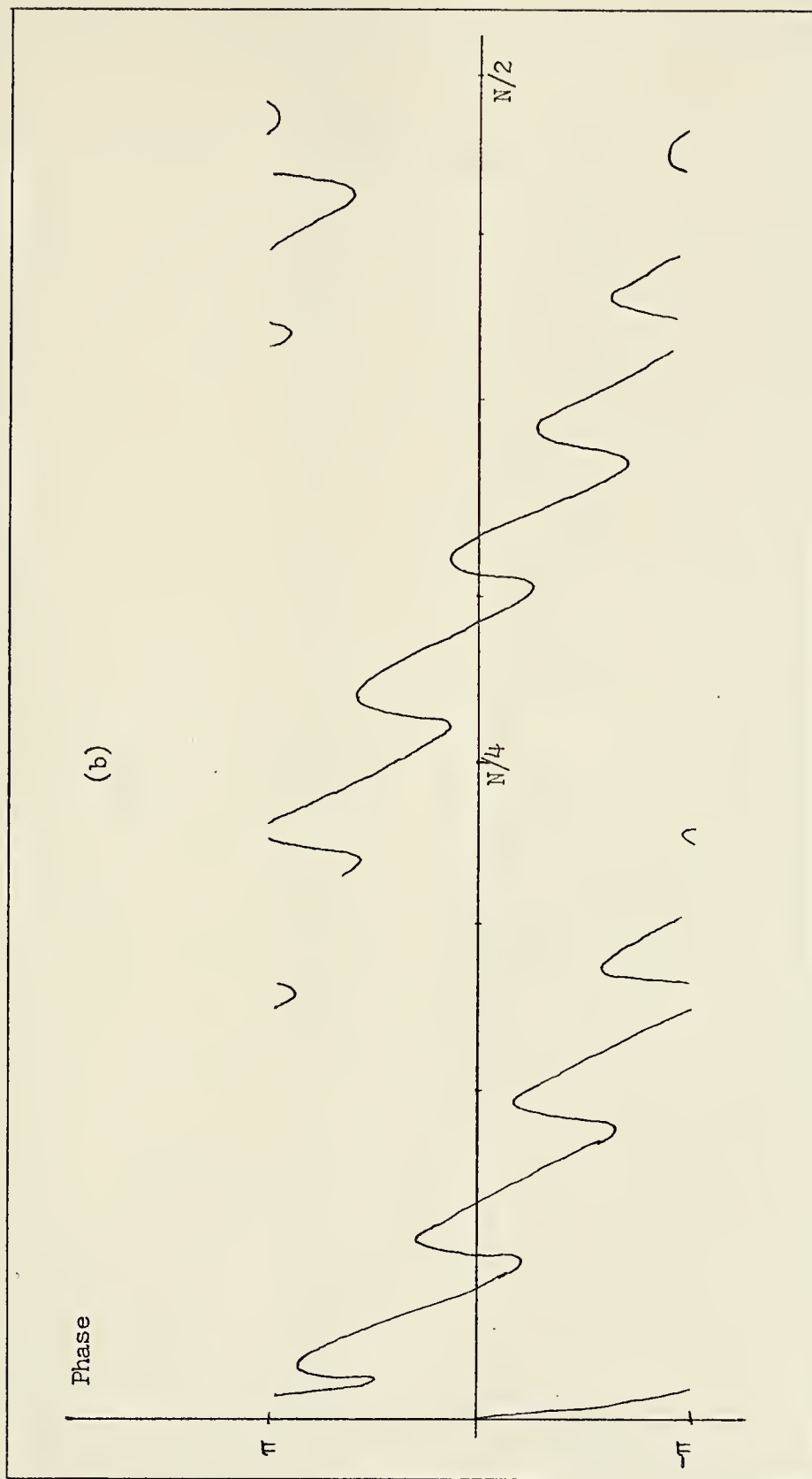


Figure B-15 (con't)



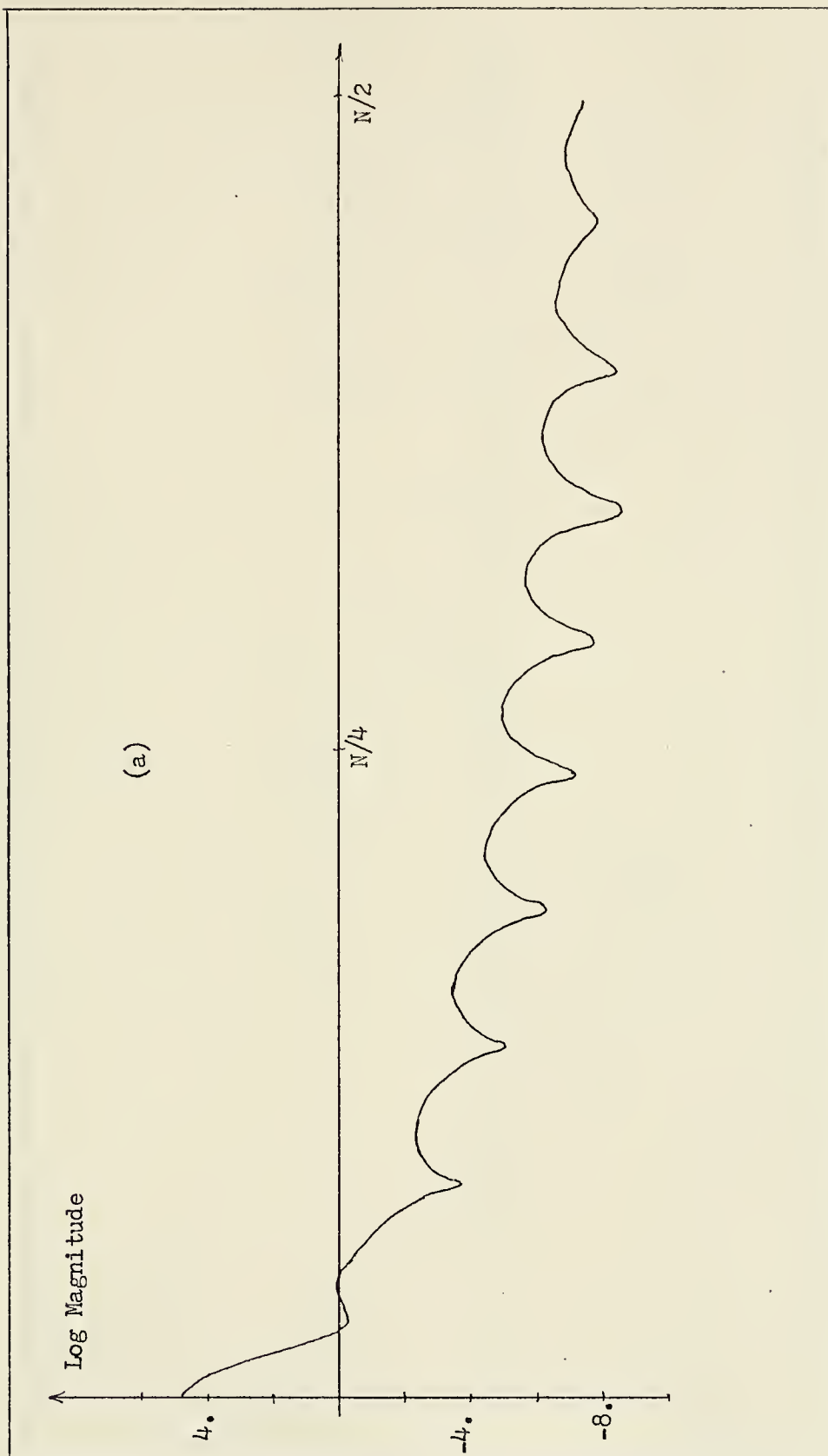


Figure B-16 Log Magnitude and Phase Curves: One Echo, Phase Aliased





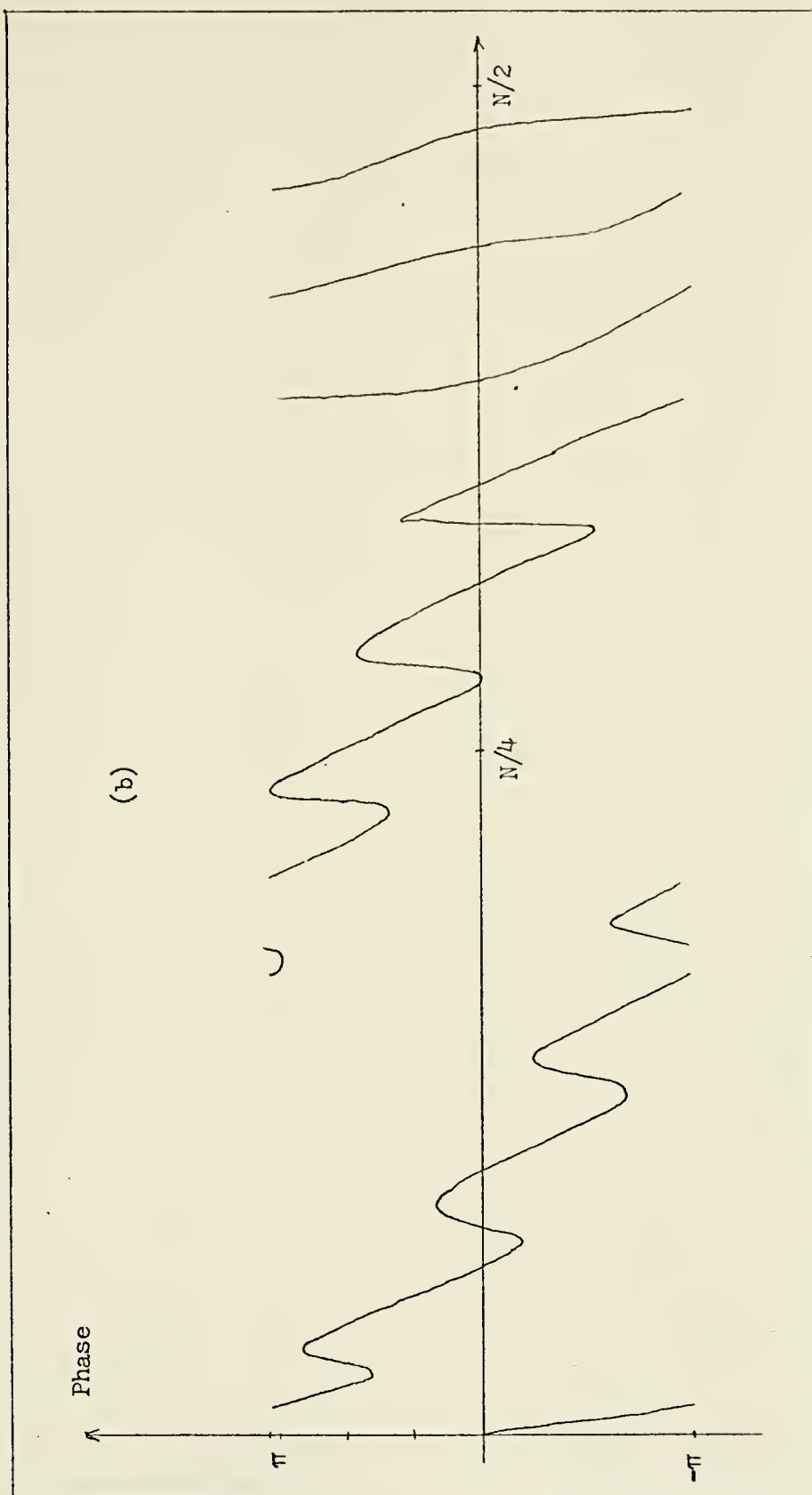


Figure B-16 (con't)



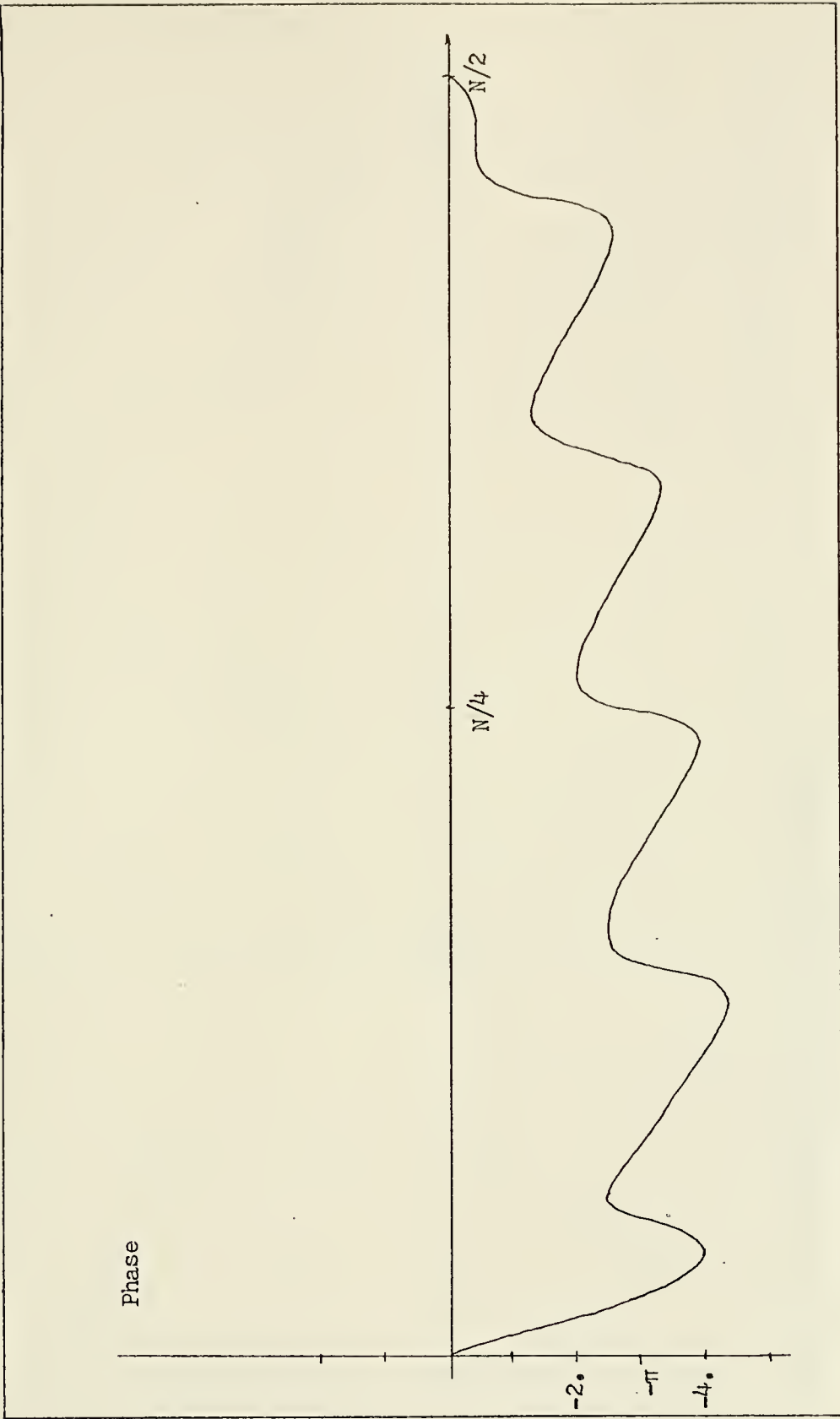


Figure B-17 Corrected Phase Curve: No Aliasing



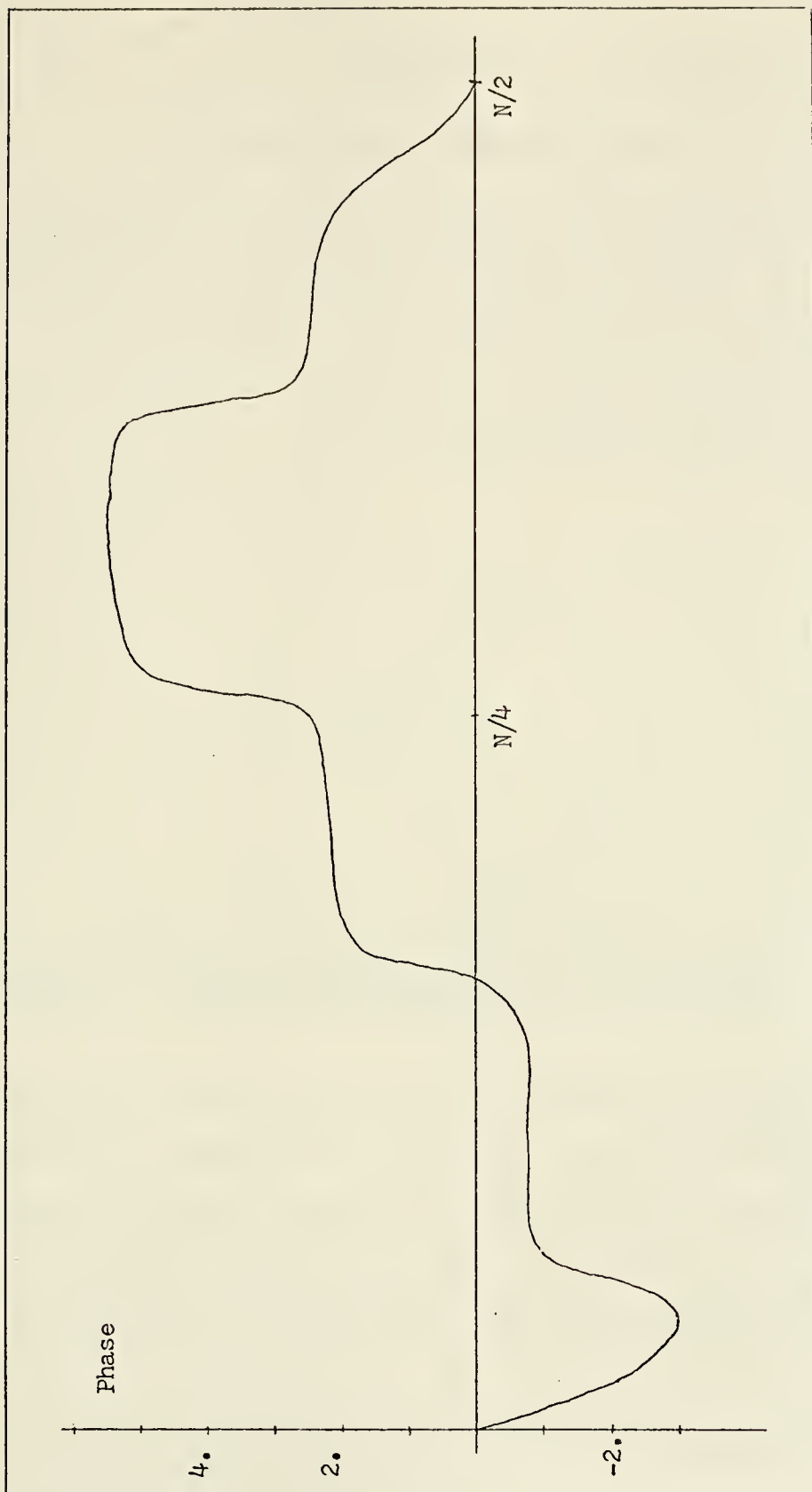


Figure B-18 Corrected Phase Curve: With Aliasing



## Appendix C

### TRANSFORM PHASE CORRECTION METHOD

This Appendix develops the technique used in this thesis to avoid the phase correction problems presented in Appendix B.

One possible solution to the problems would be to use extra exponential weighting. As an example, if the  $B_1$  in figure B-12 had a value of  $1/3$  instead of  $.8$ , the resulting vector representation would be as shown in figure C-1.

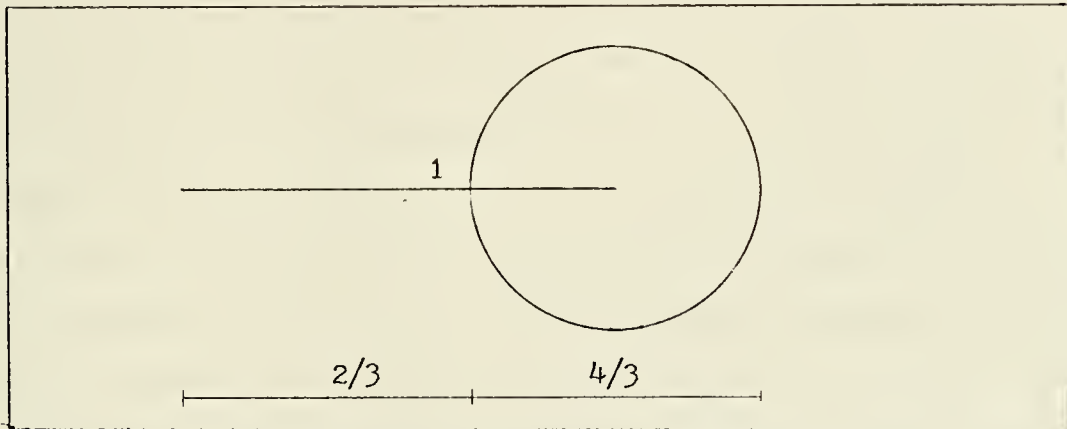


Figure C-1 Vector Representation of  $P(e^{j\omega})$  With Extra Exponential Weighting

In this case, the analog filter need only introduce a factor of 2 decrease in the transition band. However, in view of the fact that the desired exponential weighting to be used would be a complicated function of signal parameters, and since the transition band would still be very narrow, an alternate solution might be desirable.





In the cases considered in this thesis, the basic waveform is known to be of the form  $t^2 e^{-\alpha t}$  which has a phase value of almost  $-\frac{3\pi}{2}$  for large  $w$ . From figure B-13 it can be verified that the phase at  $k \approx N/4 \approx 512$  is essentially  $-1.5\pi$ . In figure B-14 it can be seen that the phase at  $k \approx 512$  is:

$$\begin{aligned} \arg X(N/4) &\approx 1.7 - 4\pi \approx -\frac{7\pi}{2} \\ &\approx -\frac{3\pi}{2} - 4(\pi/2) \end{aligned}$$

The scheme then becomes: examine the value of the phase at  $k \approx N/4$ , remove the  $-1.5\pi$  term which is due to the signal alone, and, determine the closest integer multiple of  $\pi/2$  in what remains. This integer is then  $n_0$ . The phase can then be corrected by bringing the  $N/4$  point of the phase up to zero by using the appropriate linear phase correction. This is done just as explained in Appendix B except that the straight line in figure B-2 goes from the  $k = 0$  point to the  $k = N/4$  point. The rest of the DFT record is then low pass filtered in a particular fashion - it is disregarded. A new  $N/2$  point sequence is generated:

$$\begin{aligned} X_{\text{new}}(k) &= X_{\text{old}}(k) & k = 0, 1, \dots, (N/4)-1 \\ X_{\text{new}}(k) &= X_{\text{old}}\left(\frac{N}{2} + k\right) & k = \frac{N}{4}, \dots, (N/2)-1 \end{aligned}$$

The effect of this operation is to double the effective sampling time (DT). A standard digital low pass filter is not used since zeroes in the sequence  $\log X(e^{j\omega})$  imply unity magnitude and zero phase in



the corresponding regions of the  $X(e^{j\omega})$  sequence. This would produce an even larger error in the cepstrum.

The effectiveness of this scheme can be seen by examining figure B-16 and noticing that the aliasing does not begin in the phase until well enough after  $k = N/4$  to be safe. A comparison of the resulting cepstra for the two methods of phase corrections is shown in figures C-2 and C-3.



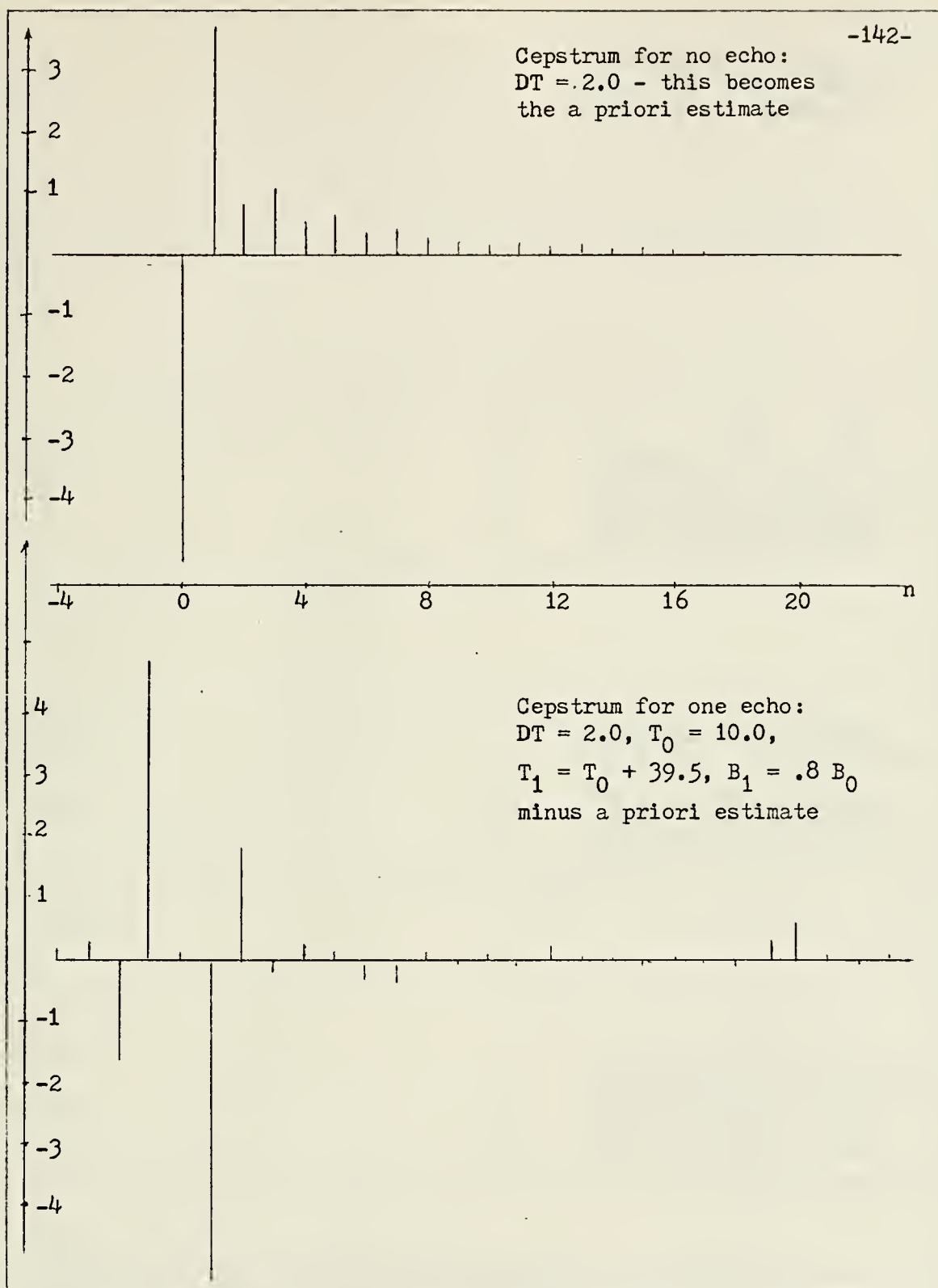


Figure C-2 Cepstrum Computed With Conventional Phase Unwrapping





Figure C-3 Cepstrum Computed With Modified Phase Unwrapping





# Appendix D MORE GENERAL NOISE DFT DERIVATION

In this Appendix, the appropriateness of the white noise model of Chapter 5 is examined to see if the results depend critically upon it.

Suppose the actual noise can be modelled as being obtained in the manner shown in figure D-1.

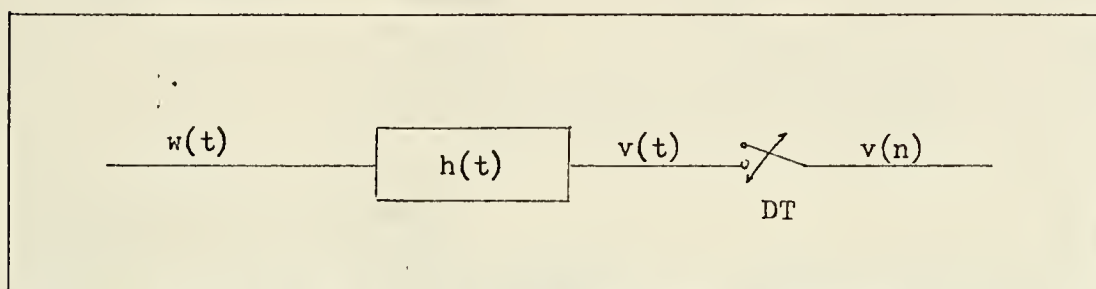


Figure D-1 Model of Non-white Noise Sample Generator

Here,  $w(t)$  is a zero mean, complex, white gaussian noise process and  $h(t)$  is some appropriate function which can model the noise structure and any receiver filters. The analysis can proceed as follows.

$$E \left[ w(t) w^*(t-\mu) \right] = \sigma^2 \delta(\mu)$$

$$E \left[ w(t) \right] = 0$$

For the purposes of this analysis it will suffice to let

$$h(t) = \beta e^{-\beta t} u_{-1}(t)$$

so that

$$v(t) = \int_{-\infty}^{\infty} w(\gamma) h(t-\gamma) d\gamma = \beta \int_{-\infty}^t w(\gamma) e^{-\beta(t-\gamma)} d\gamma$$



It follows then that

$$E \left[ v(t) \right] = \beta \int_{-\infty}^t E \left[ w(\gamma) \right] e^{-\beta(t-\gamma)} d\gamma = 0$$

and

$$E \left[ v_n \right] = E \left[ v(n \cdot DT) \right] = 0$$

Additionally,

$$\begin{aligned} E \left[ v(t) v^*(\mu) \right] &= \beta^2 \int_{-\infty}^t \int_{-\infty}^{\mu} E \left[ w(\lambda) w^*(\gamma) \right] e^{-\beta(t-\lambda)} e^{-(\mu-\gamma)} d\gamma d\lambda \\ &= \beta^2 \sigma^2 \int_{-\infty}^t \int_{-\infty}^{\mu} \delta(\lambda-\gamma) e^{-\beta(t+\mu-\lambda-\gamma)} d\gamma d\lambda \end{aligned}$$

For samples of the function,

$$R_v(n, m) = E \left[ v_n v_m^* \right] = \beta^2 \sigma^2 \int_{-\infty}^{n \cdot DT} \int_{-\infty}^{m \cdot DT} \delta(\lambda-\gamma) e^{-\beta(n \cdot DT + m \cdot DT - \lambda - \gamma)} d\gamma d\lambda$$

For  $m > n$  this becomes

$$\begin{aligned} R_v(n, m) &= \beta^2 \sigma^2 \int_{-\infty}^{n \cdot DT} e^{-\beta(n \cdot DT + m \cdot DT - 2\lambda)} d\lambda \\ &= \beta^2 \sigma^2 \left[ \frac{e^{-\beta(n \cdot DT + m \cdot DT - 2\lambda)}}{2\beta} \right]_{-\infty}^{n \cdot DT} \\ &= \frac{\beta \sigma^2}{2} e^{-\beta(m-n) \cdot DT} \end{aligned}$$

Similarly, for  $m < n$ ,

$$R_v(n, m) = \frac{\beta \sigma^2}{2} e^{-\beta(n-m) \cdot DT}$$

so that

$$R_v(1) = \frac{\beta \sigma^2}{2} e^{-\beta l \cdot DT} \quad \text{where } l = |m - n|$$



The results of Chapter 5 depend heavily on an analysis of the variance of points in the DFT - from this, the noise magnitude bound is derived. Therefore it is important to consider  $R_Y(k,k) = E \left[ x_k x_k^* \right]$ :

$$\begin{aligned} E \left[ x_k x_k^* \right] &= E \left[ \left[ v_0 + W^k v_1 + W^{2k} v_2 + \dots + W^{k(N-1)} v_{N-1} \right] \cdot \left[ v_0^* + W^{-k} v_1^* + \dots + W^{-k(N-1)} v_{N-1}^* \right] \right] \\ &= N R_V(0) + R_V(1) \cdot \left[ W^{-k} + W^k + W^{-k} + \dots + W^k \right] \\ &\quad + R_V(2) \cdot \left[ W^{-2k} + W^{2k} + \dots + W^{2k} \right] \\ &\quad + \dots \\ &= N R_V(0) + 2 \sum_{m=1}^{N-1} (N-m) \cdot R_V(m) \cdot \cos \frac{2\pi k m}{N} \end{aligned}$$

$$D-1 \quad R_Y(k,k) = \frac{\beta \sigma^2}{2} N + 2 \sum_{m=1}^{N-1} (N-m) \cdot e^{-\beta \cdot DT \cdot m} \cdot \cos \frac{2\pi k m}{N}$$

The evaluation of the sum in this expression can be simplified by making the approximation  $(N-m) \approx N$ . To see the validity of this approximation, the following would have to be specified.

$$\beta \approx 1.5 \times 10^5 \quad DT = 10 \text{ } \mu\text{sec}$$

$$\beta \cdot DT \approx 1.5 \quad \text{and} \quad e^{-\beta DT} \approx .223$$

The  $h(t)$  filter with such a pole location would have a half power point



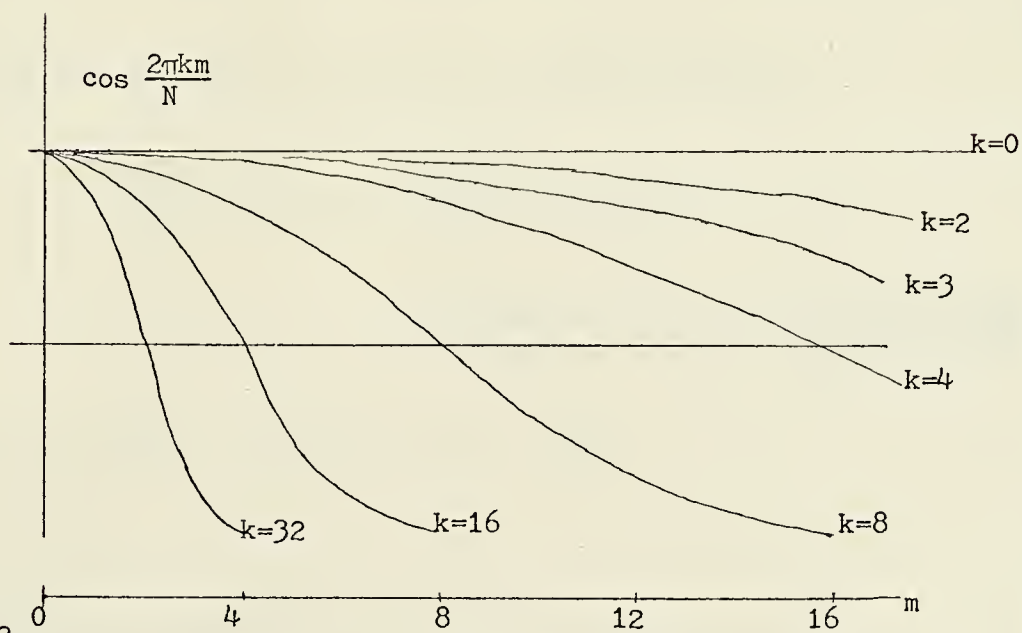
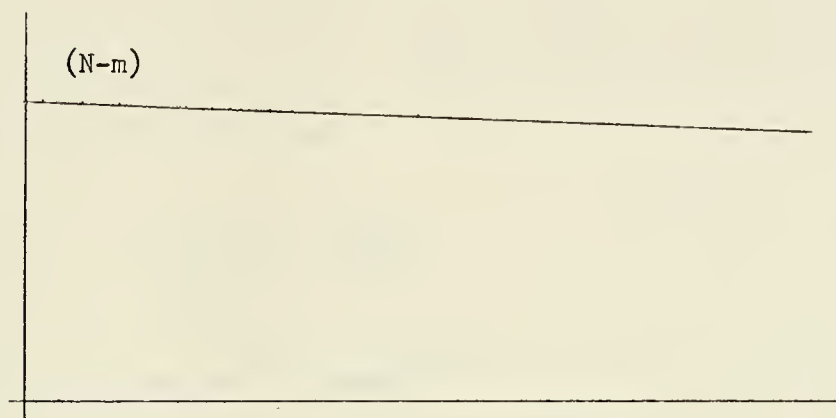
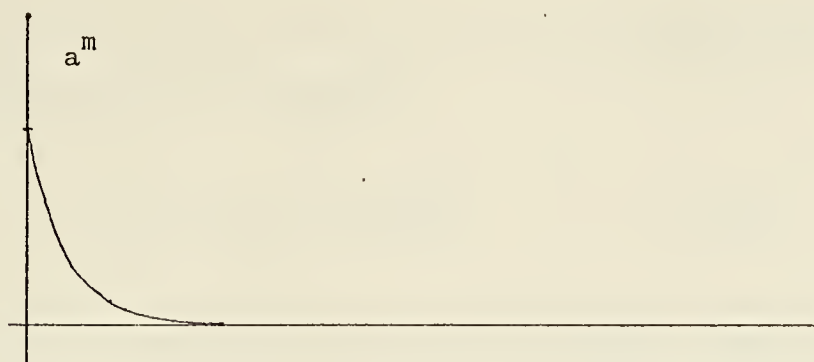


Fig. D-2





at a frequency of about 25 kHz so that  $\beta$  has a reasonable value. The sum in equation (D-1) then becomes:

$$\sum_{m=1}^{N-1} (N-m) a^m \cos \frac{2\pi k m}{N} \quad ; \quad a \approx .223$$

A plot of the three terms in the sum is shown in figure D-2 for  $N = 256$ . Since the rapid decay of the  $a^m$  term will dominate the sum, it can be seen that  $(N-m) \approx N$  is a clearly justified simplification. The sum to be considered is then

$$N \sum_{m=1}^{N-1} a^m \cos \frac{2\pi k m}{N}$$

which can be evaluated as in Jolley<sup>10</sup>

$$\sum_{m=0}^{N-1} a^m \cos m \theta = \frac{1 - a \cos \theta + a^{N+1} \cos (N-1)\theta - a^N \cos \theta}{1 - 2a \cos \theta + a^2}$$

For  $N = 256$  and  $a \approx .223$ ,  $a^N \approx a^{N+1} \approx 0$ , so that the sum is

$$\begin{aligned} \sum_{m=1}^{N-1} a^m \cos m \theta &= \left[ \sum_{m=0}^{N-1} a^m \cos m \theta \right] - 1 \\ &= \frac{a \cos \theta - a^2}{1 - 2a \cos \theta + a^2} = \frac{a [\cos \theta - a]}{|1 - a e^{-j\theta}|^2} \end{aligned}$$

The result is plotted in figure D-3 for  $\theta = \frac{2\pi k}{N}$



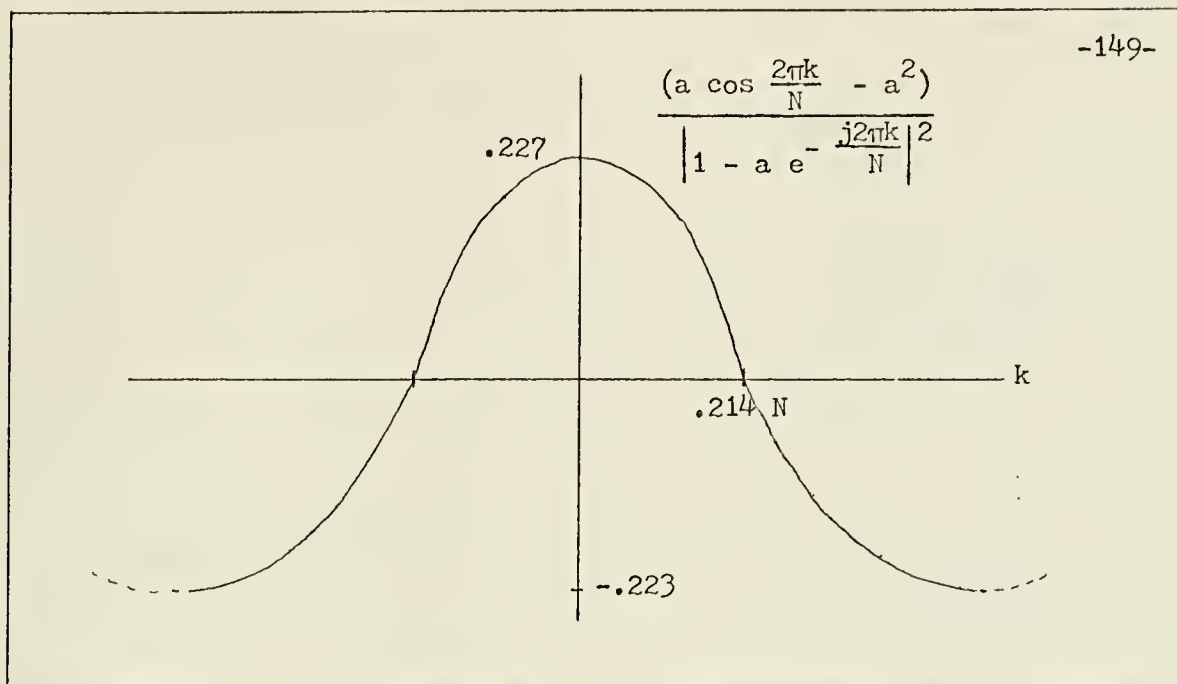


Figure D-3

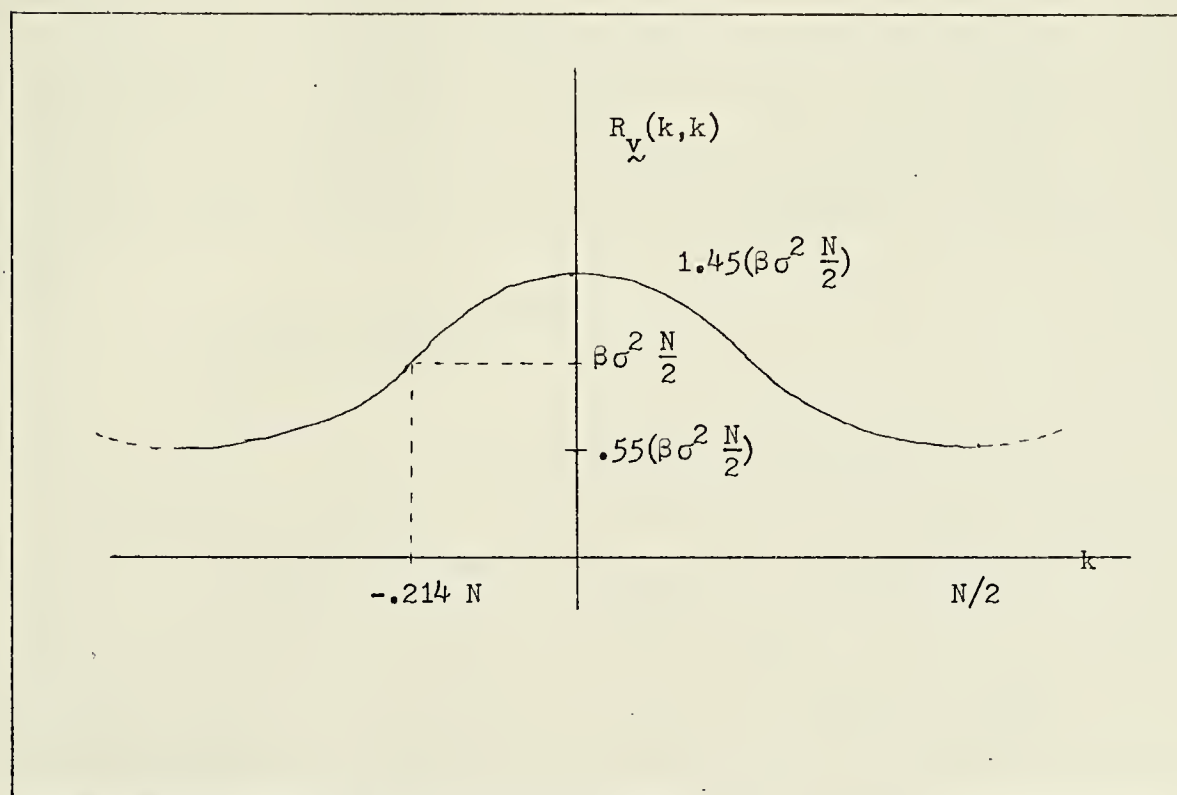


Figure D-4 Non-White Noise DFT Variance



What can be noticed is that the zero crossing is at

$$\theta = \cos^{-1} a$$

or at

$$k = \frac{N}{2\pi} \cos^{-1} .223 \approx .214 N \quad (\text{since } \theta = \frac{2\pi k}{N})$$

It follows from equation (D-1) that

$$R_{\underline{y}}(k,k) = \frac{\beta \sigma^2}{2} N \left[ 1 + 2 \sum_{m=1}^{N-1} a^m \cos m\theta \right] \quad \text{for } a \approx .223$$

$$\theta = \frac{2\pi k}{N}$$

This is plotted in figure D-4.

What can be seen is that as  $\beta \cdot DT$  increases ( $a$  decreases), the plot flattens out, approaching a value of  $N \cdot R_{\underline{y}}(0)$  as in the white noise case. The crossover point, i.e., the value of  $k$  beyond which the noise variance is less than in the white noise case, was derived from,

$$k_0 = \frac{N}{2\pi} \cos^{-1} \left( e^{-\beta \cdot DT} \right)$$

As  $\beta \cdot DT \rightarrow \infty$ ,  $e^{-\beta \cdot DT} \rightarrow 0$ , so that  $k_0$  approaches  $\frac{N}{2\pi} \left( \frac{\pi}{2} \right) = N/4$ .

As described in Appendix C, it is the values of the DFT for  $k < N/4$  that are to be retained to compute the cepstrum. Additionally, the sampling rate for any given SNR is to be determined by the noise statistics in the DFT for values of  $k$  near  $N/4$ . What the analysis has shown therefore is that for  $k \approx N/4$ , the variance of the noise is nearly the same in both the white and non-white cases so that the model used in Chapter 5 is appropriate.



5 MAY 76

23619

Thesis

153003

W464 Wenzel

An application of  
homomorphic deconvolu-  
tion to Loran-C signal  
processing.

27 SEP 76

DISPLAY

5 MAY 76

23619

Thesis

153003

W464 Wenzel

An application of  
homomorphic deconvolu-  
tion to Loran-C signal  
processing.

thesW464

An application of homomorphic deconvolut



3 2768 000 99694 6

DUDLEY KNOX LIBRARY